

## Jury Member Report – Doctor of Philosophy thesis.

**Name of Candidate:** Anastasia Gabova

**PhD Program:** Petroleum Engineering

**Title of Thesis:** Experimental investigations of thermal properties of unconventional hydrocarbon reservoirs at formation temperatures

**Supervisor:** Professor Yuri Popov

**Co-supervisor:** Dr. Evgeny Chekhonin

**Name of the Reviewer:** Prof. Alexey Cheremisin

<p>I confirm the absence of any conflict of interest</p> <p>(Alternatively, Reviewer can formulate a possible conflict)</p>	<p><b>Date: 25-12-2021</b></p>
---	--------------------------------

*The purpose of this report is to obtain an independent review from the members of PhD defense Jury before the thesis defense. The members of PhD defense Jury are asked to submit signed copy of the report at least 30 days prior the thesis defense. The Reviewers are asked to bring a copy of the completed report to the thesis defense and to discuss the contents of each report with each other before the thesis defense.*

*If the reviewers have any queries about the thesis which they wish to raise in advance, please contact the Chair of the Jury.*

### Reviewer's Report

--

The dissertation is presented in complete thesis form (128 pages, five chapters). The research topic is experimental measurements of rock thermal properties at formation (elevated) temperature for unconventional reservoirs.

The research topics are relevant for oil&gas and geothermal industries. Rock thermal properties are essential for basin modeling, enhanced oil recovery methods, and numerical simulation of oil field development.

The research results were published in four Q1 and one Q3 SCOPUS journals. The results were presented at 15 international conferences. Anastasia is a co-author of the patent. The obtained scientific results make it possible to apply the proposed approaches for measurements of thermal properties at elevated temperatures, basin modeling, and EOR simulations.

Before defending the thesis, I recommend making the following changes:

1. English proofreading
2. p. 37: Provide accuracy for both DTC and TCS measurements.
3. p. 38: Please clarify in the thesis why precision depends on temperature range.
4. p. 84: Please explain a sharp change in thermal conductivity after 180 deg. C. Please add accuracy and precision bars to all graphs.

Detailed comments, corrections, and recommendations are provided in PDF file attached to the report.

#### Provisional Recommendation

*I recommend that the candidate should defend the thesis by means of a formal thesis defense*

*I recommend that the candidate should defend the thesis by means of a formal thesis defense only after appropriate changes would be introduced in candidate's thesis according to the recommendations of the present report*

*The thesis is not acceptable and I recommend that the candidate be exempt from the formal thesis defense*

Skolkovo Institute of Science and Technology

EXPERIMENTAL INVESTIGATIONS OF THERMAL PROPERTIES OF  
UNCONVENTIONAL HYDROCARBON RESERVOIRS AT FORMATION  
TEMPERATURES

*Doctoral Thesis*

by

ANASTASIA GABOVA



DOCTORAL PROGRAM IN PETROLEUM ENGINEERING

Supervisor  
Professor Yuri Popov

Co-supervisor  
Dr. Evgeny Chekhonin

I hereby declare that the work presented in this thesis was carried out by myself at Skolkovo Institute of Science and Technology, Moscow, except where due acknowledgment is made and has not been submitted for any other degree.

Candidate (Anastasia Gabova)

Supervisor (Prof. Yuri Popov)

Co-supervisor (Dr. Evgeny Chekhonin)

## Abstract

Experimental data on thermal properties (thermal conductivity, coefficient of linear thermal expansion (CLTE), volumetric heat capacity (VHC)) of rocks at elevated temperatures is necessary for heat flow density determination, enhanced oil recovery methods, basin and petroleum system modeling, wellbore stability analysis, designing radioactive waste repositories, etc. Such information is especially actual for organic-rich shales that exhibit significant thermal anisotropy and heterogeneity and were not studied comprehensively previously. Nowadays, there is a lack of experimental data on thermal properties of organic-rich rocks at elevated temperatures and reliability of results is  provided. A new sophisticated technique was developed to carry out thermal conductivity measurements **on** organic-rich rocks from various unconventional formations in a temperature range of 30-300 °C. Divided-bar and optical scanning methods were combined in the thermal conductivity measurements in order to account for thermal anisotropy and heterogeneity of the rocks and improve the quality of the experimental data. This approach enabled us to reveal and overcome systematic errors in previous measurements of oil shale samples using the divided-bar method and to develop an approach for the correction of measurement results. It allowed us to account for the thermal contact resistance, non-parallelism of rock samples surfaces, and changes in rock samples structure during heating the samples. The coefficient of linear thermal expansion (CLTE) of shale samples was studied with a quartz dilatometer specially adapted for the measurements on standard core plugs. Strong correlations between the CLTE, thermal conductivity, and total organic carbon were established. Detailed profiles of CLTE along studied wells were obtained for the first time due to the application of the optical scanning technique and established correlations between the thermal conductivity and CLTE. These profiles fit well with total organic carbon obtained with pyrolysis. CLTE anisotropy was assessed for organic-rich shale samples together with thermal conductivity anisotropy. The new methodology for determining volumetric heat capacity at elevated temperatures for unconventional reservoir rocks allowed us to obtain new equations which relate thermal conductivity to temperature. New developed methodology of thermal conductivity measurements on rock cuttings at elevated temperatures provides measurements for unconventional reservoir rocks. It allowed us to obtain new equations  which relate the thermal conductivity of the matrix to temperature. 114 rock samples from  7 oil fields were totally studied with the techniques developed and enhanced to establish the behavior of the thermal properties at elevated temperatures within the temperature range of 25-300 °C.

## Publications

### *Peer-Reviewed Articles in International Scientific Journals*

1. **Gabova A.**, Popov Y., Savelev E., Romushkevich R., Chekhonin E., Plotnikov V., Emelyanov D., Akhmadishin A. Experimental investigation of the effect of temperature on thermal conductivity of organic-rich shales. *Journal of Petroleum Science and Engineering*. Q1.2020. Scopus.
2. **Gabova A.**, Chekhonin E., Popov Yu., Savelev E., Romushkevich R., Popov E., Kozlova E. Experimental Investigation of Thermal Expansion of Organic-Rich Shales. *International Journal of Rock Mechanics and Mining Sciences*. Q1. 2020. Scopus&WoS.
3. Chekhonin E., Popov E., Popov Y., **Gabova A.**, Romushkevich R., Spasennykh M., Zagranovskaya D. High-Resolution Evaluation of Elastic Properties and Anisotropy of Unconventional Reservoir Rocks via Thermal Core Logging. *Rock Mechanics and Rock Engineering*. Q1. 2018. Scopus&WoS.
4. Popov, Y., Spasennykh, M., Shakirov, A., Chekhonin, E., Romushkevich, R., Savelev, E., **Gabova, A.**, Zagranovskaya, D., Valiullin, R., Yuarullin, R., Golovanova, I., Sal'manova, R. Advanced Determination of Heat Flow Density on an Example of a West Russian Oil Field. *Geosciences*. Q1. 2021. Scopus.
5. Popov Y., Popov E., Chekhonin E., **Gabova A.**, Romushkevich R., Spasennykh M., Zagranovskaya D. Investigations of Bazhenov formation using thermal core logging technique. *Oil Industry*. Q3. 2017. Scopus.

### *Patent*

Gabova A., Goncharov A., Popov Y., Chekhonin E., Spasennykh M., 2020. Approach for determining the thermal conductivity of particles of solid materials at elevated temperatures. Russian patent, №220.017.FB7B.

### *Extended abstracts in conference proceedings*

1. **Gabova A.**, Chekhonin E., Popov E., Savelev E., Kozlova E., Popov Y., Karpov I. Experimental investigations of thermal expansion coefficient of Bazhenov formation rocks. *Proceedings of ISRM European Rock Mechanics Symposium EUROCK 2018*. Scopus, 2018
2. **Gabova A.**, Chekhonin E., Popov E., Savelev E., Kozlova E., Popov Y., Karpov I. Investigation of coefficient of linear thermal expansion of Bazhenov formation rocks. *In: Proceedings of 19th Scientific-Practical Conference on prospecting and development of oil and gas fields «Geomodel-2017»*, 4 p. Scopus, 2017.

3. Popov E., **Gabova A.**, Chekhonin E., Romushkevich R., Savelev E. Bazhenov formation characterization with rock thermal property profiling technique. *79th EAGE Conference & Exhibition 2017, Paris, June 12-15, 2017*. Scopus.
4. Popov Y., Spasennykh M., Valiullin R., Yarullin R., Ramazanov A., Zagranovskaya D., Zakharova O., Golovanova I., Chekhonin E., Savelev E., **Gabova A.**, Popov E., Shakirov A. First experience of maintenance of basin modeling with up-to-date complex of experimental geothermic investigations. *Proceedings of 19th Scientific-Practical Conference on prospecting and development of oil and gas fields «Geomodel-2018»*, 4 p. Scopus, 2018.
5. Popov Y., Chekhonin E., Romushkevich R., Popov E., Savelev E., **Gabova A.**, Emelyanov D., Ahmadshin A., Smyshlyaeva M., Grischenko M. The modern role of thermal petrophysics in prospecting, exploration and development of HC deposits by example of Em-Egovskoye oilfield. *Proceedings of 19th Scientific-Practical Conference on prospecting and development of oil and gas fields «Geomodel-2018»*, 4 p. Scopus, 2018.
6. Popov Y., Popov E., Chekhonin E., **Gabova A.**, Savelev E. New role of thermal petrophysical technologies at exploration, prospecting and development of oil-gas fields. *Proceedings of 5th International Conference on prospecting and development of oil and gas fields «GeoBaikal 2018»*, 4 p. Scopus, 2018.
7. Popov E., Goncharov A., Popov Y., Spasennykh M., Chekhonin E., Shakirov A., **Gabova A.** Advanced techniques for determining thermal properties on rock samples and cuttings and indirect estimating for atmospheric and formation conditions. *IOP Conference Series: Earth and Environmental Science*. Scopus, 2019.
8. Popov Y., Romushkevich R., **Gabova A.**, Chekhonin E., Popov Yu., Spasennykh M., Zagranovskaya D., Belenkaya I., Karpov I. Development of database on Bazhenov formation thermal properties for hydrodynamic and basin and petroleum system modeling. *In: Proceedings of 18th Scientific-Practical Conference on prospecting and development of oil and gas fields «Geomodel-2016»*, 4 p. Scopus, 2016.
9. Popov Y., Popov E., Chekhonin E., Romushkevich R., Spasennykh M., Bogdanovich N., Kozlova E., **Gabova A.**, Zhukov V., Zagranovskaya D., Karpov I., Belenkaya I., Ovcharenko Y., Alekseev A., Kalmykov G., Gutman I., Oksenoyd E. Thermal core logging as new technique of Bazhenov formation investigations for prospecting, exploration and recovery of hydrocarbons. *In: Proceedings of 18th Scientific-Practical Conference on prospecting and development of oil and gas fields «Geomodel-2016»*, 4 p. Scopus, 2016.
10. Popov E., **Gabova A.**, Karpov I., Zagranovskaya D., Romushkevich R., Spasennykh M., Chekhonin E., Popov Y. Correlations between thermal core logging, gamma logging and

- gamma spectrometry data. *In: Proceedings of 18th Scientific-Practical Conference on prospecting and development of oil and gas fields «Geomodel-2016»*, 4 p. Scopus, 2016.
11. Popov E., Popov Y., **Gabova A.**, Chekhonin E., Romushkevich R., Spassenykh M., Stenin V., Kozlova E., Deliya S., Shayakhmetov T., Drandusov K. Results of combined investigations of Domanic formation with continuous thermal core profiling. *In: Proceedings of 19th Scientific-Practical Conference on prospecting and development of oil and gas fields «Geomodel-2017»*, 4 p. Scopus, 2017.
  12. Popov E., Romushkevich R., **Gabova A.**, Popov Y., Savelev E., Romanov Y., Spiridonov D. Thermal Properties of Bazhen Formation Rocks of Surgut and Nizhnevartovsk Arches of Western-Siberian Plate from Continuous Core Profiling. *In: Proceedings of 19th Scientific-Practical Conference on prospecting and development of oil and gas fields «Geomodel-2017»*, 4 p. Scopus, 2017.
  13. Popov Y., Popov E., Chekhonin E., **Gabova A.**, Romushkevich R., Spasennykh M. Thermal core logging as new method of investigations of Bazhenov formation at exploration, prospecting and development of hydrocarbon fields. *Conference "New GIS-technologies for oil-gas companies"*. Ufa, 14-16 November, 2017.
  14. Popov Y. Popov E., Romushkevich R., Chekhonin E., **Gabova A.**, Spasennykh M., Zagranovskaya D., Karpov I., Ovcharenko Y. Interrelations of Bazhenov shale properties and their significance at exploration, prospecting and development of hydrocarbon fields. *Conference "Shale science: Problems of prospecting and development"*, Moscow, 10-11 April, 2017.
  15. Spasennykh M., Popov E., Chekhonin E., Romushkevich R., Zagranovskaya J., Belenkaya I., Zhukov V., Karpov I., Saveliev E., **Gabova A.** Thermal properties of Bazhen formation sediments from thermal core logging. *Proceedings volume of EGU General Assembly*, Vienna, Austria, April 19-22, 2016. Scopus.

## Acknowledgments

I would like to express gratitude to the people which helped and supported me during my Ph.D. study and research.

First of all, I want to say many thanks to my supervisor, Professor Yuri Popov, for being a supportive mentor and advisor. Especially thanks for practice in experimental research, writing publications, scientific discussions, and for the opportunity to be a part of a world-leading team of thermal petrophysics.

Also, I thank my co-supervisor Dr. Evgeny Chekhonin for constant support in my research, for giving useful recommendations and advice, and for very efficient discussions.

Many thanks to Raisa Romushkevich for her support and advice in the geological part of my research.

I am very grateful to Dr. Elena Kozlova for her support and constant help with pyrolysis experiments.

I would like to say thanks to the laboratory team that helped to conduct experiments for my research. Thanks to Dr. Evgeny Popov who helped with equipment adjustment and samples preparation for my research and also for constant advice and support. Thanks to Egor Savelev, Dr. Alexander Goncharov, Dmitry Ostrizhny, Sergey Pohilenko, Valentin Solomatin for help in the experimental part of my research.

Many thanks to Professor Mikhail Spasennykh for the opportunity to conduct research in the center for Hydrocarbon Recovery, for constant help and support.

Also, I would like to mention the help of the Educational Office of the Skolkovo Institute of Science and Technology in my Ph.D. study and say many thanks to all team members.

Many thanks to all my colleagues from the Center for Hydrocarbon Recovery for a friendly and positive atmosphere during my Ph.D. study and research.

## Table of contents

Abstract.....	3
Publications .....	4
Acknowledgments .....	7
Table of contents .....	8
List of figures.....	10
List of tables .....	15
Chapter 1. Introduction.....	17
1.1 The necessity of experimental data on thermal properties at elevated temperatures for the solution of actual problems in oil&gas science and industry .....	17
1.2 Statement of the problem.....	21
1.3 Goals and objectives .....	21
1.4 Outline of the Thesis.....	22
Chapter 2. Literature review and the current state of the problem .....	23
2.1 Thermal conductivity dependence of unconventional reservoirs at elevated temperatures – current state of art .....	23
2.2 Coefficient of linear thermal expansion at elevated temperatures – current state of art ...	28
2.3 Volumetric heat capacity at elevated temperatures – current state of art .....	31
2.4 Thermal conductivity measurements on rock cuttings and unconsolidated rocks at elevated temperatures – current state of art .....	32
2.5 Summary.....	33
Chapter 3. Research methods .....	35
3.1 Enhancement of experimental basis for thermal conductivity measurements at elevated temperatures.....	35
3.1.1 Method of measuring thermal conductivity at elevated temperatures.....	35
3.1.2 New measuring technique based on the integration of DTC-300 instrument and Thermal Conductivity Scanner.....	41
3.1.3 Modification of DTC-300 technique .....	45
3.2 The technique of measurements of thermal conductivity of rock cuttings and non-consolidated rocks at elevated temperatures.....	48
3.2.1 Materials and methods.....	48
3.2.2 Theoretical approach .....	49
3.3 Enhancement of experimental basis for CLTE measurements at elevated temperatures on core samples.....	52
3.3.1 Experimental basis of CLTE measurements .....	52
3.3.2 Integration of dilatometer and Thermal Conductivity Scanner.....	55
3.4 The technique of measurements of volumetric heat capacity of rocks at elevated temperatures.....	57
3.4.1 Measurements of specific heat capacity at elevated temperatures .....	57

3.4.2	Integration of differential scanning calorimeter and dilatometer for measuring volumetric heat capacity at elevated temperatures .....	59
Chapter 4.	Experimental results.....	60
4.1	Unconventional reservoir rocks under study .....	60
4.2	Thermal conductivity at elevated temperatures .....	61
4.2.1	Rock collection for studying thermal conductivity at elevated temperatures .....	61
4.2.2	Results of measurements .....	63
4.2.3	Equations that relate thermal conductivity to temperature for unconventional reservoir rocks .....	80
4.2.4	Changes in thermal conductivity of unconventional reservoir rocks during heating and cooling .....	80
4.2.5	Measurements on kerogen sample.....	83
4.3	CLTE investigations for unconventional reservoir rocks .....	84
4.3.1	Rock collections for studying CLTE .....	84
4.3.2	CLTE and thermal conductivity measurements at room temperature.....	86
4.3.3	CLTE anisotropy at room temperature.....	89
4.3.4	Integrated analysis and core state control.....	91
4.3.5	CLTE measurements at elevated temperatures .....	94
4.4	Volumetric heat capacity of unconventional reservoir rocks at elevated temperatures ....	98
4.4.1	Rock collection for studying volumetric heat capacity at elevated temperatures ...	98
4.4.2	Results of measurements for unconventional reservoir rocks .....	99
4.4.3	Equations that relate volumetric heat capacity to temperature for unconventional reservoir rocks .....	111
4.4.4	Analysis of volumetric heat capacity with temperature characteristic of unconventional reservoir rocks in comparison with other sedimentary rocks .....	111
4.5	Experimental investigations of thermal conductivity on rock cuttings and non-consolidated rocks at elevated temperatures.....	112
Chapter 5.	Conclusion .....	117
5.1	Summary.....	117
5.2	Conclusions.....	118
Bibliography	.....	121

## List of figures

<b>Figure 1.</b> DTC-300 instrument for measuring Thermal conductivity of rock samples at elevated temperatures.....	35
<b>Figure 2.</b> The precision of thermal conductivity measurements on technical glass K-8 with temperature, obtained with DTC-300 instrument.....	38
<b>Figure 3.</b> The precision of thermal conductivity measurements on marble with temperature, obtained with DTC-300 instrument.....	38
<b>Figure 4.</b> The precision of thermal conductivity measurements on plexiglass with temperature, obtained with DTC-300 instrument.....	39
<b>Figure 5.</b> The precision of thermal conductivity measurements on quartz with temperature, obtained with DTC-300 instrument.....	39
<b>Figure 6.</b> The precision of thermal conductivity measurements on titanium alloy VT-6 with temperature, obtained with DTC-300 instrument.....	40
<b>Figure 7.</b> The precision of thermal conductivity measurements on vespel with temperature, obtained with DTC-300 instrument.....	40
<b>Figure 8.</b> Dependence of accuracy of thermal conductivity measurements (DTC-300 instrument) on thermal conductivity values of studied materials (Table 4). ....	41
<b>Figure 9.</b> Influence of difference in rock sample thickness on the relative difference between thermal conductivity measured with DTC-300 and TCDS instruments at room temperature. $R$ is the correlation coefficient, $RMSE$ is the root mean square error.....	46
<b>Figure 10.</b> Thermal conductivity of marble samples with different diameters with the temperature. ....	47
<b>Figure 10a.</b> The dependence of thermal conductivity of marble samples on samples diameter. ....	47
<b>Figure 11.</b> Corrected thermal conductivity values of marble samples with different diameters within the temperature. ....	48
<b>Figure 12.</b> Main (a) and auxiliary equipment (b, c) used in the study; a - Quartz dilatometer with an installed core sample, b - Thermal Conductivity Scanner, c - HAWK pyrolysis instrument...56	56
<b>Figure 13.</b> Differential scanning calorimeter NETZSCH - DSC 214 Polyma. ....	58
<b>Figure 14.</b> Thermal conductivity decrease for rock samples from the Bazhenov and Abalak formations in the 30-300 °C temperature range. Different colors refer to different rock samples: ♦ – 1AB, ▲ – 2AB, ● – 5AB, ■ – 3BF, ■ – 4BF, ● – 5BF. ....	66
<b>Figure 15.</b> Curves drawn on a scatter diagram of average thermal conductivity change with temperature for rock samples from different formations: ♦ – Abalak formation, ● – Bazhenov formation, ■ – sample 3BF from the Bazhenov formation, - – correction for the Bazhenov	

formation, - – correction for the Abalak formation, - – correction for sample 3BF from the Bazhenov formation. ....	66
<b>Figure 16.</b> Changes in thermal conductivity for rock samples of the Golchikh and Abalak formations of oil field 2 with increasing temperature. Black dotted line - curve obtained by averaging thermal conductivity over all rock samples of the Golchih formation; brown dotted line - curve obtained by averaging thermal conductivity over all rock samples of the Abalak formation. ....	68
<b>Figure 17.</b> Relative change in thermal conductivity for rock samples from the Golchih and Abalak formations of oil field 2 with increasing temperature. Black dotted line - curve obtained by averaging the relative change in thermal conductivity for all rock samples of the Golchih formation; brown dotted line - curve obtained by averaging the relative change in thermal conductivity for all rock samples of the Abalak formation. ....	69
<b>Figure 18.</b> Changes in thermal conductivity for rock samples of Bazhenov formations of oil field 3 with increasing temperature.....	71
<b>Figure 19.</b> Relative change in thermal conductivity for rock samples from the Bazhenov formation of oil field 3 with increasing temperature. Black dotted line - curve obtained by averaging the relative change in thermal conductivity for all rock samples of the Bazhenov formation.....	71
<b>Figure 20.</b> Changes in thermal conductivity for rock samples of Bazhenov formations of oil field 4 with increasing temperature.....	72
<b>Figure 21.</b> Relative change in thermal conductivity for rock samples from the Bazhenov formation of oil field 4 with increasing temperature. Black dotted line - curve obtained by averaging the relative change in thermal conductivity for all rock samples of the Bazhenov formation.....	73
<b>Figure 22.</b> Curves drawn on the thermal conductivity-temperature scatter diagram for Mendym samples (■ – 1Md, ● – 2Md, ▲ – 3Md, ◆ – 4Md, ■ – 5Md, ● – 6Md, ● – 7Md, ● – 8Md, ▲ – 9Md, ● – 10Md) in the 30-300 °C temperature range. ....	75
<b>Figure 23.</b> Curves lines drawn on the thermal conductivity-temperature scatter diagram for Domanic samples (■ – 1Dm, ● – 2Dm, ▲ – 3Dm, ● – 4Dm, ● – 5Dm, ● – 6Dm, ◆ – 7Dm) in the 30-300 °C temperature range. ....	76
<b>Figure 24.</b> Curves lines drawn on the thermal conductivity-temperature scatter diagram for Sargaev samples (◆ – 1S, ■ – 2S, ▲ – 3S, ● – 4S) in the 30-300 °C temperature range.....	76
<b>Figure 25.</b> The curve drawn on the thermal conductivity-temperature scatter diagram for the Timan sample (Tm) in the 30-300 °C temperature range. ....	77
<b>Figure 26.</b> Curves drawn on the average thermal conductivity- temperature scatter diagram for lithotypes from different formations in the 30-300 °C temperature range. Different colors are	

related to different lithotypes: ● – dolomites (Mendym), ▲ – limestones (Mendym), ◆ – limestones (Domanic), ● – limestones (Sargaev), ▲ – sandstone (Timan), ■ – argillites (Domanic), ■ – clayey limestones (Mendym), ◆ – clayey limestones (Sargaev).....77

**Figure 27.** Curves drawn on the average thermal conductivity- temperature scatter diagram for different lithotypes from different formations (● – clayey limestones, ▲ – dolomites and sandstones, ■ – limestones and argillites, - - clayey limestones with correction, - - dolomites and sandstones with correction, - - limestones and argillites with correction) in the 30-300 °C temperature range. ....78

**Figure 28.** A Bazhenov sample before heating (a) and after heating to 300 °C (b).....79

**Figure 29.** Thermal conductivity values of Golchih and Abalak formations rocks measured with the DTC-300 instrument during heating and cooling.....81

**Figure 30.** Relative change in thermal conductivity for unconventional and other sedimentary rock samples with increasing temperature.....83

**Figure 31.** A synthetic sample of kerogen. ....84

**Figure 32.** Thermal conductivity of kerogen sample at elevated temperatures measured with DTC-300 instrument. ....84

**Figure 33.** Results of CLTE (measurement unit is  $10^{-6} \text{ K}^{-1}$ , the data are shown by red lines and numbers) and thermal conductivity (measurement unit is  $\text{W}/(\text{m}\cdot\text{K})$ , black line and numbers) measurements of BF core plugs at different directions to the bedding plane (a, c, e, g, i, k). The results of solving the optimization problem by the ellipse parameters method (blue lines) and the CLTE measurement results (red markers) are shown in corresponding figures b, d, f, h, j, l.....91

**Figure 34.** Correlation TC vs CLTE for core plugs from BF from 3 oil fields. ....92

**Figure 35.** Correlations density vs CLTE (parallel to bedding at temperature range 25-50 °C) (a), density vs TOC (b), and density vs TC (c) for core plugs from BF from 3 oil fields. ....92

**Figure 36.** Detailed profile of CLTE and pyrolysis data (red markers) for BF rocks from well 4 (c), well 5 (b) and well 1 (a). ....93

**Figure 37.** Correlation CLTE vs TOC for BF rocks form 3 wells.....94

**Figure 38.** CLTE variations with a temperature increase for core plugs from the BF (a) and the AF (b) (well 1).....95

**Figure 39.** CLTE values change with temperature for core plugs from the BF (wells 4, 5). ....95

**Figure 40.** CLTE variations with a temperature increase for core plugs from the BF (well 3)....96

**Figure 41.** CLTE variations with a temperature increase for core plugs from the GF and AF (well 2).....96

<b>Figure 42.</b> Variations of CLTE with a relative change of core plug mass after measurements at 300 °C for BF rocks (Samples №4, 5, 6, 7, 8, 10, 12-13, 15-23).....	97
<b>Figure 43.</b> Photo of sample №1 before (a) and after high-temperature measurements with a zoomed area of bitumen exudation (b). .....	97
<b>Figure 44.</b> The dependence of the density on temperature, calculated by the formula (15), for a sample from the studied collection of rocks, which has the maximum CLTE ( $\alpha = 15.9 \cdot 10^{-6} \text{ K}^{-1}$ ). .....	103
<b>Figure 45.</b> The dependence of the volumetric heat capacity on temperature for Bazhenov formation rock samples from oil field 1. ....	103
<b>Figure 46.</b> The dependence of the volumetric heat capacity on temperature for Abalak formation rock samples from oil field 1.....	104
<b>Figure 47.</b> The percentage of volumetric heat capacity increasing relatively to initial volumetric heat capacity ( $T = 25 \text{ }^\circ\text{C}$ ) for Bazhenov formation rocks. ....	104
<b>Figure 48.</b> The percentage of volumetric heat capacity increasing relatively to initial volumetric heat capacity ( $T = 25 \text{ }^\circ\text{C}$ ) for Abalak formation rocks.....	105
<b>Figure 49.</b> Experimental data on the change in the specific heat capacity of rock samples from the Golchih and Abalak formations (Oil field 2) with temperature increasing. The black dotted line is the curve obtained by averaging the specific heat capacity for all samples.....	106
<b>Figure 50.</b> Dependence of density on temperature for rock samples of the Golchih and Abalak formations (Oil field 2).....	107
<b>Figure 51.</b> The dependence of the volumetric heat capacity of the matrix for all rock samples of the Golchih and Abalak formations (Oil field 2) on temperature. The dashed line is the curve obtained by averaging the volumetric heat capacity of the matrix over all samples.....	108
<b>Figure 52.</b> Experimental data on the change in the specific heat capacity of rock samples of the Bazhenov formation with an increase in temperature. The black dotted line is the curve obtained by averaging the specific heat capacity for all samples.....	109
<b>Figure 53.</b> The dependence of the volumetric heat capacity, averaged over all rock samples of the Bazhenov formation (Oil field 4), on temperature. The dashed line is the curve obtained by averaging the volumetric heat capacity of all samples. ....	110
<b>Figure 54.</b> The percentage of volumetric heat capacity increasing relatively to initial volumetric heat capacity ( $T = 25 \text{ }^\circ\text{C}$ ) for Bazhenov formation and other sedimentary rocks.....	112
<b>Figure 55.</b> The results of determining the dependences of the thermal conductivity of the matrix on temperature from the results of measuring the thermal properties on rock cuttings. The	

equations show the average decreasing of thermal conductivity for the corresponding lithotype.

.....115

**Figure 56.** Comparison of the results of determining the dependences of the thermal conductivity of the matrix on temperature (according to the results of measurements on rock cuttings) with the results of determining the dependences of the thermal conductivity of rocks on temperature (according to the results of measurements on standard samples). The dashed lines represent the dependences obtained from the results of measurements on rock cuttings, the solid lines represent the dependences obtained from the results of measurements on standard rock samples. ....116

## List of tables

<b>Table 1.</b> Thermal conductivity of shales and experimental conditions of high-temperature measurements for different shale formations obtained from the literature. ....	27
<b>Table 2.</b> Summary of published CLTE studies of shales. ....	30
<b>Table 3.</b> Summary of published specific heat capacity studies of shales.....	31
<b>Table 4.</b> Accuracy of thermal conductivity measurements of standard samples on DTC-300 instrument at room temperature obtained with TCS and DTC-300 instrument measurements. ...	37
<b>Table 5.</b> Main technical characteristics of the calorimeter DSC NETZSCH 214 Polyma.....	58
<b>Table 6.</b> Number of unconventional reservoir rocks for studying thermal conductivity, CLTE, and VHC at elevated temperatures. ....	60
<b>Table 7.</b> The collection of studied rocks from Oil field 1. ....	61
<b>Table 8.</b> The collection of studied rocks from Oil field 2. ....	61
<b>Table 9.</b> The collection of studied rocks from Oil field 3. ....	62
<b>Table 10.</b> The collection of studied rocks from Oil field 4. ....	62
<b>Table 11.</b> The collection of studied rocks from Oil field 5. ....	63
<b>Table 12.</b> Results of thermal property measurements of rock samples from Bazhenov and Abalak formations at room temperature with a TCS before measurements at elevated temperatures. ....	64
<b>Table 13.</b> TCS measurements of thermal properties of Bazhenov and Abalak samples at room temperature after heating to 300 °C and subsequent cooling. ....	67
<b>Table 14.</b> Results of thermal property measurements of rock samples from Golchih and Abalak formations at room temperature with a TCS before measurements at elevated temperatures. ....	68
<b>Table 15.</b> TCS measurements of thermal properties of Golchih and Abalak samples at room temperature after heating to 300 °C and subsequent cooling. ....	69
<b>Table 16.</b> TCS measurements of thermal properties of Bazhenov formation samples at room temperature after heating to 300 °C and subsequent cooling. ....	70
<b>Table 17.</b> TCS measurements of thermal properties of Mendym, Domanic, Sargaev, and Timan samples at room temperature before measurements at high temperatures. ....	74
<b>Table 18.</b> TCS measurements of thermal properties after heating to 300 °C and subsequent cooling of Mendym, Domanic, Sargaev, and Timan samples. ....	79
<b>Table 19.</b> Equations which relate average thermal conductivity to temperature in the 30-300 °C temperature range for studied lithotypes from different formations. ....	79
<b>Table 20.</b> Changes in thermal properties of unconventional reservoir rocks from 5 oil fields before and after heating. ....	81
<b>Table 21.</b> Characteristics of studied rock samples from oil field 1. ....	85

<b>Table 22.</b> Characteristics of studied rock samples from oil field 2.....	85
<b>Table 23.</b> Characteristics of studied rock samples from oil field 3.....	86
<b>Table 24.</b> Results of CLTE, CLTE anisotropy coefficient, density, TOC and thermal properties measurements .....	88
<b>Table 25.</b> Characteristics of studied rock samples from oil field 1.....	98
<b>Table 26.</b> Characteristics of studied rock samples from oil field 2.....	98
<b>Table 27.</b> The results of measurements of the specific heat capacity of sample №1.....	100
<b>Table 28.</b> The results of measurements of the specific heat capacity of sample №3.....	100
<b>Table 29.</b> The results of measurements of the specific heat capacity of sample №4.....	100
<b>Table 30.</b> The results of measurements of the specific heat capacity of sample №5.....	100
<b>Table 31.</b> The results of measurements of the specific heat capacity of sample №6.....	100
<b>Table 32.</b> The results of measurements of the specific heat capacity of sample №7.....	101
<b>Table 33.</b> The results of measurements of the specific heat capacity of sample №8.....	101
<b>Table 34.</b> The results of measurements of the specific heat capacity of sample №9.....	101
<b>Table 35.</b> The results of measurements of the specific heat capacity of sample №10.....	101
<b>Table 36.</b> The results of measurements of the specific heat capacity of sample №11.....	102
<b>Table 37.</b> Density measurement results by the hydrostatic weighing method.....	102
<b>Table 38.</b> The density of the studied rock samples of the Golchih and Abalak formations.....	106
<b>Table 39.</b> Density of the studied rock samples of the Bazhenov Formation.. <b>Ошибка! Закладка не определена.</b>	
<b>Table 40.</b> Equations of VHC vs temperature for studied unconventional reservoir rocks.....	111
<b>Table 41.</b> The results of determining the thermal conductivity of the matrix (at 25, 50, and 75 °C) and the volumetric heat capacity of the matrix (at 25 °C) based on the results of measurements on rock-cuttings. ....	<b>Ошибка! Закладка не определена.</b>
<b>Table 42.</b> The results of determining the dependences of the thermal conductivity of the matrix on temperature from the results of measurements on rock cuttings.....	117

## **Chapter 1. Introduction**

### **1.1 The necessity of experimental data on thermal properties at elevated temperatures for the solution of actual problems in oil&gas science and industry**

Experimental data on the thermal properties of hydrocarbon reservoirs and surrounding formations at elevated temperatures are important for a variety of purposes: determining heat flow density, designing and optimizing thermal methods of enhanced oil recovery (EOR), basin and petroleum system modeling, exploitation of geothermal reservoirs and design of radioactive waste disposal. However, there is an acute shortage of such data at present, particularly for unconventional reservoir rocks. Modeling of sedimentary basins and petroleum systems using any basin simulator requires data on the deep heat flow and thermal rock properties (thermal conductivity, specific heat or volume) and reservoir properties at elevated temperatures (Hantschel and Kauerauf, 2009). However, the experimental work of recent years established the serious problems to obtain baseline data on thermal properties of rocks and heat flow, reducing the reliability of basin modeling.

Nowadays equipment (e.g. thermal conductivity scanner) is already developed for thermal properties measurements on cores at room temperatures. The optical scanning method and instruments were developed for non-contact, non-destructive measurements of thermal conductivity and thermal diffusivity of rocks and minerals. This technology allowed us to provide economical, fast, detailed, and reliable data of thermal conductivity, thermal diffusivity, and volumetric heat capacity measured on thousands of cores from many scientific boreholes (Popov et al, 2016b). However, there are disadvantages of methodologies of thermal properties measurements at elevated temperature, including thermal conductivity, coefficient of linear thermal expansion, and volumetric heat capacity.

A number of researchers have reported the results of experimental investigation of thermal conductivity of various rocks and minerals at high temperatures and pressures (Abdulagatova et al., 2009; Vosteen and Schellschmidt, 2003; Clauser, 2006; Miklashevskiy et al., 2006; Ramazanov and Magdiev, 2014). Experiments to investigate the simultaneous influence of high temperature and high pressure are extremely hard to arrange, so an “additive” approach is normally used where the dependencies “thermal conductivity vs temperature” and “thermal conductivity vs pressure” are studied separately (Seipold, 1998; Clauser and Huenges, 1995). The studies have shown that thermal conductivity is most dependent on temperature (Clauser, 2006; Vosteen and Schellschmidt, 2003). Experimental data on thermal conductivity of hydrocarbon reservoirs and

surrounding formations at elevated temperatures are important for determining heat flow density (Sekiguchi, 1984), modeling basin and petroleum systems (Hantschel and Kauerauf, 2009), and developing and improving thermal methods of enhanced oil recovery (EOR), such as steam-assisted-gravity-drainage (Irani and Cokar, 2016). Data on the thermal conductivity of rocks are also necessary for calculating heat losses from underground steam and hot water pipes including those used in thermal EOR, and for exploitation of geothermal reservoirs (Somerton, 1992; Clauser, 2006; Khan and Maqsood, 2007). Heat transfer calculations have also become increasingly important in the analysis of in-situ combustion and underground nuclear explosions (Somerton and Boozer, 1960).

Estimation of thermal conductivity of rocks with increasing temperature is also important for the design of radioactive waste disposal where heat generation induces thermal stresses that influence the stability of disposal (Gilliam and Morgan, 1987; Durham and Abey, 1981; Garitte et al, 2014). The thermal conductivity of rock samples decreases at elevated temperatures mainly due to corresponding changes in the thermal conductivity of the rock-forming minerals. Changes in mineral composition, pore structure, and propagation of microcracks prompted by heating of the rock sample often cause an additional reduction of thermal conductivity. The complexity of the heat transfer mechanism in rocks makes it difficult to correctly calculate the thermal conductivity of porous materials from theoretical modeling of the effective thermal conductivity of rocks (Clauser, 2006; Sun et al, 2016). This makes it important to use representative experimental data concerning thermal properties in simulations, as uncertainties about thermal conductivity have a significant impact on modeling results (Popov et al, 2013).

Extensive studies of the thermal properties of various types of rocks have been carried out. But the results obtained by different measurement techniques often contain systematic errors due to poor contact with the studied rock sample (Merriman et al, 2017). Methods of thermal core logging exist, which allow Kukkonen and Suppala, 1999 to measure the thermal conductivity of rocks in-situ, but they are not widely used due to significant duration of the required measurements, insufficient radius of influence, and difficulties in analyzing the influence of borehole fluid (Miklashevsky et al., 2006; Novikov et al., 2008).

In general, according to numerous data, unconventional reservoir formations have a very complex mineral composition, different and rather complex textures. Physical parameters of such rocks, necessary for the numerical simulations can hardly be estimated by analogy, or determined by calculation, based on the parameters of the rocks included in the composition components. To obtain the initial data, systematic laboratory petrophysical research should be obtained (Yudin et al, 2015). Shale rocks are more sensitive to temperature increase than other rocks due to their

specific physical and mechanical properties. The organic matter is pyrolyzed at high temperatures, which increases the porosity and propagation of cracks in rock samples (Wang et al, 2018). The thermal conductivity of shales is influenced by many factors, including composition, porosity, anisotropy, temperature, and pressure (Gillian and Morgan, 1987; Ilozobhie et al, 2016). As mentioned above, the experimental procedure for thermal conductivity measurements, which give simultaneous consideration to temperature and pressure, is very complicated and only a few such experiments have been carried out (Abdulagatova et al., 2009; Durham and Abey, 1981; Horai and Susaki, 1989; Miklashevsky et al., 2006; Smith, 1978; Prats and O'Brien, 1975; DuBow et al., 1980). It is also difficult to ensure reliable metrology in such experiments.

Information about the coefficient of linear thermal expansion (CLTE) of rock samples is necessary for the estimation of the thermal stress of rock mass that is caused by the thermal expansion of rocks. Knowledge of CLTE allows us to predict how rocks will behave under thermal stress (Siratovich et al., 2015) and to establish depth intervals with possible borehole wall collapse for prevention of rock drilling equipment damage (Wong and Brace, 1979). CLTE estimation is important in designing repositories for radioactive wastes for safety control as well (Heard and Page, 1982; Delage, 2015) as the long-term influence of high temperatures can change mechanical characteristics of shales (Smith, 1978). Another application of the thermal expansion data is related to cap rock integrity assessment for thermal EOR methods (Chekhonin et al., 2012).

A lot of factors can influence the thermal expansion of rocks: temperature, pressure, mineralogical composition, crystal orientation, texture, porosity, pore fluid properties, and micro-fracturing (Siegesmund, 2000; Huotari and Kukkonen, 2004). One of the reasons for rocks damage is different thermal expansion of rock components (minerals, pore fluids). As thermal expansion coefficients are anisotropic and different for rock-forming minerals, it results in stress accumulation at grain boundaries of different minerals. The minerals with the largest thermal expansion have the strongest influence on the strain of the studied rock sample as a whole (Harvey, 1967; Somerton, 1992; Pitts, 2017). Exceeding breaking points at the contact of mineral grains can lead to rocks disruption. The thermal expansion causes cracks propagation between mineral grains that increases porosity, and lead to changes in elastic moduli of rocks and rock stresses (Wong and Brace, 1979; Bauer and Handin, 1983; Cooper and Simmons, 1977).

Phase change reactions in minerals that occurred due to high temperatures can cause induced thermal stresses (Somerton, 1992). As coefficients of linear and volumetric strain are often given for constant volume and pressure systems, thermal cycling cracking during thermal expansion at atmospheric pressure occurs (Wong and Brace, 1979; Cooper and Simmons, 1977).

In general, the published data on rock thermal expansion are not numerous and involve a narrow range of minerals and rocks. Previously published CLTE data often do not provide the necessary quality of CLTE measurements for oil-rich shales. Particularly, the CLTE measurements with different orientations of principal axes of CLTE were previously performed only on several shale samples drilled from full-size core samples that cannot allow accounting for the influence of essential heterogeneity of organic-rich shales on the quality of rock anisotropy characterization (Wong and Brace, 1979). At the same time, accounting for significant heterogeneity and anisotropy of oil-rich shales is important for studying correlations of CLTE with other physical properties of rocks to provide all measurements on the same rock sample that allows us to exclude heterogeneity

Very often, CLTE anisotropy is not considered in previous publications at all (Popov et al, 2008). However, high anisotropy of shales and unstable CLTE behavior with temperature can influence the thermal stress of rocks and stability of formation (Grebowicz, 2014).

In most publications, experimental data on CLTE is given as average values within wide temperature ranges (50 °C and more), while results of differential CLTE measurements with a heating interval of 20-250 °C were not published previously, although detailed information on CLTE vs temperature variations for different temperature ranges is necessary for rock stress modeling (Yanchenko, 2009).

Volumetric heat capacity as one of the thermal properties of rocks and other materials determines the dynamics of the thermal regime of a heating or cooling medium. The volumetric heat capacity  $C$  is related to the thermal conductivity and the thermal diffusivity by the ratio  $C = \lambda/a$ . The volumetric heat capacity is related to the specific heat  $c$  and the density of the medium by the ratio  $C = c \cdot \rho$ . Volumetric heat capacity is one of the initial parameters, data on which are required when calculating the characteristics of dynamic heat transfer processes in rock massifs. In geological and geophysical work, such calculations are necessary, for example, in the development of thermal methods for the production of high-viscosity oils, modeling the thermal evolution of sedimentary basins and oil and gas systems, studying paleoclimatic processes, and in many other cases.

In the practice of geological and geophysical work, another common approach is to determine the volumetric heat capacity from data on thermal conductivity and thermal diffusivity of rocks, obtained independently from the results of measurements of these properties on different instruments and different rock samples.

In the absence of experimental data, the approximate value of the heat capacity can be obtained by calculation. The volumetric heat capacity can be calculated using the formula  $C = f_m \cdot$

$c_m \cdot \rho_m + f_o \cdot c_o \cdot \rho_o + f_w \cdot c_w \cdot \rho_w$ , where  $f$  is the volume fraction of a substance,  $c$  is the specific heat capacity of a substance,  $m$  is a mineral substance,  $o$  is an organic matter,  $w$  - water (Hillel, 1980). However, the results obtained in this way in most cases cannot be assessed as accurate because it is not always possible to accurately determine the volume fraction of the substance contained in the rock. The presented simple analytical and empirical formulas for calculating the specific heat capacity of rocks can be used only as a first approximation for qualitative estimates of its value.

## 1.2 Statement of the problem

Preliminary studies that have already been performed provide a basis for the measurements of thermal properties of core samples at reservoir temperatures. Nevertheless, nowadays there are problems that relate to:

- number of experimental data on thermal conductivity, CLTE with temperature is not representative for unconventional reservoir rocks;
- experimental data on VHC is absent for unconventional reservoir rocks;
- measurement techniques often contain systematic errors;
- the absence of metrological analysis;
- lack of anisotropy analysis for thermal conductivity and CLTE of unconventional reservoir rocks;
- lack of correlation analysis of CLTE with other physical properties;
- absence of measurements of thermal conductivity of non-consolidated rocks at elevated temperatures;
- thermal properties of unconventional reservoir rocks at elevated temperatures can not be estimated analytically due to complex mineral composition and texture.

## 1.3 Goals and objectives

The disadvantages of methods for measuring thermal properties of unconventional reservoir rocks at elevated temperatures and nowadays problems mentioned above encouraged to:

- develop new methodologies for determining thermal properties of unconventional reservoir rocks at elevated temperatures;
- get representative data on thermal properties of unconventional reservoir rocks at elevated temperatures;
- provide metrological analysis of measurements;

- provide anisotropy analysis of CLTE for unconventional reservoir rocks;
- provide correlation analysis for thermal conductivity and CLTE;
- provide measurements of thermal conductivity of particles of solid material at elevated temperatures.

New methodologies should be used on the basis of reliable and non-contact measurement techniques as unconventional reservoir rocks are enough fragile due to numerous fractures. One of the equipment that can provide such measurements is the Thermal Conductivity Scanner (TCS) (Popov et al., 2016). The combination of TCS with equipment for measurements of thermal properties at elevated temperatures gives the possibility to exclude nowadays disadvantages and problems. Lack of anisotropy analysis is also can be excluded by combination with TCS, as it allows us to measure core samples in different directions to the core axis. It also helps to compare thermal conductivity and CLTE anisotropy for unconventional reservoir rocks that was not provided before. Also, it gives the possibility to find a new correlation of thermal conductivity with other properties such as CLTE. It also can be the basis for measurements of the thermal conductivity of rock particles of solid material at elevated temperatures.

#### **1.4 Outline of the Thesis**

For obtaining goals mentioned above it is necessary to carry out the following steps:

- to develop a new approach to the measurement of rock thermal properties at elevated temperatures for unconventional reservoir rocks and non-consolidated rocks;
- to apply the approach to organic-rich rocks from unconventional reservoirs and improve the quality of thermal conductivity measurements;
- to determine the degree of CLTE anisotropy and range of CLTE values for unconventional reservoir rocks;
- to compare directions of CLTE anisotropy main axes with the direction of the main axes of thermal conductivity tensor;
- to analyze new correlations between CLTE, thermal conductivity, TOC, and density for unconventional reservoir rocks;
- to analyze temperature behavior of CLTE of unconventional reservoir rocks;
- to develop a new methodology of VHC measurements and establish new equations which relate VHC to temperature for unconventional reservoir rocks.

## **Chapter 2. Literature review and the current state of the problem**

### **2.1 Thermal conductivity dependence of unconventional reservoirs at elevated temperatures –current state of art**

The investigation of thermal properties of shales at high temperatures has recently acquired new importance (Grebowicz, 2014) but experimental data on such properties remain scant (Jha et al, 2016). The thermal conductivity of four rock samples from the Green River oil field at high temperatures (40-400 °C) and high pressure was studied by DuBow et al. (1976) using the comparative method. It was observed that the effect of pressure on thermal conductivity only becomes significant at high temperatures (above 300-400 °C). In contrast to other studies, the experimental data showed that the thermal conductivity of shales remains steady or increases with increasing temperature. This is because, when oil shales approach retorting temperatures (when they are heated to 200-400 °C) the role of solid-fluid and fluid-fluid heat transfer mechanisms increases and, at relatively low porosities, may predominate over thermal transfer properties. Analysis of shale anisotropy has only rarely been carried out (Popov et al, 2017; Yu et al, 2015; Wang et al, 2018). Unfortunately, even in these rare investigations, thermal anisotropy was estimated from a comparison of measurement results obtained for different rock samples, which fails to exclude the influence of rock heterogeneity on the anisotropy estimation. The heterogeneity of the studied rock samples and their changes as a result of heating was not taken into account in the above-mentioned experiments.

Sokolova et al. (1986) studied thermal conductivity of three samples of bituminous argillites from Bazhenov formation (West Siberia, Russia) with a dynamic calorimeter using an IT- $\lambda$ -400 instrument and observed abnormally low thermal conductivity (1.1-1.3 W/(m·K)) within a temperature range of 25-200 °C. A very weak reduction of thermal conductivity of shale rocks with temperature (10% at 100 °C) was observed in comparison with other sedimentary rock samples. Unfortunately, the orientation of the studied rock samples relative to the heat flow direction was not recorded and analysis of rock heterogeneity and anisotropy was not carried out, although the high thermal heterogeneity and anisotropy of shale rocks are generally acknowledged (Popov et al., 2016a; Popov et al., 2017).

Another investigation of thermal conductivity, both parallel and perpendicular to the bedding plane, for two anisotropic shales (at the Liaoning Fushun open-cast mine in China), was carried out by Wang et al. (2018) using a Netzsch LFA laser thermal conductivity analyzer at temperatures ranging from room temperature to 600 °C. The authors concluded that the main

reason for the change in the thermal characteristics of the shales and their anisotropy were thermal cracks caused by the temperature increase. Numerous cracks appear parallel to bedding when the temperature increases up to 400 °C that leads to increasing the anisotropy coefficient of both thermal conductivity and some other physical parameters. However, as in the other experiments mentioned above, the number of studied rock samples dealt with by Wang et al. (2018) is not representative and the procedure of core sampling is not described.

Yu et al. (2015) measured thermal conductivity of six oil shale samples (Fushun, China) parallel and perpendicular to bedding using a Netzsch LFA laser thermal conductivity analyzer in a temperature range of 25-300 °C. The authors found a weak decrease of thermal conductivity with temperature (about 10% at 100 °C) and a high value of the rock thermal anisotropy coefficient (1.8), which remained unchanged with temperature. The variations of the thermal conductivity component parallel to bedding with temperature are 1.35-1.85 W/(m·K) and variations perpendicular to bedding are 0.75-1.00 W/(m·K). The organic content of the studied rock samples was not analyzed and the core sampling procedure was not described.

Jha et al. (2016) measured the thermal conductivity of Jhiri shale (India) using the single guarded hot parallel plate method (ASTM C177-13, 2013). Heating to 200 °C causes a marked reduction of thermal conductivity (by 32%), possibly due to the evaporation of moisture from the pores. Thermal conductivity changes by 10% at temperature range 200-400 °C that can be related to pore volume increasing of the studied rock sample. At high temperatures (400-700 °C) thermal conductivity changes only by (2-3%) due to, probably, ductile behavior of rock samples at such high temperatures. No information is provided about the orientation of the rock samples, their anisotropy, heterogeneity, and organic content.

Gilliam and Morgan (1987) studied thermal conductivity variations within a temperature range of 25-200 °C using the comparative method for Devonian, Pierre, and Green River formations and established a conductivity range of 0.68-1.09 W/(m·K). The authors noted that variables, which ought to be considered, are temperature, pressure, rock composition, and anisotropy of thermal conductivity in the rocks (not all of these were considered in the studies).

Key findings of the previous publications are summarized in *Table 1* to (1) show ranges of thermal conductivity variations of shales in different temperature intervals, and (2) to present information about the experimental procedures used for different shale formations. It can be seen that samples from different shale formations have a broad range of thermal conductivity (0.25-4.36 W/(m·K)). Specific thermal conductivity behavior of shales at high temperatures can be seen, including a weak decrease of thermal conductivity (2-10%) at 100 °C in comparison with other sedimentary rock samples (about 10-15%, according to Popov et al. (2013)). The publications

show that thermal conductivity of shales at high temperatures depends on many factors, including orientation of the core sample relative to the direction of heat flow, temperature range, organic content in core samples, and the environment in which experiments are performed (air, nitrogen, argon, etc.).

Orientation of the shale samples relative to the direction of heat flow in measurements using the divided-bar technique (Popov et al., 2016b) has a major impact on thermal conductivity values since most of the shale samples have a high degree of anisotropy. Thermal conductivity measured parallel to bedding is normally 30-50% higher than thermal conductivity measured perpendicular to bedding (Gilliam and Morgan, 1987; Nottenburg et al., 1978; Rajeshwar and DuBow, 1980; Popov et al., 2016a).

Different thermal conductivity of shales in different temperature ranges can be explained by the specific nature of the decomposition of organic matter at high temperatures (Rajeshwar and DuBow, 1980). A slight decrease of thermal conductivity with temperature is observed in most shales (Rajeshwar and DuBow, 1980; Sokolova et al., 1986; Nottenburg et al., 1978; Gilliam and Morgan, 1987). However, in some shales, thermal conductivity behavior is essentially related to a particular temperature range. At 25-200 °C free and bound water loss is observed (Wang et al., 2018), at 200-400 °C there is loss of mineral water and volatile components (Wang et al., 2018), at 400-600 °C organic matter decomposes (Wang et al., 2018; Rajeshwar et al., 1980) and cracks appear (Jha et al., 2016). The influence of kerogen decomposition on thermal conductivity is questionable as the degree of kerogen decomposition depends on the length of time during which the high temperature is maintained. For example, 90% kerogen decomposition required 100 hours at a temperature of 350 °C (Prats and O'Brien, 1975).

The results of experiments have shown that pressure has only a small effect on the thermal conductivity of shales in a temperature range of 25-400 °C. For Conasauga formation the thermal conductivity of shales at the initial temperature increased by 2% with a pressure increase from 2.5 MPa to 10 MPa (Smith, 1978). For shale samples from the Green River formation, thermal conductivity also increased by 2% with pressure increase from 0.7 MPa to 12 MPa (Prats and O'Brien, 1975). However, pressure increase from 0.8 MPa to 4.1 MPa at high temperatures of 400-600 °C was shown to increase the thermal conductivity of shales much more significantly, by 10-20 % (DuBow et al., 1980).

The degree of reduction in thermal conductivity is related to the percentage of organic content in shale samples. It was shown for the Green River formation that the dependence of thermal conductivity of shale samples with various oil yields (7-82 gal/t) on temperature is weak.

However, an increase in oil yield in a shale sample is associated with a lower decrease in thermal conductivity as the temperature rises (Rajeshwar et al., 1980).

The thermal behavior of oil shales was observed to be sensitive to the atmosphere surrounding the sample during measurements. Differential thermal analysis (DTA) carried out on shale samples from the Green River formation showed the difference in the thermal behavior of shales in air and inert atmosphere (nitrogen) when rock sample temperature exceeds 300 °C. Thermal decomposition of kerogen was observed at two DTA peaks (440 and 500 °C) in the presence of air and one DTA peak (500 °C) in the presence of nitrogen (Rajeshwar et al., 1979). Similar thermal behavior was observed for samples from the Green River, Kentucky, and Michigan formations using differential scanning analysis. Exotherms observed in the range 300-500 °C are related to oxidation effects and decomposition of kerogen. Decomposition of organic matter in shale in an inert atmosphere occurred in a temperature range of 400-500 °C (Rajeshwar et al., 1980).

**Table 1.** Thermal conductivity of shales and experimental conditions of high-temperature measurements for different shale formations obtained from the literature.

Literature reference	Shale formation	Heat flow direction relative to the bedding plane	Thermal conductivity range, W/(m·K)	Temperature range, °C	Atmosphere	Number of studied samples	Oil yield, g/t*	Measurement technique	Metrological control of measurement quality
Prats and O'Brien, 1975	Green River, US	Parallel	0.44-1.82	25-400	Nitrogen	5	0-35	Transient line heat-source (probe) method	Tested on pyrex
Smith, 1978	Conasauga, US	30°/40°/45°	1.00-2.80	55-400	Nitrogen	5	Not mentioned	Comparator / guarded hot plate method	Tested on pyroceram, average error-2.6%
Nottenburg et al., 1978	Green River, US	Parallel	0.90-1.50	25-350	Inert gas	3	6-79	Comparator	Tested on pyroceram (standard deviation (STD) = 5%) and pyrex (STD = 6%)
		Perpendicular	0.25-1.75			4			
DuBow et al., 1980	Green River, US	Parallel	0.40-1.70	35-430	Air	5	21.6-47.9	Comparator	Tested on pyrex (STD = 4%)
Rajeshwar et al., 1980	Kentucky, US	Parallel	0.80-1.00	25-350	Nitrogen	1	52	Comparator	Tested on pyroceram (STD = 5%) and pyrex (STD = 6%)
	Michigan, US					1	28		
	Utah, US					11	7-82		
	Wyoming, US					3	18-40		
Sokolova et al., 1986	Bazhenov, Russia	Not mentioned	0.90-1.60	25-200	Air	3	Not mentioned	Comparator	Not mentioned
Gilliam and Morgan, 1987	Devonian, US	Parallel	0.73-1.09	25-200	Not mentioned	19	Not mentioned	Comparator	Tested on pyrex
	Pierre, US		0.68-1.01			4			
	Green River, US		1.00-1.45			2			
Yu et al., 2015	Fushun, China	Parallel	1.35-1.84	25-300	Air	3	Not mentioned	Laser analyzer	Not mentioned
		Perpendicular	0.75-1.00			3			
Jha et al., 2016	Jhiri, India	Not mentioned	1.77-4.36	25-900	Air	1	Not mentioned	Guarded hot plate method	Tested on mild steel and asbestos (uncertainty** = 6%)
Wang et al., 2018	Fushun, China	Parallel	0.70-1.89	20-600	Argon	1	Not mentioned	Laser analyzer	Not mentioned
		Perpendicular	0.25-0.73	20-600		1	Not mentioned		

\*g/t – gallons per ton; \*\* – uncertainty is based on an estimated accounting for accuracy and precision.

## 2.2 Coefficient of linear thermal expansion at elevated temperatures – current state of art

The experimental data on CLTE of shales with different orientations of rock samples relatively to bedding plane and within a wide temperature range (up to 800 °C) were published earlier. The data demonstrate that CLTE of shales increases with temperature, but sometimes CLTE stops its increasing within a particular temperature range. For example, for Devonian formation (USA) some shale samples went deformation above 200 °C, and CLTE started to decrease (Gilliam and Morgan, 1987). Such deformation is explained by the collapse of contained clays that can have a reduction of the spacing between platelets (Gilliam and Morgan, 1987). Similar oil-rich shale behavior was observed for Fushun formation (China) and Devonian formation (US) where CLTE decrease began at temperature 60 °C and 430 °C correspondingly (Gilliam and Morgan, 1987; Yu et al., 2015). These experimental data show the complicated character of CLTE variations of shales with temperature. The previous experimental data show a wide range of CLTE variations when a CLTE component parallel to bedding varies within a range of  $(8-80) \cdot 10^{-6} \text{ K}^{-1}$ , a CLTE component perpendicular to bedding varies within a range of  $(6-350) \cdot 10^{-6} \text{ K}^{-1}$ , and CLTE component inclined by 45° to the bedding plane varies within a range of  $(40-200) \cdot 10^{-6} \text{ K}^{-1}$  at temperature range (25-800 °C) (Smith, 1978; Gilliam and Morgan, 1987; Yu et al., 2015; MacGillivray and Dusseault, 1998). For Queenston and Mancos formations, a study of CLTE anisotropy coefficient of shales was performed on samples with orientation parallel, perpendicular, and 45° to bedding within a temperature range 25-75 °C when the CLTE anisotropy coefficient values were found to be 1.04-1.29 for Queenston shales and 1.04-1.71 for Mancos shale (MacGillivray and Dusseault, 1998). Experiments on CLTE variations of shales with different heating rates, organic matter content, and orientations showed that:

- the heating rate has a little effect on thermal rock expansion;
- organic matter content has no effect on CLTE behavior with temperature before kerogen starts decomposing;
- perpendicularly oriented shale samples have the largest CLTE values (Duvall et al., 1983).

The previous results of CLTE measurements on shales and characteristics of the experimental procedure for different shale formations are shown in *Table 2*.

An effect of oil grade on thermal expansion was observed for the Anvil Points Mine shale samples cut at a different orientation to bedding (Duvall et al., 1983). An increase in the grade of oil shale leads to thermal expansion increase within a temperature range of 350-450 °C when decomposition of kerogen occurs. Within a temperature range of 100-200 °C, the effect of oil grade was observed only for samples cut perpendicular to bedding.

Shale samples have a high degree of thermal anisotropy (Popov et al., 2016a); therefore studying CLTE anisotropy is important for such samples. However, investigation of CLTE anisotropy of rocks and rock-forming minerals was previously provided rarely: for clay minerals (McKinstry, 1965), dolomitic marbles (Luque et al., 2011), sandstones (Zhou et al., 2016), and Mancos and Queenstone shales (MacGillivray and Dusseault, 1998). Detection of main axes direction of CLTE anisotropy for shale samples was not performed previously according to our analysis of publications, except our previous study (Gabova et al., 2017).

**Table 2.** Summary of published CLTE studies of shales.

Shale formation	Temperature range, °C	Pressure, MPa	Number of samples	Bedding orientation	CLTE range, $10^{-6} \text{ K}^{-1}$	Atmosphere	CLTE Anisotropy	Measurement technique	Presence of CLTE standards for testing, description of metrology	Literature
Conasauga	25-400	No pressure	4	parallel	8-13	—	—	NETZSCH 402E dilatometer	Borosilicate glass, measurement error $\pm 1.2\%$	Smith, 1978
			4	perpendicular	6-16					
Anvil Points Mine	25-800	No pressure	3	parallel	20-80	Nitrogen	?	In-house*	$\pm 40\%^{**}$ , no information on standards and metrology	Duvall et al., 1983
			3	perpendicular	50-350				$\pm 12\%^{**}$ , no information on standards and metrology	
			3	45°	40-200				$\pm 30\%^{**}$ , no information on standards and metrology	
Devonian	25-300	No pressure	4	perpendicular	9-325	Nitrogen	—	NETZSCH 402E dilatometer	Vacromium reference material, no information on metrology	Gilliam and Morgan, 1987
Queenstone	25-75	0-13.8 MPa	4	axial	10.1-15.3	—	1.0-1.5	Waterloo TE Cell	Aluminum sample, no information on metrology	MacGillivray and Dusseault, 1998
Mancos	25-75	0-7 MPa	4	diametric	9.6-11.9					
			3	axial	16-22					
Green River	25-800	No pressure	3	axial	16-22	Nitrogen	?	Thermomechanical Analyzer 2490 model	—	Grebowicz, 2014
			3	diametric	13.7-15.4					
Fushun	25-300	No pressure	1	parallel	100	—	1.7	NETZSCH dilatometer	—	Yu et al., 2015
			1	perpendicular	3500					
Bazhenov	25-300	No pressure	3	parallel	14	Air	1.2-2.2	Quartz dilatometer	Precision not more than 4%, absolute error $1.8 \cdot 10^{-7} \text{ K}^{-1}$	Gabova et al., 2017
			3	perpendicular	23.6					
Bazhenov	25-300	No pressure	4	parallel	4.4-22.8	Air	1.2-2.2	Quartz dilatometer	Precision not more than 4%, absolute error $1.8 \cdot 10^{-7} \text{ K}^{-1}$	Gabova et al., 2017
			5	perpendicular	14.4-143.0					

Remarks:

Dash (—) means the absence of corresponding information in the literature source.

Question mark (?) means that anisotropic behavior was observed, but no values are presented.

\*Setup was designed and built in the laboratory of the Department of Metallurgy and Metallurgical Engineering, University of Utah.

\*\* Values calculated from the error bars shown in graphs representing the maximum and minimum values of the relative linear thermal expansion values observed in the temperature range 25-300 °C.

### 2.3 Volumetric heat capacity at elevated temperatures – current state of art

The volumetric heat capacity of rocks depends on the volumetric heat capacity of the components - the mineral matrix, pore fluid, organic matter, as well as the temperature of the rocks. The volumetric heat capacity of rock-forming minerals varies in the range of 1.8 - 2.6 MJ/(m<sup>3</sup>·K). For water, the volumetric heat capacity is 4.19 MJ/(m<sup>3</sup>·K), for oil - 1.3-1.7 MJ/(m<sup>3</sup>·K), for air - 0.001 MJ/(m<sup>3</sup>·K)) (Dobrynin et al., 2004).

The previous results of specific heat capacity measurements on shales and characteristics of the experimental procedure for different shale formations are shown in *Table 3*. Gilliam and Morgan (1987) studied the specific heat capacity of shale formations with a differential scanning calorimeter. For Devonian formation slight decrease of specific heat capacity at 200 °C is observed. The average percent of specific heat capacity increasing at temperature range 25-200 °C is 40% for Devonian shale formation, 55% - for Pierre shale formation, 50 % - for Green River shale formation. Investigations of Kendyrylyk and Shubarkol shale formations provided by Kasenov et al. (2016) showed that specific heat capacity increases more than by 100% at temperature range 25-200 °C. Investigations of specific heat capacity for Baltic oil shale showed that increasing kerogen content increases the value of heat capacity. The average percent of specific heat capacity increasing at temperature range 0-350 °C is 90%. Rajeshwar and DuBow (1980) also studied the specific heat capacity of shale formations with differential scanning calorimeter. The average percent of specific heat capacity increasing at temperature range 100-350 °C is 50% for Michigan shale, 20% - for Kentucky shale. Smith (1978) studied 5 samples from Conasauga shale formations that showed that the average percent of specific heat capacity increasing at temperature range 20-400 °C is 35%. Somerton (1992) studied the specific heat capacity of 1 shale sample with a Bunsen-type calorimeter. The average percent of specific heat capacity increasing at temperature range 25-350 °C is 48%. Determination of volumetric heat capacity for shales is not presented in publications, only analytical solutions can be found.

**Table 3.** Summary of published specific heat capacity studies of shales.

Literature reference	Shale formation	Specific heat capacity range, J/(kg·K)	Temperature range, °C	Number of studied samples	Measurement technique
Gilliam and Morgan, 1987	Devonian, US	840-1465	25-200	14	differential scanning calorimeter
	Pierre, US	1047-1675		3	
	Green River, US	1047-1570		1	
	Kendyrylyk,	400-1600	25-200	1	

Kasenov et al., 2016	Kazakhstan				IT-S-400 calorimeter
	Shubarkol, Kazakhstan	600-1400		1	
Savest and Oja, 2013	Baltic shale	1000-1900	0-350	1	aqueous calorimeter
Rajeshwar and DuBow, 1980	Michigan shale	840-1260	100-350	1	differential scanning calorimeter
	Kentucky shale	1050-1260		1	
Smith, 1978	Conasauga shale	800-1200	20-400	5	differential scanning calorimeter
Somerton, 1992	Shale	800-1180	25-530	1	Bunsen-type calorimeter

## 2.4 Thermal conductivity measurements on rock cuttings and unconsolidated rocks at elevated temperatures – current state of art

Nowadays, there are a few methods of measuring the thermal properties of particles of solid materials at elevated temperatures. One of them is a divided-bar method, which allows us to measure the thermal conductivity of solid material at different temperatures in a specified temperature range on samples with fixed dimensions, cylindrical shape, and parallel-sided surfaces (Lemenager et al., 2018). Another method consists of mixing particles of solid material with water, determining the volume fractions of particles of solid material and water in the mixture, measuring the effective thermal conductivity of the mixture of particles of solid material with water at different temperatures using the linear source method, determining the thermal conductivity of particles of solid material at different temperatures using a ratio (Lichtenecker model) describing the effective thermal conductivity of a mixture of solid particles with water (Pribnow and Sass, 1995). The methods mentioned above have the following disadvantages:

- measurements are carried out on solid samples that can withstand hold-down pressure (without any failure) required to reduce the thermal resistance on the surfaces of the sample under study;
- the effect of free convection in a liquid mixed with particles of a solid material before measurements during heating by a heat source in the process of measurements on the results of measurements of the thermal conductivity of the mixture; uncontrolled convection of a liquid introduces significant distortions in the measurement results, which are obtained using a formula that does not take into account the effect of convection of a liquid;

- the temperature range in which measurements of the thermal conductivity of a mixture of particles of solid material with a liquid can be made is limited by the boiling point of the liquid.

Disadvantages mentioned above were excluded in the method of determination of thermal conductivity of rock cuttings and non-consolidated rocks (Popov et al., 2018) including grinding particles of non-consolidated material, preparation of the mixture of grinded particles with material-filler, and following mixture pressing until the solid sample of the pressed mixture. Then volume fractions of particles of non-consolidated material, material-filler and volume fraction of air in the sample of the pressed mixture are determined. Next, the effective thermal conductivity of the sample of the pressed mixture is measured and the thermal conductivity of particles of non-consolidated material is determined by the ratio, describing the link between the effective thermal conductivity of the sample of a pressed mixture of particles of non-consolidated material with material-filler with thermal conductivity of particles of non-consolidated material. However, this method does not provide the determination of the thermal conductivity of particles of solid material at elevated temperatures and does not include operations that determine the thermal conductivity of particles of solid material at elevated temperatures. Another disadvantage of the method is that preparation of a solid sample of the pressed mixture does not ensure the choice of material filler that allows the sample made from the mixture withstanding the hold-down pressure required for measurements and maintain strength properties in the studied temperature range.

## 2.5 Summary

As can be seen from the overview of previous publications, very little of the research has used careful metrological analysis, or has assessed measurement quality and levels of uncertainty in the results. This is unfortunate since shale rocks are very sensitive to mechanical treatment. It is not easy to obtain the flatness of the rock, which is required for the divided-bar method, so it is essential to check the degree of uncertainty in the results due to deviation from flatness. Most of the rock sample collections, which have been the objects of previous studies, were not representative; only two previous publications (Gilliam and Morgan, 1987; Rajeshwar et al., 1980) have a representative number of samples. Shale rocks are highly anisotropic, so the main axes of thermal conductivity and the anisotropy coefficient of studied rock samples should be defined before high-temperature measurements. It should be taken into account that the point position of the temperature sensors (thermocouples) when the divided-bar method is applied to highly

heterogeneous shales (Popov et al., 2017) results in a significant measurement uncertainty so that careful control of heterogeneity of the selected rock samples is required.

The previous studies have found different degrees of thermal conductivity decrease in the 25-300 °C temperature range for each shale formation, with variations of 5-35% (Prats and O'Brien, 1975; Smith, 1978; Nottenburg et al., 1978; DuBow et al., 1980; Rajeshwar et al., 1980; Sokolova et al., 1986; Gilliam and Morgan, 1987; Yu et al., 2015; Jha et al., 2016; Wang et al., 2018). There is a necessity in new experimental investigations on representative shale sample collections, taking account of the experimental problems described above.

Analysis of published experimental data on rock CLTE showed insufficient information on thermal expansion of shales at different temperatures, namely:

- non-representative collections of investigated samples for organic-rich shale formations;
- lack of CLTE anisotropy analysis;
- the absence of standard procedure of sampling core plugs for CLTE investigation (the sampling point significantly influences results of shale formation characterization as most shale samples and formations are highly heterogeneous);
- lack of combined integrated investigations of CLTE together with other physical characteristics of shales (density, thermal conductivity, total organic carbon, etc.).

Reliable information on thermal expansion of particular shale formation could not be obtained from literature data and requires experimental investigation of CLTE on particular representative rock samples collection with advanced equipment and methodology, accounting for rock anisotropy.

The volumetric heat capacity of unconventional reservoir rocks at elevated temperatures is not presented in publications and requires a new approach for determining this parameter. Only specific heat capacity values are presented and the number of studied rock samples is not represented (see *Table 3*).

Methods of determination of thermal conductivity of rock cuttings and non-consolidated rocks do not provide the determination of the thermal conductivity of particles of solid material at elevated temperatures and require a new approach.

## Chapter 3. Research methods

### 3.1 Enhancement of experimental basis for thermal conductivity measurements at elevated temperatures

#### 3.1.1 Method of measuring thermal conductivity at elevated temperatures

##### 3.1.1.1 Characteristics of DTC-300 instrument

Thermal conductivity measurements in a temperature range of 30-300 °C were carried out with the well-known divided-bar method (Popov et al., 2016b) using a DTC-300 instrument (*Figure 1*) (TA Instruments, <http://www.tainstruments.com/dtc-300>). By the manufacturer's instructions, the rock samples were treated before the measurements and were prepared as cylindrical core plugs with a diameter of (50±1) mm and a height of (20±1) mm. The thermal conductivity measurements are based on the guarded heat flow meter method (Popov et al., 2016b) and satisfy the requirements of ASTM E1530-11 (2016). The instrument scheme can be found in (Popov et al., 2016b; TA Instruments, <http://www.tainstruments.com/dtc-300>).



**Figure 1.** DTC-300 instrument for measuring Thermal conductivity of rock samples at elevated temperatures.

Technical characteristics of the DTC-300 are as follows (TA Instruments, <http://www.tainstruments.com/dtc-300>):

- thermal conductivity range: 0.1-30 W/(m·K)

- temperature range: -20 °C to 300 °C with an interval between measurements of at least 5 °C;
- range of compressive pressure: 0.03 – 0.41 MPa;
- measurement rate: 40-60 min at a particular temperature;
- measurement accuracy (systematic error): from  $\pm 3$  to  $\pm 8\%$  (depends on the thermal resistance of studied sample);

### **3.1.1.2 Thermal conductivity measurements procedure using a DTC-300 instrument**

For measurements with the DTC-300, the samples should have a cylindrical form with a thickness of  $20\pm 1$  mm and a diameter of  $50\pm 1$  mm. The samples must have smooth and parallel-sided surfaces without any damage or cracks. Before the measurements, a thermal compound is applied on the flat surfaces of the sample to minimize thermal resistance between the sample and the closeout surfaces according to the recommendations of the DTC-300 manufacturer. The studied sample with some amount of thermal compound is set between two parallel flat surfaces (each of them has incorporated thermocouple inside) regulated by different temperatures. The temperature difference applied to the rock from the upper to lower surface is 30 °C. During measurements, a compressive load is applied to the stack (to minimize contact resistance) and axial temperature gradient is provided in the stack as heat is supplied from the upper surface through the sample to the lower surface. Compressive load for all experimental data was 7kPa and constant with temperature. Thermal expansion of studied rock samples does not exceed 0.1 mm (that is just 0.5% of the height of studied samples). It results in negligible changing in the compressive load and does not has an effect on thermal conductivity during heating that takes about 1 hour for each temperature to reach a steady state. The thermal conductivity of studied samples is calculated using measured temperature drop along with the sample and the sample thickness. An automatically controlled system provides continuing measurements during the studied temperature range. The heat isolation is performed by the guard that surrounds the stack during the experiment and is kept at the mean temperature of the two plates, to minimize lateral heat flow to and from the stack. A number of samples with known thermal resistance that covers the necessary range of studied samples are used for calibration of the instrument. Six certified reference standards (Vespel, titanium alloy VT-6, marble, plexiglass, single-crystal quartz, and technical glass K-8) within the temperature range of 30-300 °C have been used for calibration and the accuracy and precision determination.

### 3.1.1.3 Metrological study of DTC-300 instrument

For the metrological study of thermal conductivity measurements at elevated temperatures with DTC-300 instrument following standard samples were used: plexiglass, vespel, technical glass K-8, marble, single-crystal quartz, titanium alloy VT-6. These materials were chosen in such a way because their thermal conductivity covers the range of thermal conductivity of rocks – 0.19-6.40 W/(m·K) (see *Table 4*). For all materials precision of thermal conductivity measurements with temperature was obtained. A number of measurements are presented in *Table 4*. The precision of thermal conductivity measurements on technical glass K-8, quartz, and titanium with temperature showed polynomial behavior. For technical glass K-8 it is in the range of 0-3%, for single-crystal quartz – 0-8%, for titanium alloy VT-6 – 2-7% (*Figures 2, 5, 6*). The precision of thermal conductivity measurements on marble and vespel with temperature showed unstable behavior and for marble, it is in the range of 4-10%, for vespel – 0.5-2.5% (*Figures 3, 7*). The precision of thermal conductivity measurements on plexiglass showed stable behavior with temperature and is in the range of 0.4-0.6% (*Figure 4*). For determining the accuracy of thermal conductivity measurements on the DTC-300 instrument at room temperatures Thermal Conductivity Scanner (TCS) (Popov et al., 2016) was used. The values of thermal conductivity measurements with TCS and DTC-300 instrument at room temperature are shown in *Table 4*. The accuracy of thermal conductivity measurements for studied materials is in the range of -14-0.2%.

**Table 4.** Accuracy of thermal conductivity measurements of standard samples on DTC-300 instrument at room temperature obtained with TCS and DTC-300 instrument measurements.

Material	$\lambda$ (TCS), W/(m·K)	$\lambda_{\text{average}}$ (DTC-300), W/(m·K)	Number of measurements (DTC-300)	Accuracy of DTC-300 measurements, %
Plexiglass	0.194	0.179	4	-8
Vespel	0.374	0.371	6	-1
Glass K-8	1.094	0.96	5	-12
Marble	2.70	2.32	5	-14
Quartz, single crystal	6.05	5.66	5	-6
Titanium alloy VT-6	6.52	6.37	5	-2

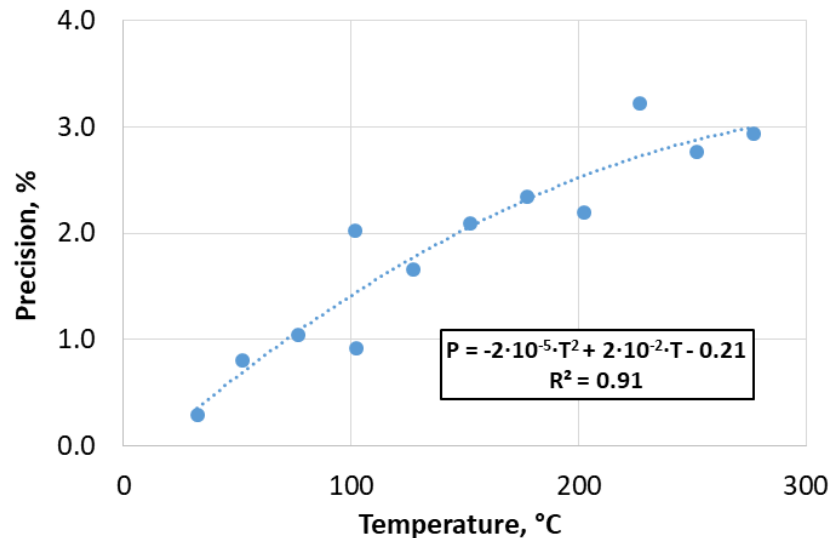


**Figure 2.** The precision of thermal conductivity measurements on technical glass K-8 with temperature, obtained with DTC-300 instrument.

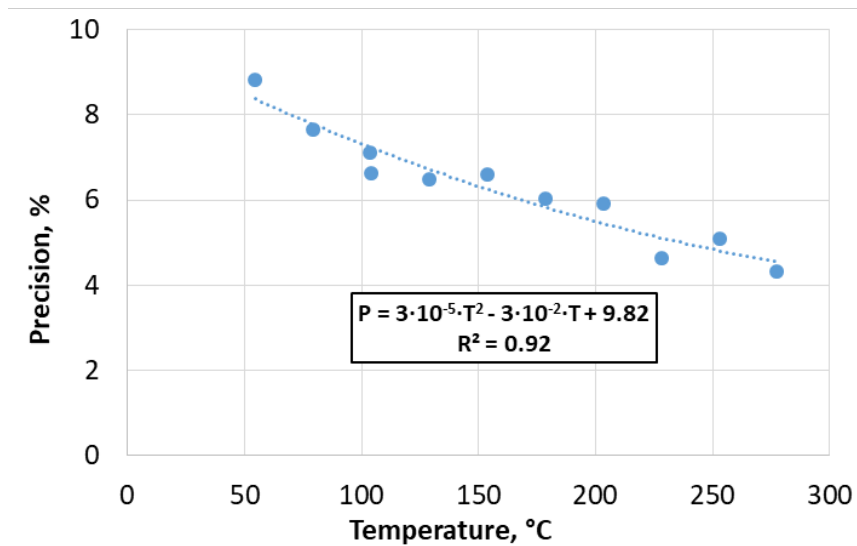


**Figure 3.** The precision of thermal conductivity measurements on marble with temperature, obtained with DTC-300 instrument.

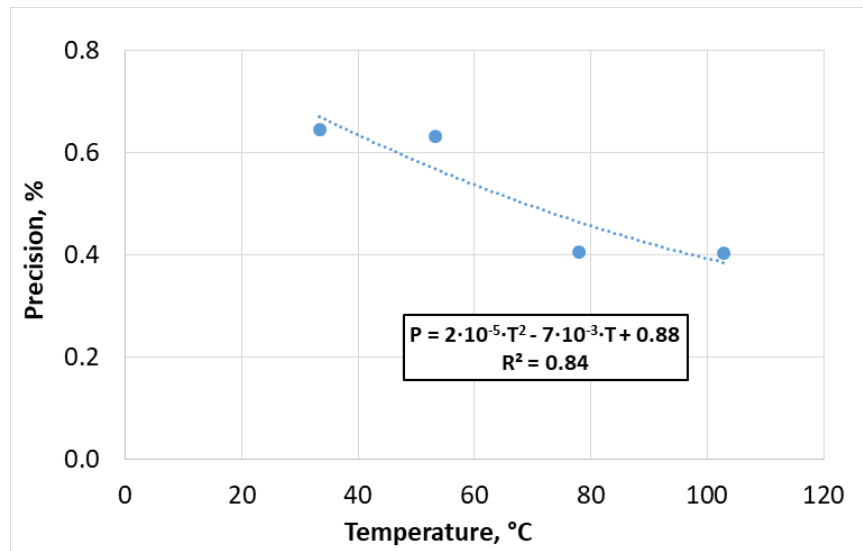


**Figure 4.** The precision of thermal conductivity measurements on plexiglass with temperature, obtained with DTC-300 instrument.

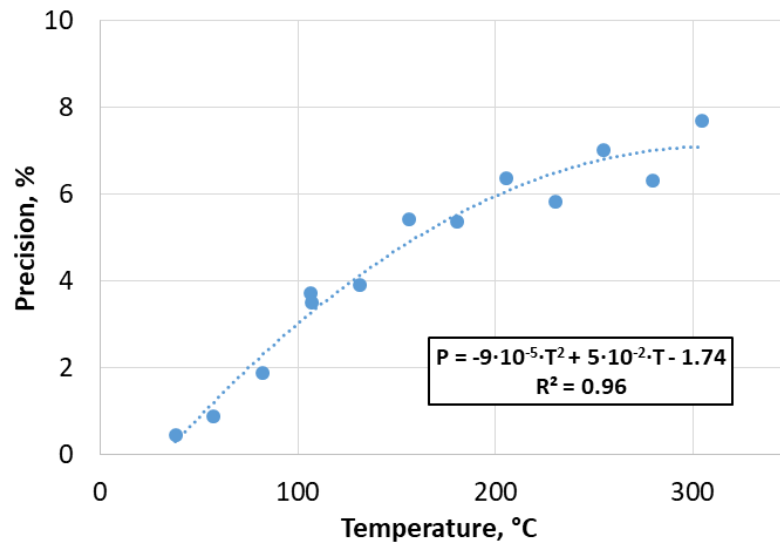


**Figure 5.** The precision of thermal conductivity measurements on single-crystal quartz with temperature, obtained with DTC-300 instrument.

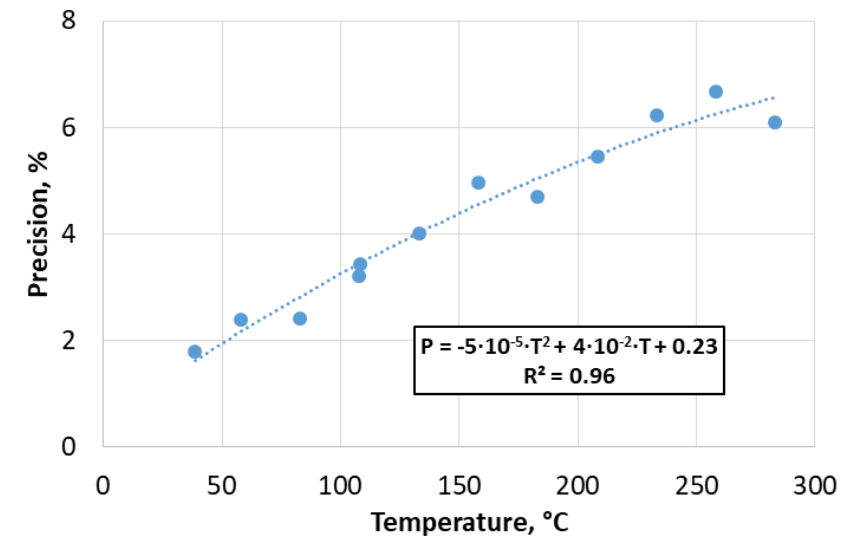


**Figure 6.** The precision of thermal conductivity measurements on titanium alloy VT-6 with temperature, obtained with DTC-300 instrument.

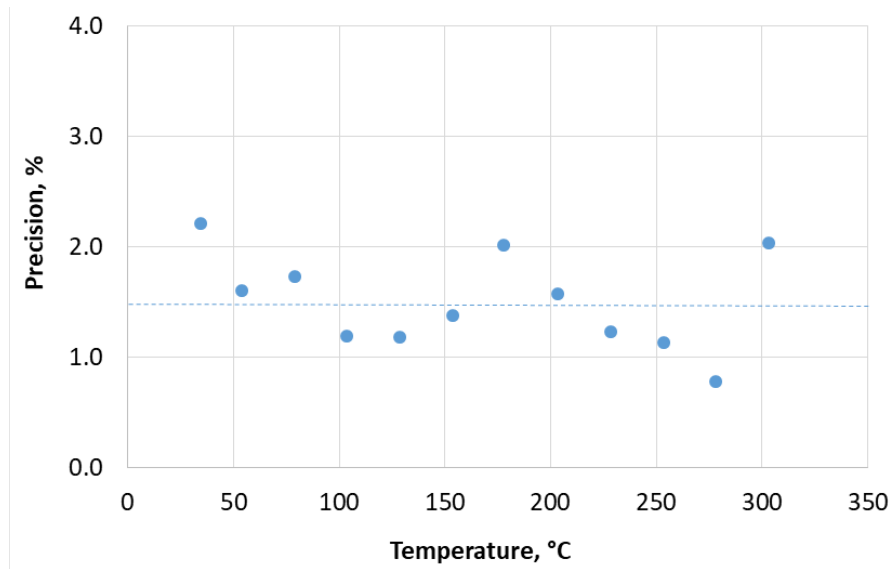


**Figure 7.** The precision of thermal conductivity measurements on vespel with temperature, obtained with DTC-300 instrument.

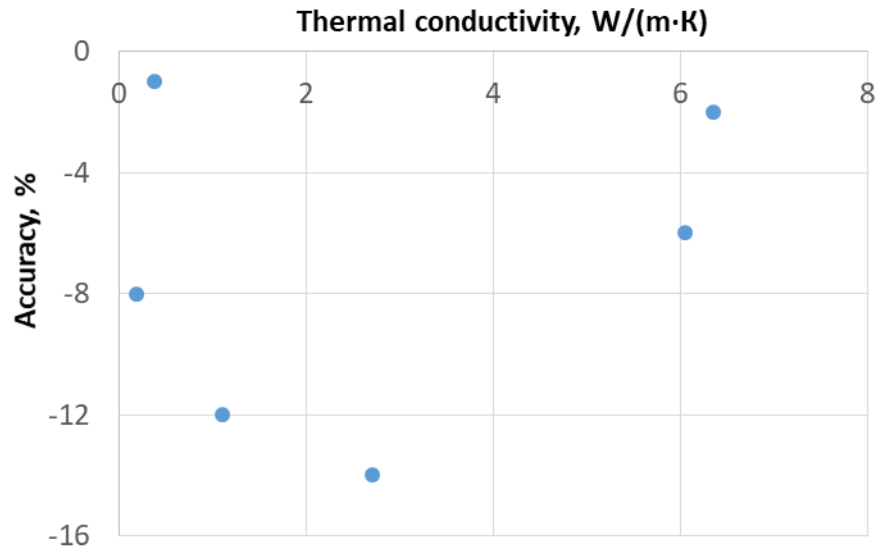


**Figure 8.** Dependence of accuracy of thermal conductivity measurements (DTC-300 instrument) on thermal conductivity values of studied materials (*Table 4*).

Metrological study of thermal conductivity measurements of standard samples on DTC-300 instrument showed that precision and accuracy of measurements are enough high and can reach 9% and -14% respectively. A new approach for thermal conductivity measurements at elevated temperatures is required to provide better measurement quality.

### 3.1.2 New measuring technique based on the integration of DTC-300 instrument and Thermal Conductivity Scanner

To account for rock anisotropy and heterogeneity and to provide better measurement quality, the DTC-300 was used in combination with Thermal Conductivity Scanner (TCS). The TCS offers non-contact non-destructive profiling of rock thermal conductivity and thermal diffusivity on the flat or cylindrical surface of full-diameter or split core samples. It measures thermal properties (thermal conductivity parallel ( $\lambda_{||}$ ) and perpendicular ( $\lambda_{\perp}$ ) to bedding, thermal diffusivity, the thermal heterogeneity factor obtained from scanning the sample along ( $\beta_1$ ) and perpendicular ( $\beta_2$ ) to the core axis, and the thermal anisotropy coefficient ( $K = \lambda_{||}/\lambda_{\perp}$ ) as well as the volumetric heat capacity of rock samples with flat or cylindrical surfaces in atmospheric conditions. The thermal conductivity component parallel to the bedding plane ( $\lambda_{||}$ ) is determined by optical scanning in a direction perpendicular to the rock bedding plane (normally equivalent to scanning along the axis of the core sample on the cylindrical surface of full-diameter core samples

for sub-vertical wells). The additional optical scan in a direction parallel to the rock bedding plane provides a determination of the thermal conductivity component perpendicular to the bedding plane ( $\lambda_{\perp}$ ) using the formula:

$$\lambda_{\perp} = \lambda_{\text{app}}^2 / \lambda_{\parallel}, \quad (1)$$

where  $\lambda_{\text{app}}$  is ‘apparent’ thermal conductivity measured by optical scanning in a direction perpendicular to the rock bedding plane (Popov et al., 2016b). The instrument scheme can be found in (Popov et al., 2016b).

The procedure of thermal conductivity measurements using the TCS instrument is following. The studied rock samples are placed between two reference standards on the platform. The reference standards are chosen in accordance with the range of thermal conductivity of the studied rock samples. Eight certified reference standards (VespeI, stainless steel, pyrex, plexiglass, fused quartz, technical glass K-8, titanium alloy VT-6 and anisotropic single crystal of quartz) have been used for calibration and the accuracy and precision determination (description of standards can be found in Popov et al., 2016b). The samples and two reference standards are scanned successively by three infrared temperature sensors that indicate temperature distribution along with the samples and reference standards before and after heating. Thermal conductivity values are calculated by comparing the temperature excess of the samples with that of reference standards (with known thermal conductivity), in accordance with the theoretical model of the optical scanning method (Popov et al., 2016b). The thermal heterogeneity factors ( $\beta_1, \beta_2$ ) of every studied rock sample are determined from the thermal conductivity profile in order to establish the degree of rock heterogeneity caused by variations of texture, structure, porosity, and mineral composition of the rocks (Popov et al., 2003). The thermal heterogeneity factor is defined as  $\beta = (\lambda_{\text{max}} - \lambda_{\text{min}}) / \lambda_{\text{aver}}$ , where  $\lambda_{\text{max}}$ ,  $\lambda_{\text{min}}$  and  $\lambda_{\text{aver}}$  are the maximum, minimum, and average values of the thermal conductivity component with the recorded thermal conductivity profile of the rock sample. The number of experimental data points along the thermal conductivity profiles for  $\beta$  calculation is about 40.

The advantages of TCS instruments are as follows (Popov et al., 2016b):

- the high spatial resolution of continuous profiling of thermal properties (about 1 mm);
- non-destructive non-contact approach to measurement;
- measurement of principal components of the thermal conductivity tensor;
- high quality of the thermal conductivity measurements with accuracy (A) and precision (P) not exceeding, respectively:



- $\pm 2\%$  (A) and  $\pm 1.5\%$  (P) for thermal conductivity  $\lambda_{\parallel}$  parallel to a rock bedding plane,
- $\pm 3\%$  (A) and  $\pm 2.5\%$  (P) for thermal conductivity  $\lambda_{\perp}$  perpendicular to a rock bedding plane (confidence level in both cases is 0.95).

That corresponds to measurement uncertainties of  $\pm 3\%$  for thermal conductivity  $\lambda_{\parallel}$  parallel to a rock bedding plane and  $\pm 4\%$  for thermal conductivity  $\lambda_{\perp}$  perpendicular to a rock bedding plane as the uncertainty  $U$  is determined as:

$$U = (A^2 + P^2)^{1/2} \quad (2)$$

Thermal conductivity measurements with the TCS were carried out on every rock sample before and after thermal conductivity measurements with the DTC-300 at high temperatures in order to:

- determine principal axes of the thermal conductivity tensor by making measurements with rotation of the flat surface of the samples at different angles to the scanning line (Popov et al., 2016b);
- determine principal components of the rock thermal conductivity tensor;
- analyze thermal heterogeneity and variations of the thermal anisotropy coefficient along with the core samples, from which the rock samples (core plugs) are taken for measurements with the DTC-300; this enables us to select a homogeneous zone with representative thermal anisotropy, from which to take a small cylindrical specimen (50 mm in diameter and 20 mm in height) for subsequent measurements with the DTC-300 (Popov et al., 2014) taking account of the local (point) location of temperature sensors in the metal layers of the DTC-300;
- enable metrological control of thermal conductivity measurements, since the optical scanning method provides non-contact thermal conductivity measurements with significantly better accuracy and precision for heterogeneous shale samples, which may be damaged by mechanical treatment, so that is it not possible to properly polish and obtain parallelism of flat surfaces of the rock sample, as would be required in order to achieve accurate measurements using the divided-bar technique;
- compare the above-mentioned thermal properties before and after measurements with the DTC-300 instrument at high temperatures.

Continuous profiling of full-diameter core samples from the studied depth intervals was carried out with the TCS before the measurements using the DTC-300 instrument. Full-diameter core samples with a small thermal heterogeneity factor were then selected from the thermal conductivity profile along the well. The cylindrical samples sized 50×20 mm for measurements at high temperatures with the DTC-300 were drilled from the least heterogeneous zones of the full-diameter core samples. We thus select core samples with representative thermal properties for measurements of thermal conductivity at high temperatures, according to the research objectives, and avoid significant variations of thermal properties along the core sample (Popov et al., 2014) that could cause uncertainty in the DTC-300 measurement results. In order to control for any changes in the rock samples within the temperature range studied, all of the cylindrical rock samples were scanned by the TCS to obtain thermal conductivity in two mutually perpendicular directions – parallel and perpendicular to bedding – for the determination of the thermal anisotropy coefficient before and after high-temperature measurements by the DTC-300.

Correction for change in the structure of the rock samples during heating (due to the appearance of cracks) was carried out using thermal conductivity data obtained with the TCS after heating. Considering that thermal conductivity changes are related to the appearance of cracks after heating the difference between thermal conductivity before and after heating obtained with TCS was included as correction for results (obtained with DTC-300). Correction of experimental data at high temperatures using the TCS data consisted of the following steps:

1. Thermal conductivity measuring at room temperature with TCS before heating.
2. Thermal conductivity measuring at temperature range 30-300 °C with DTC-300.
3. Correcting the dependence obtained at step 2 using the value of thermal conductivity obtained at step 1.
4. Thermal conductivity measuring at room temperature with TCS after heating up to 300 °C.
5. Calculating the proportional relative decrease in thermal conductivity values (obtained with TCS) within temperature interval between atmospheric temperature and 300 °C using results of steps 1 and 4.
6. Gradual correcting (from 0% at room temperature up to the value obtained in step 5 at 300 °C) of the data obtained at step 3.

Changing in rock samples structure during heating is supposed to be a gradual process and the percentage of correction of thermal conductivity monotonically increases with temperature.

### 3.1.3 Modification of DTC-300 technique

#### 3.1.3.1 Accounting for rocks flatness deviation

The difference in the rock sample thickness, caused by non-parallelism of the two flat surfaces of the core plug, leads to uncertainty in the thermal conductivity measurements obtained using the DTC-300 instrument. *Figure 9* shows experimental data, which demonstrate how a difference  $\Delta h$  in the rock sample thickness produces a difference  $\delta\lambda$  between thermal conductivity  $\lambda_{DTC-300}$  obtained with the DTC-300 at room temperature and thermal conductivity  $\lambda_{TCS}$  measured with the TCS. Determination coefficient  $R^2 = 0.70$ , root mean square error (*RMSE*) is 5.8%. The parameter  $\delta\lambda$  was defined by the formula:

$$\delta\lambda = (\lambda_{TCS} - \lambda_{DTC-300})/\lambda_{TCS} \quad (3)$$

The difference in rock sample thickness  $\Delta h$  was measured using a dimensional height gauge and relative difference  $\delta h$  in the core plug thickness was calculated as:

$$\delta h = \Delta h/h, \quad (4)$$

where  $\Delta h$  is a maximum difference in the rock sample thickness and  $h$  is the average height of the rock samples.

The deviation  $\delta\lambda$  is caused by the uncontrolled increase of thermal resistance between rock samples and metallic layers of the DTC-300 surrounding the rock sample when parallelism of the two flat surfaces of the core plug is disturbed. Peculiarities of organic-rich rocks do not permit adequate mechanical treatment of the rock samples to remove non-parallelism of the rock sample surfaces and exclude the thermal conductivity measurement error  $\delta\lambda$  when using the DTC-300. The combined use of the TCS and DTC-300 enables the correction of the thermal conductivity values obtained using the DTC-300. In the actual performed experiments collection of organic-rich rocks was used with the range of  $\delta h$ : 0.5-5%.

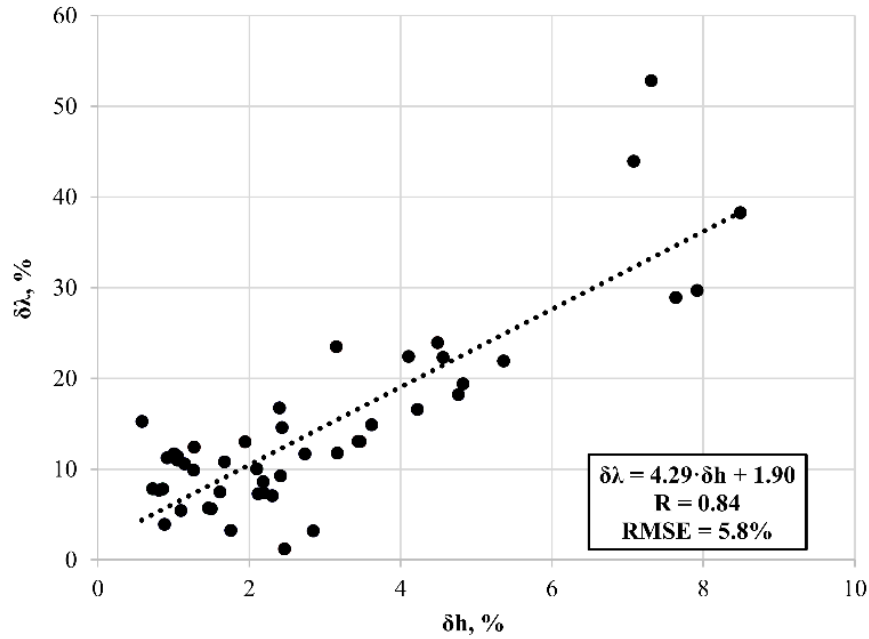


**Figure 9.** Influence of difference in rock sample thickness on the relative difference between thermal conductivity measured with DTC-300 and TCS instruments at room temperature.  $R$  is the correlation coefficient,  $RMSE$  is the root mean square error.

### 3.1.3.2 Variations in rock sample diameters

DTC-300 instrument allows us to measure the thermal conductivity of samples with a diameter of 50 mm. However, there is a necessity in measurements of rock samples with less diameter, as it is not always possible to drill rock samples or to make synthetic samples with a diameter of 50 mm. For checking the possibility of thermal conductivity measurements on samples with a diameter less than 50 mm a number of experiments on synthetic samples of marbles with different diameters were carried out. Marble samples with different diameters (25-50 mm) were made using a press machine (PP 25, Retsch). Results of thermal conductivity measurements on marble samples at elevated temperatures with the DTC-300 instrument are presented in *Figure 10*. The dependence of thermal conductivity of marble samples on samples diameter is shown in *Figure 10a*. The results showed that the thermal conductivity of samples is decreasing with decreasing of samples diameter. To exclude dependence of thermal conductivity of samples on diameter following correction was applied:

$$\lambda_{corr} = \lambda \cdot \left(\frac{D_{50}}{D}\right)^2, \quad (5)$$

where  $\lambda_{corr}$  – correction of thermal conductivity value on diameter,  $\lambda$  – measured thermal conductivity,  $D_{50}$  – diameter of 50 mm,  $D$  – diameter of the studied sample.

Results of thermal conductivity correction using formula (5) are presented in *Figure 11*. It was observed that correction of thermal conductivity values on diameter can be used for samples with diameters 38-50 mm.

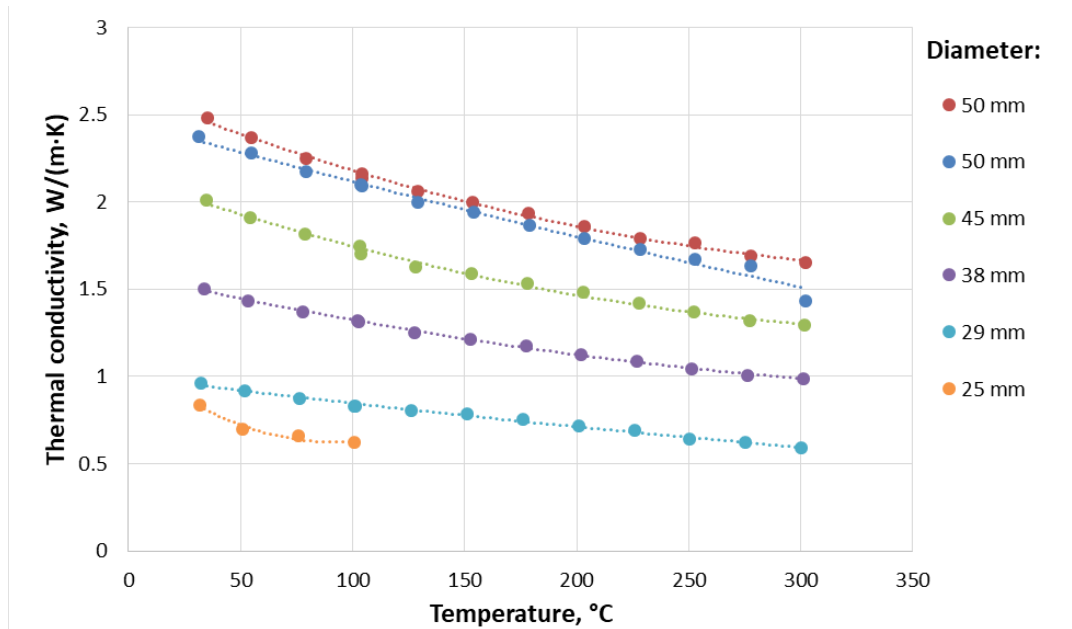


*Figure 10.* Thermal conductivity of marble samples with different diameters with the temperature.

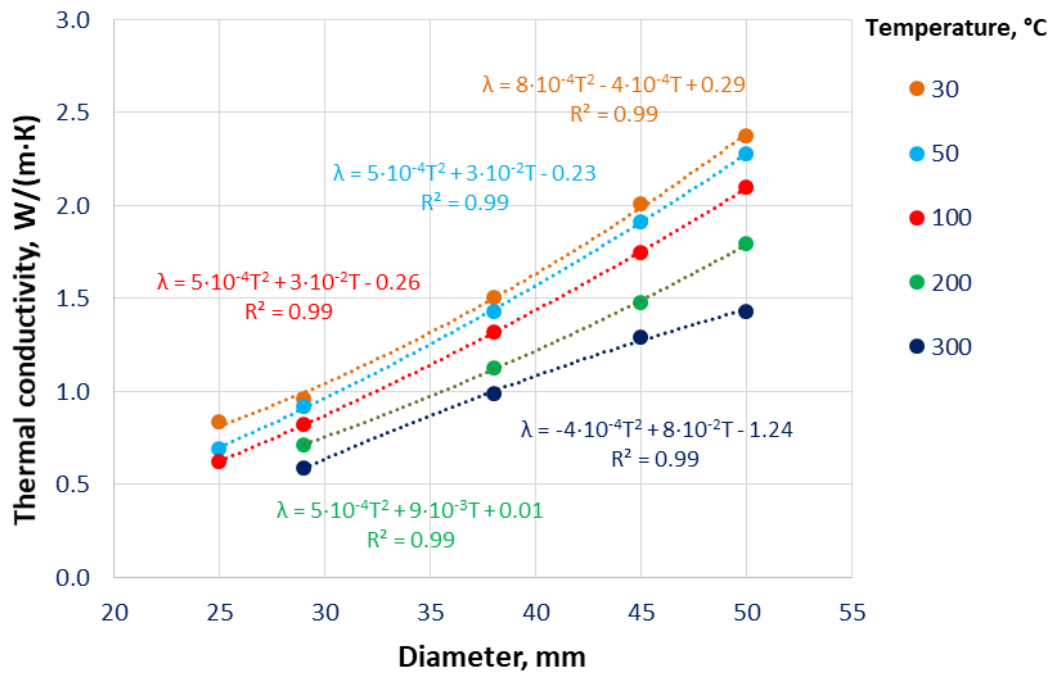


*Figure 10a.* The dependence of thermal conductivity of marble samples on samples diameter.

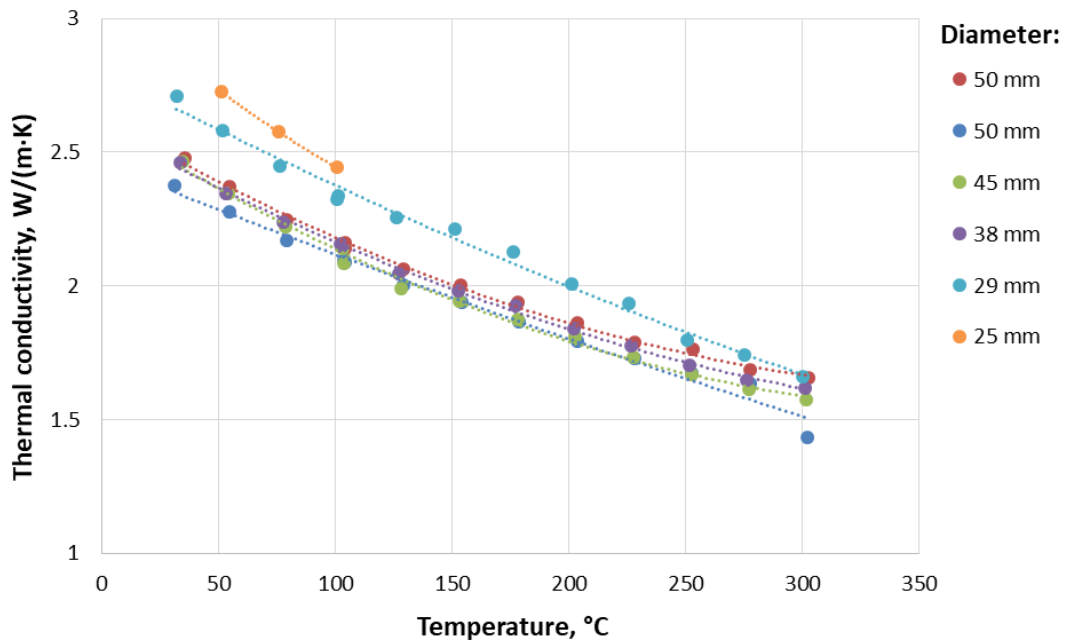


**Figure 11.** Corrected thermal conductivity values of marble samples with different diameters within the temperature.

### 3.2 The technique of measurements of thermal conductivity of rock cuttings and non-consolidated rocks at elevated temperatures

#### 3.2.1 Materials and methods



Method of determining the thermal conductivity of particles of solid materials at elevated temperatures includes the following steps:

1. Thermal conductivity of the material-filler (solid-state) is measured at different temperatures in the specified temperature range and the dependence of the thermal conductivity of the material-filler on temperature is determined in the specified temperature range. It is also possible to measure thermal diffusivity and volumetric heat capacity of the material-filler (solid-state) at different temperatures in a given temperature range and determine the dependence of thermal diffusivity and volumetric heat capacity of material-filler (solid-state) on temperature.
2. Rock cuttings are prepared with a ball mill with a certain particle size, which is controlled by the duration and frequency of the ball mill oscillation. The frequency and the duration of the ball mill oscillation are chosen based on the results of preliminary studies of the influence of these factors, as well as the properties of the rock cuttings (hardness, porosity, etc.) on the size of the particles.

3. The mixture of rock cuttings with material-filler is prepared at a specified proportion. It is also possible to use a mixture of several different materials (one of which is in a liquid state) as a material filler. At first, rock cuttings are mixed with solid components of the material filler until a homogeneous mixture is obtained and then the liquid component of the material filler is added and the mixture is put into a homogeneous state. Removing as much air as possible from the mixture a solid sample mixture is formed.
4. The volume fractions of the following components of the solid sample mixture are determined: rock cuttings, material filler, and air.
5. The effective thermal conductivity of the solid sample mixture is measured at different temperatures in a specified temperature range. It is also possible to measure the effective thermal diffusivity or volumetric heat capacity of solid sample mixture at different temperatures.
6. The thermal conductivity of rock cuttings is determined at different temperatures in a specified temperature range by the ratio describing the effective thermal conductivity of a solid sample mixture of rock cuttings and material filler. If the temperature dependence of the thermal diffusivity of the material-filler is determined in a specified temperature range, then the temperature diffusivity of rock cuttings vs temperature in a specified temperature range can be calculated from measurements of the effective thermal diffusivity of rock cuttings at different temperatures in a specified temperature range.

### 3.2.2 Theoretical approach

The thermal diffusivity of a material can be calculated from the relation connecting thermal diffusivity, thermal conductivity, and volumetric heat capacity of materials:

$$\alpha(T) = \frac{\lambda(T)}{c(T)} \quad (6)$$

where  $C(T)$ ,  $\lambda(T)$ , and  $\alpha(T)$  are volumetric heat capacity, thermal conductivity, and the thermal diffusivity of the material at temperature  $T$  correspondingly.

The effective volumetric heat capacity of solid sample mixture is determined from the measurement results of the effective thermal conductivity and thermal diffusivity of a solid sample mixture using the following relationship:

$$C_{mixture}(T) = \frac{\lambda_{mixture}(T)}{\alpha_{mixture}(T)} \quad (7)$$

where  $C_{mixture}(T)$ ,  $\lambda_{mixture}(T)$ , and  $\alpha_{mixture}(T)$  are effective volumetric heat capacity, effective thermal conductivity, and effective thermal diffusivity of solid sample mixture at temperature T correspondingly.

The volumetric heat capacity of rock cuttings is determined by the ratio connecting the volumetric heat capacity of rock cuttings with the effective volumetric heat capacity of the solid sample mixture, the volumetric heat capacities of material-filler and air, as well as the volume fractions of the components of the solid sample mixture:

$$C_{mixture}(T) = C_M(T) \cdot V_M + C_A(T) \cdot V_A + C_B(T) \cdot V_{AB} \quad (8)$$

where  $C_M(T)$  is the volumetric heat capacity of rock cuttings at temperature T,  $C_A(T)$  is the volumetric heat capacity of air at temperature T,  $C_B(T)$  is the volumetric heat capacity of material-filler at temperature T,  $V_M$  is the volume fraction of rock cuttings,  $V_A$  is the volume fraction of air,  $V_B$  is the volume fraction of material-filler in the solid sample mixture.

Thermal diffusivity of rock cuttings can be determined from relations (6)-(8):

$$\alpha_M(T) = \lambda_M(T) \cdot \frac{V_M}{\left(\frac{\lambda_{mixture}(T)}{\alpha_{mixture}(T)} - \lambda_A(T) \cdot \frac{V_A}{\alpha_A(T)} - \lambda_B(T) \cdot \frac{V_B}{\alpha_B(T)}\right)} \quad (9)$$

where  $\lambda_A(T)$  is the thermal conductivity of air at temperature T,  $\lambda_B(T)$  is the thermal conductivity of material-filler at temperature T,  $\alpha_A(T)$  is thermal diffusivity of air at temperature T,  $\alpha_B(T)$  is thermal diffusivity of material-filler at temperature T.

The thermal conductivity of rock cuttings can be determined in two ways. In accordance with the first method, the thermal conductivity of rock cuttings is determined by the Lichtenecker-Asaad ratio (Asaad, 1995), which links the effective thermal conductivity of a solid sample mixture with the thermal conductivity of rock cuttings, the thermal conductivity of air, the thermal conductivity of a material-filler, their volume fractions in a solid sample mixture and a parameter characterizing the structural features of the material under study:

$$\lambda_M(T) = \left(\lambda_{mixture}(T) \cdot \lambda_A(T)^{-\beta(T) \cdot V_A} \cdot \lambda_B(T)^{-\beta(T) \cdot V_B}\right)^{1/(1-\beta(T) \cdot (V_A+V_B))}, \quad (10)$$

where  $\beta(T)$  is a parameter characterizing structural features of the material under study at temperature T. The parameter  $\beta(T)$  is chosen on the basis of prior information about the material under study. If there is no prior information the parameter  $\beta(T)$  is assumed to be 1.

In accordance with the second way of the method for determining the thermal conductivity of rock cuttings, the value of thermal conductivity of rock cuttings is calculated by solving an equation based on the modified Lichtenecker formula (Edvabnik, 2015):

$$\lambda_{mixture}(T) - \left(V_M \cdot \lambda_M(T) + V_A \cdot \lambda_A(T) + V_B \cdot \lambda_B(T)\right)^{\beta(T)} \left(\frac{V_M}{\lambda_M(T)} + \frac{V_A}{\lambda_A(T)} + \frac{V_B}{\lambda_B(T)}\right)^{\beta(T)-1} = 0, \quad (11)$$

where parameter  $\beta(T)$  is chosen on the basis of prior information about the material under study. If there is no prior information, the parameter  $\beta(T)$  is calculated using the empirical formula depending on the measured parameters of the solid sample mixture.

A material filler consisting of a solid and a liquid phase is prepared by mixing solid and liquid phases in a mass ratio of 2:1. After that air bubbles are removed from the material filler by vacuuming and the material filler is placed for 12 hours in the oven at 70 °C until complete crystallization. Crystallization of material filler occurs due to the chemical reaction of material filler components during which crystalline hydrates are formed. After removal from the furnace, the material-filler is weighed and a sample of a cylindrical shape with required dimensions determined by the requirements of the measuring equipment is made of material-filler. Using the DTC-300 instrument (TA Instruments) the effective thermal conductivity of a sample of material-filler is measured at different temperatures in a specified temperature range, limited by the temperature at which the structure of the material filler is destroyed. According to the measurement results, the dependence of the thermal conductivity of the material-filler on the temperature in a temperature range is determined. Particles of solid material are ground with a ball mill (MM 400, Retsch) for 2 minutes at an oscillation frequency of 25 Hz. Then, 20 g of ground particles of unconsolidated material are mixed with 9 g of the solid phase of the initial material-filler using a ball mill for 2 minutes at a frequency of 15 Hz. The mixture is weighed and put into a shape with an internal diameter of 40 mm and mixed with 5 g of the liquid phase of the material-filler to homogeneous condition. Then, air bubbles are removed from the mixture using a vacuum, and the mixture is weighed again. Next, the mixture is put for 12 hours in an oven at 70 °C until complete crystallization. After removal from the furnace, the mixture is weighed and a cylindrical sample of the required size is made from it. The solid sample mixture, consisting of a mixture of ground particles of solid material, material-filler, and air, is weighed, its thickness and diameter are measured as well as the porosity to determine the volume fractions of the components of the solid sample mixture. Using the DTC-300 instrument, the effective thermal conductivity of a solid sample mixture is measured at different temperatures in a specified temperature range. After that according to the dependencies of thermal conductivity of material-filler and air on the temperature in a specified temperature range, the thermal conductivity of the solid material particles is determined for the specified temperature values by relations (10) or (11), describing the effective thermal conductivity of the mixture of ground solid particles, material-filler, and air.

Using a sample made of CEREOX wax (BM-0002-1 FLUXANA) molten under vacuum for maximizing air removal and cooled to a solid wax state at room temperature, the effective thermal conductivity of solid wax is measured using a DTC-300 instrument (TA Instruments) at

different temperatures in a specified temperature range, which is limited by the melting point of wax - 140 °C. Then, the dependence of the thermal conductivity of solid wax on the temperature is determined in a specified temperature range. Particles of solid material are ground using a ball mill (MM 400, Retsch) for 2 minutes at an oscillation frequency of 25 Hz. Then 20 g of ground particles of solid material is mixed with 4 g of the initial powdered wax using the same ball mill for 2 minutes at a frequency of 15 Hz. The prepared mixture is put into a press cell with an internal diameter of 40 mm of a press machine (PP 25, Retsch) and heated to 105 °C in an oven, after which it is pressed at a pressure of 1800 bar for 5 minutes. After removing from the press machine a solid sample mixture consisting of a mixture of ground particles of solid material, wax, and air, is weighed, its thickness and diameter are measured, and the porosity of the solid sample mixture is measured to determine the volume fraction of its components. Using the instrument DTC-300 (TA Instruments) the effective thermal conductivity of a solid sample mixture at different temperatures in a specified temperature range is measured. After that according to the dependences of thermal conductivity of air and wax on the temperature in a specified temperature range the thermal conductivity of the solid material particles is determined for the specified temperature values by the relations (10) or (11) describing the effective thermal conductivity of the mixture of ground solid particles with wax and air.

### **3.3 Enhancement of experimental basis for CLTE measurements at elevated temperatures on core samples**

#### **3.3.1 Experimental basis of CLTE measurements**

The CLTE measurements at elevated temperatures were performed with a quartz dilatometer (*Figure 12a*) specially adapted for the measurements on standard core plugs (cylinders 30×30 mm) within a temperature range of 25-300 °C. The basic requirements of the ASTM standard (Popov et al., 2012; ASTM D4535-85, 2000) were accounted for during CLTE measurements.

Quartz dilatometers are widely used for both laboratory and industrial studies of CLTE that is related to the following reasons (Yanchenko, 2009):

- dilatometers design is simple enough for construction;
- studied rock samples do not require complicated special treatment as the main requirement for the tested samples is the presence of two plane-parallel surfaces;

- the dilatometers provide sufficient elongation sensitivity for the satisfactory quality of the CLTE measurements.

The instrument used in our experiments has been developed specially for the CLTE measurements on rock samples (Popov et al., 2012) and allows us to measure CLTE on standard core plugs (30×30 mm) or cubes (30×30×30 mm). It allows us to measure differential CLTE within every temperature interval of 20 °C on core plugs with different bedding orientations and obtaining CLTE anisotropy on the same core plug. The technical characteristics of the dilatometer are as follows:

- temperature range is 20...300 °C;
- accuracy of the elongation measurement is 0.05÷0.1 μm;
- accuracy of the temperature measurement is 0.1 °C;
- range of the heating rate is 0.1÷3.0 °C/min;
- the precision of the CLTE measurements is not more than 4%;
- uncertainty of the CLTE measurements is not more than  $1.8 \cdot 10^{-7} \text{ K}^{-1}$  (all at the confidence level 0.95).

Average CLTE is calculated from the following formula:

$$\alpha = \Delta l_0 / (l_0 \cdot (T_f - T_i)) + \alpha_{q.s.}, \quad (12)$$

$\alpha$  – CLTE of the sample in the temperature range  $T_i - T_f$ ,  $\Delta l_0$  – samples elongation, defined by the instrument with initial and final values difference,  $l_0$  – initial the length of the sample at the temperature  $T_i$ ,  $\alpha_{q.s.}$  – correction for expansion of dilatometer the quartz system at the temperature range  $T_i - T_f$ ,  $T_i$  – initial temperature,  $T_f$  – final heating temperature. The initial temperature is related to surrounding air temperature providing samples holding at room temperature for a time that is enough for samples thermodynamical equilibrium with the atmosphere inside the furnace.

Considering that transmitting elements of dilatometer (tube and push bar) can be made of different quartz glass with unknown CLTE values and temperatures of push bar and tube are different, it is necessary to correct expansion of dilatometer quartz system. Such correction is made with a standard sample of quartz glass with a calibration certificate. CLTE of quartz glass is calculated with the following formula:

$$\alpha_q = \Delta l_q / (l_0 \cdot (T_f - T_i)) + \alpha_{q.s.} \quad (13)$$

where the correction for expansion of dilatometer the quartz system is given by

$$\alpha_{q.s.} = \alpha_q - \Delta l_q / (l_0 \cdot (T_f - T_i)), \quad (14)$$

Here  $\alpha_q$  – average CLTE value of quartz glass standard sample in particular temperature range according to certificate,  $\Delta l_q$  – elongation of quartz glass standard sample with dilatometer quartz

system, defined by the instrument for length calibration (Micron-02). Calculations are checked considering elongation measured by instrument Micron-02. Quartz glass standard sample is measured a minimum of three times in a particular temperature range and average  $\Delta l_q$  is applied for calculation  $\alpha_{q.s.}$  by formula (14), which is used in basic formula (12).

Metrological studies of quartz dilatometer were provided with recommendations mentioned in (Miklashevsky, 2007).

For the CLTE measurements, cylindrical core plugs with a diameter and height of  $30 \pm 1$  mm were drilled from full-size core samples perpendicularly to the full-size core axis (i.e., parallel to bedding). Core plug dimensions were controlled by triple measurements of diameter and height with a slide-gauge. The preparation procedure included quality control when the core plugs having damages and cracks were excluded from the following measurements. Surfaces of studied core plugs were cleaned from dust particles, surfaces of dense samples, and standard samples were cleaned with ethanol. For the CLTE measurements on core plugs in radial direction polishing of side, the surface was performed in contact points with a sample holder of the dilatometer. A sampling of small pieces of core plugs was done and TOC measurements with the pyrolysis method for each small core piece were performed before the CLTE measurements.

Measurement workflow on the core plugs included the following step-by-step operations:

1. Density measurements with the gas volumetric method.
2. The measurements of thermal conductivity, thermal heterogeneity, and anisotropy on both flat surfaces of every core plug with the laser optical scanning instrument at seven different directions of the optical scanning (including directions parallel and perpendicular to bedding) (Popov et al., 2016b). Firstly, CLTE of 6 core plugs were measured in different directions (through every  $30^\circ$ ) in the temperature range 25-50 °C for detection of the direction of CLTE main axes. Each core plug was placed in two mutually perpendicular directions and was measured in axial direction and seven different points in the radial direction with sample rotation by every  $30^\circ$ . For these measurements, special preparation of a core plug was provided with a smoothing surface in measurement points. The temperature regime that was used during measurements is heating from room temperature (25 °C) to 50 °C. Room temperature was held for 60 minutes, 50 °C was kept for 90 minutes for the thermodynamical equilibrium of core plug and atmosphere inside the furnace.
3. The measurements of the mass of every core plug before the CLTE measurements.
4. Measurements of CLTE values on six core plugs at seven different directions (including directions parallel and perpendicular to bedding) at temperature range 25-50 °C.

5. Measurements of CLTE within a temperature range of 25-300 °C in the direction parallel and perpendicular to the bedding plane.
6. The measurements of the mass of every core plug after the CLTE measurements and cooling the core plugs up to room temperature.

### **3.3.2 Integration of dilatometer and Thermal Conductivity Scanner**

#### **3.3.2.1 Influence of rock anisotropy**

For studying CLTE anisotropy of shales a measurement methodology was developed that consists of two stages. At the first stage, the CLTE measurements were carried out for the heating temperature range of 25-50 °C on the core plugs with different bedding orientations relative to the dilatometer axis for anisotropy estimation (detection of main axis direction and values of principal components). Such a heating temperature range of 25-50 °C for the CLTE anisotropy study is chosen to avoid irreversible changes of structure and properties of studied shale samples. At the second step, the CLTE measurements were carried out within a wide temperature range of 25-300 °C when the bedding orientation of the core plug corresponded to the principal axes of the CLTE established in the first stage.

The high-precision measurements of the thermal conductivity of shale samples under study were performed within the CLTE investigation. The principal thermal conductivity tensor components were determined for every core plug and additional measurements were performed with several optical scanning lines inclined to the rock bedding plane with different angles to determine principal axes of the rock thermal conductivity. The complemented thermal conductivity measurements were performed for every core plug twice - before and after the CLTE measurements. The goals of the thermal conductivity measurements were as follows:

- to fix changes in the shale sample properties happened during the CLTE measurements when the shale samples were heated up to 300 °C;
- to determine principal axes of the rock thermal conductivity to compare the principal thermal conductivity axes directions with the principal CLTE axes directions.



**Figure 12.** Main (a) and auxiliary equipment (b, c) used in the study; a - Quartz dilatometer with an installed core sample, b - Thermal Conductivity Scanner, c - HAWK pyrolysis instrument.

The laser thermal conductivity scanner was used for the thermal conductivity measurements and thermal anisotropy investigation including detection of principal axes of the studied core plug thermal conductivity (*Figure 12b*) (Popov et al., 2016b). The instrument provides determination of the following rock characteristics:

- thermal conductivity components parallel ( $\lambda_{||}$ ) and perpendicular to bedding plane ( $\lambda_{\perp}$ );
- coefficient of thermal conductivity anisotropy  $K = \lambda_{||} / \lambda_{\perp}$ ;
- thermal heterogeneity factor calculated separately for scanning parallel ( $\beta_1$ ) and perpendicular to bedding plane ( $\beta_2$ );  $\beta = (\lambda_{\max} - \lambda_{\min}) / \lambda_{\text{average}}$ , where  $\lambda_{\max}$ ,  $\lambda_{\min}$ ,  $\lambda_{\text{average}}$  – maximum, minimum and average values of TC along every scanning line.

The laser thermal conductivity scanner (TCS) allows us to measure thermal conductivity on standard core plugs prepared for the CLTE measurements and on full-size core samples as well. It gives the possibility for comprehensive studying correlations CLTE vs thermal conductivity excluding the influence of essential heterogeneity of shales if the correlation studying is performed with CLTE and TC measurements on different core plugs. The laser thermal conductivity scanner

was used for the same shale collection in combination with the quartz dilatometer for the following objectives:

- control of thermal anisotropy and heterogeneity of shales from the measurements on full-size core samples and core plugs as well;
- selection of a representative collection of full-size core samples along a well under study for the following CLTE investigations;
- selection of representative areas with the full-size core samples selected for the following core plug drilling accounting for heterogeneity and variations in thermal conductivity anisotropy coefficient within the full-size core samples selected;
- detection of the direction of thermal conductivity main axes;
- investigation of the correlation thermal conductivity vs CLTE.

### **3.4 The technique of measurements of volumetric heat capacity of rocks at elevated temperatures**

#### **3.4.1 Measurements of specific heat capacity at elevated temperatures**

A differential scanning calorimeter DSC 214 Polyma (NETZSCH) was used to measure the specific heat of the rocks. Technical characteristics and image of the calorimeter are given in *Table 5* and *Figure 13*.

The measurement results were processed using the Proteus 7.0 software. NETZSCH - Concavus aluminum crucibles were used for measurements. To calibrate the heat flux, a synthetic sapphire weighing 25.02 mg was used. Calibration was carried out every day before the start of measurements.

The measurement program in various temperature ranges consists of three stages:

1. Isothermal segment at 35 °C - 10 min;
2. Dynamic segment 35 - 310 °C, heating rate - 10 °C / min;
3. Isothermal segment at 310 °C - 10 min.

High purity nitrogen (99.999%) was used as a purge and shielding gas. The volumetric flow rates of the purge and shielding gases were 40 and 60 ml/min, respectively. The mass of the samples was determined with an accuracy of  $\pm 0.01$  mg. Measurements and calculations of specific heat were carried out in accordance with the requirements of ASTM E1269-11 (ASTM E1269-11, 2018).



**Figure 13.** Differential scanning calorimeter NETZSCH - DSC 214 Polyma.

**Table 5.** Main technical characteristics of the calorimeter DSC NETZSCH 214 Polyma.

<b>Description of characteristics</b>	<b>Value</b>
Temperature reading range T, °C	-170-600
Temperature measurement range, °C	30-600
Specific heat measurement range, kJ/kg	10-1000
Specific heat capacity measurement range, J/(kg·K)	200-2000
Limits of permissible uncertainty of temperature measurements, °C	±0.8
Limits of permissible relative error of specific heat measurements, %	±3.0
Limits of permissible relative error of specific heat capacity measurements, %	±2.5
Temperature change rate, °C/min	0.001-500
Supply voltage, V	230
Supply voltage frequency, Hz	50
Power consumption, κV·A,	1.0
<b>Operating conditions</b>	
Ambient temperature range, °C	15-35
Atmospheric pressure range, κPa	84-106.7
Relative humidity range, %	5-80

### 3.4.2 Integration of differential scanning calorimeter and dilatometer for measuring volumetric heat capacity at elevated temperatures

For volumetric heat capacity, determination new methodology was applied as only analytical solutions are applied for the calculation of this parameter (*Chapter 1.1*). Experimental data for shale formations are presented only for specific heat capacity (*Chapter 1.1*). The methodology is based on a combination of measurements on differential scanning calorimeter, dilatometer, and hydrostatic weighing method. It includes the following steps:

1. Specific heat capacity of rock sample  $c_p(T)$  within temperature is measured with differential scanning calorimeter
2. The coefficient of linear thermal expansion on rock sample sized 30×30 mm  $\alpha(T)$  within temperature is measured with dilatometer DKT-40 (*Chapter 3.3.1*)
3. The density of rock sample at room temperature  $\rho_0$  is measured by hydrostatic weighing method (GOST 25281-82, 1982)
4. The dependence of density of rock sample on temperature is determined using the following formula (Zhdanov, 1984):

$$\rho(T) = \frac{\rho_0}{(1+\beta \cdot T)} \quad (15)$$

$\rho_0$  – density of rock sample at room temperature  $T = 25^\circ\text{C}$ ,  $\beta = 3\alpha$ ,  $\alpha$  – coefficient of linear thermal expansion of rock sample.

5. Volumetric heat capacity of rock sample within temperature is determined by the following formula:

$$C_p(T) = c_p(T) \cdot \rho(T), \quad (16)$$

where  $c_p(T)$  – specific heat capacity of a rock sample,  $\rho(T)$  – density of rock sample within the temperature.

For volumetric heat capacity of rock sample determination the following formula can be applied:

$$C_p(T) = C_p^M(T) \cdot (1-x) + c_a(T) \cdot \rho_a(T) \cdot x, \quad (17)$$

$C_p^M(T)$  – volumetric heat capacity of the matrix,  $x$  – air fraction in the sample,  $c_a$ ,  $\rho_a$  – heat capacity and density of air.

From formula (17) volumetric heat capacity of the matrix can be determined:

$$C_p^M(T) = \frac{(c^m(T) \cdot \rho_0 - c^a(T) \cdot \rho^a(T) \cdot x)}{(1-x)} \quad (18)$$

where  $c^m$ ,  $\rho_0$  – measured heat capacity and density of a sample at room temperature.

## Chapter 4. Experimental results

### 4.1 Unconventional reservoir rocks under study

The collections of organic-rich sedimentary rock samples, which were studied, are from unconventional reservoirs in Russia's West-Siberian and Volga-Ural oil and gas basins. The number of unconventional reservoir rocks for studying thermal conductivity, CLTE, and VHC at elevated temperatures is shown in *Table 6*. The organic-rich samples were selected after continuous non-destructive non-contact profiling of all core samples recovered during the drilling of the respective wells. The profiling was carried out using TCS (Popov et al., 2016b) in bench conditions on all full-diameter cores from wells for the formations to be studied (Popov et al., 2017; Chekhonin et al., 2018). Thermal core logging provided a thermal conductivity profile along every core sample. A thermal conductivity tensor component was defined along the bedding plane with a spatial resolution of 1 mm (Popov et al., 2017; Chekhonin et al., 2018). Additional profiling for a perpendicular direction on every core sample (along one or several lines on the core sample surface) enabled the definition of thermal conductivity tensor components for a direction perpendicular to the bedding plane (Popov et al., 2016b; Popov et al., 2017). The thermal anisotropy coefficient was then determined as a ratio of the parallel and perpendicular components of thermal conductivity. The most representative core samples for every formation were selected based on statistical processing of the thermal core logging data and geological description of all the core samples (accounting for data on multiscale rock thermal heterogeneity and anisotropy obtained from the thermal core logging).

**Table 6.** Number of unconventional reservoir rocks for studying thermal conductivity, CLTE, and VHC at elevated temperatures.

Formation	Thermal conductivity	CLTE	VHC
Bazhenov	19	31	27
Abalak	9	6	4
Golchih	4	7	-
Domanic	7	-	-
Total	39	44	31

## 4.2 Thermal conductivity at elevated temperatures

### 4.2.1 Rock collection for studying thermal conductivity at elevated temperatures

Rock collection for studying thermal conductivity at elevated temperatures includes 5 oil fields of West-Siberian and Volga-Ural oil and gas basins.

#### Oil field 1

The collection of 6 West-Siberian rock samples (50×20 mm) of Oil field 1 are from Bazhenov and Abalak formations and were all drilled along a single well (see *Table 7*). The Bazhenov formation (3 samples) is composed of organic-rich clayey-siliceous and carbonaceous siliceous-clayey rocks with total organic carbon (TOC) of 3-15%. The Abalak formation (3 samples) is composed of silty argillites with TOC of about 1-3%.

**Table 7.** The collection of studied rocks from Oil field 1.

№ of sample	Formation	Lithology
3BF	Bazhenov	Clayey-siliceous with lentils siltstone
4 BF	Bazhenov	Clayey-siliceous
5 BF	Bazhenov	Clayey-siliceous
1AB	Abalak	Silty argillite
2 AB	Abalak	Silty argillite
5 AB	Abalak	Silty argillite

#### Oil field 2

The collection of 8 West-Siberian rock samples (50×20 mm) of Oil field 2 are from Golchih and Abalak formations and were all drilled along a single well (*Table 8*). The Golchih and Abalak formations are composed of bituminous argillites with total organic carbon (TOC) of 2-6%.

**Table 8.** The collection of studied rocks from Oil field 2.

№ of sample	Formation	Lithology
1G	Golchih	bituminous argillite
2G	Golchih	bituminous argillite
3G	Golchih	bituminous argillite
4G	Golchih	bituminous argillite
5A	Abalak	bituminous argillite
6A	Abalak	bituminous argillite
7A	Abalak	bituminous argillite
8A	Abalak	bituminous argillite

### Oil field 3

The collection of 5 West-Siberian rock samples (50×20 mm) of Oil field 3 are from Bazhenov formation and were drilled along and perpendicular to a single well (*Table 9*). The Bazhenov formation is composed of clayey-siliceous and carbonaceous siliceous-clayey rocks with total organic carbon (TOC) of 3-14%.

**Table 9.** The collection of studied rocks from Oil field 3.

№ of sample	Formation	Axis direction of the cylinder to be drilled	Lithology
1B	Bazhenov	perpendicular	Clayey-siliceous
2B	Bazhenov	perpendicular	Clayey-siliceous
3B	Bazhenov	perpendicular	carbonaceous siliceous-clayey
4B	Bazhenov	parallel	Clayey-siliceous
5B	Bazhenov	perpendicular	Clayey-siliceous

### Oil field 4

The collection of 12 West-Siberian rock samples (50×20 mm) of Oil field 4 are from Bazhenov formation and were drilled along a single well (*Table 10*). The total organic carbon (TOC) of studied rocks is 5-8%.

**Table 10.** The collection of studied rocks from Oil field 4.

№ of sample	Formation	Lithology
1	Bazhenov	bituminous argillite
2	Bazhenov	bituminous argillite
3	Bazhenov	bituminous argillite
4	Bazhenov	bituminous argillite
5	Bazhenov	bituminous argillite
6	Bazhenov	bituminous argillite
7	Bazhenov	bituminous argillite
8	Bazhenov	bituminous argillite
9	Bazhenov	bituminous argillite
10	Bazhenov	bituminous argillite
11	Bazhenov	bituminous argillite
12	Bazhenov	bituminous argillite

### Oil field 5

The collection of 22 Volga-Ural rock samples (50×20 mm) are from Mendym, Domanic, Sargaev, and Timan formations, also along one well (*Table 11*). The Mendym formation (10 samples) is composed of dolomites, limestones, and clayey limestones, with TOC of 0.3-0.6%. The Domanic formation (7 samples) is composed of carbonaceous clayey limestones and siliceous

limestones, with TOC of 0.5-17.8%. The Sargaev formation (4 samples) consists of interbedded limestones and clayey limestones with TOC of 0.6-0.8%. And the Timan formation (1 sample) is represented by silty sandstone.

**Table 11.** The collection of studied rocks from Oil field 5.

№ of sample	Formation	Lithology
1Md	Mendym	Dolomite
2Md	Mendym	Dolomite
3Md	Mendym	Limestone
4Md	Mendym	Clayey limestone
5Md	Mendym	Limestone with fractures
6Md	Mendym	Limestone
7Md	Mendym	Limestone
8Md	Mendym	Clayey limestone
9Md	Mendym	Limestone with fractures
10Md	Mendym	Limestone
1Dm	Domanic	Clayey limestone
2Dm	Domanic	Clayey limestone
3Dm	Domanic	Limestone
4Dm	Domanic	Calcareous argillite
5Dm	Domanic	Calcareous argillite
6Dm	Domanic	Limestone
7Dm	Domanic	Limestone
1S	Sargaev	Limestone with fractures
2S	Sargaev	Limestone with fractures
3S	Sargaev	Limestone
4S	Sargaev	Clayey limestone
1Tm	Timan	Sandstone

#### 4.2.2 Results of measurements

##### Oil field 1

The thermal conductivity values of 6 rock samples from the Bazhenov (BF) and Abalak (AB) formations were measured with a TCS at room temperature and then with a DTC-300 instrument in a temperature range of 30-300 °C. The results of the measurements with the TCS are shown in *Table 12*. The BF and AB rocks have high variations in both thermal conductivity components: parallel to the bedding plane ( $\lambda_{||} = 2.08-2.73$  W/(m·K)) and perpendicular to the bedding plane ( $\lambda_{\perp} = 1.27-2.20$  W/(m·K)). Wide range of values of the thermal anisotropy coefficient (up to 1.79) and thermal heterogeneity factors ( $\beta_1 = 0.08-0.56$ ,  $\beta_2 = 0.04-0.15$ ) were established. High values of the heterogeneity factor  $\beta_1$  relative to  $\beta_2$  for the Bazhenov formation

are explained by the local development of organic matter along the sample with the sub-parallel layering of organic matter that has lower thermal conductivity (0.2-0.5 W/(m·K)) than that of the surrounding rock matrix (2.5-3.2 W/(m·K)). The marked contrast between the thermal conductivity of organic matter and the mineral matrix as well as the significant content of organic matter and its sub-layering distribution in samples have a major effect on thermal conductivity, heterogeneity, and thermal anisotropy of organic-rich rock samples (Popov et al., 2016a). High values of the thermal heterogeneity factor in the Bazhenov rock samples are related to high values and variations in TOC (3-15%) within the formation as well as within the rock samples.

Abalak rock samples are less heterogeneous than the Bazhenov rocks due to low variations of TOC (0-3%). TOC values for the rock samples were measured using a HAWK pyrolysis instrument (<http://www.wildcattechnologies.com>). Additional reasons for the high thermal anisotropy coefficient of Bazhenov and Abalak rocks are (1) sub-oriented layers of organic matter; and (2) oriented natural microcracks in the rocks and artificial microcracks caused by changes during core recovery from the well and further mechanical treatment of the core samples.

**Table 12.** Results of thermal property measurements of rock samples from Bazhenov and Abalak formations at room temperature with a TCS before measurements at elevated temperatures.

No sample	Rock type	$\lambda_{  }$ , W/(m·K)	$\lambda_{\perp}$ , W/(m·K)	K	$\beta_1$	$\beta_2$
Bazhenov formation						
3BF	Clayey-siliceous with lentils siltstone	2.22	2.20	1.00*	0.56	0.15
4BF	Clayey-siliceous	2.08	1.33	1.56	0.25	0.04
5BF	Clayey-siliceous	2.42	1.48	1.63	0.18	0.13
Abalak formation						
1AB	Silty argillite	2.28	1.27	1.79	0.09	0.10
2AB	Silty argillite	2.22	1.30	1.70	0.20	0.07
5AB	Silty argillite	2.73	1.55	1.77	0.08	0.09

\*All measurements of the thermal anisotropy coefficient in a range of 1.00-1.02 were approximated as 1.00 due to real uncertainty concerning measurements of the thermal conductivity components  $\lambda_{||}$  and  $\lambda_{\perp}$ .

Thermal conductivity measurements in the 30-300 °C range show curvilinear dependences of thermal conductivity on temperature along bedding ( $\lambda_{||}$ ) of rock samples from the Bazhenov and Abalak formations. *Figure 14* shows the percentage decrease of thermal conductivity of corresponding rocks at a particular temperature relative to the initial temperature  $T_0 = 30$  °C. As the temperature increases, thermal conductivity decreases and the average value of thermal

conductivity (for 6 studied samples) becomes lower than its value at 30 °C by 3-5% at 100 °C and 5-14% at 300 °C. However, the thermal conductivity change with temperature for sample 3BF is unique: average thermal conductivity at 100 °C and 300 °C is respectively 6% and 25% lower than its value at 30 °C. Such a sharp decrease of thermal conductivity with temperature can be explained by the presence of quartz grains with a size of ~0.1 mm in this sample as the thermal conductivity of quartz decreases by 30% at 100 °C and 50% at 300 °C (Clauser, 2006). Scattering the data of the sample 1AB compare to the other samples does not exceed the measurement error (*Chapter 3.1.1.1*) and, probably, explained by the increased volume of clay minerals: endothermic reactions in clay minerals around 130-190 °C (Milner, 1962) may decrease measured thermal conductivity due to features of the measurement technique. The increment values within the temperature range of 240-300 °C can be seen for two AB samples from three AB samples: 1AB and 2AB. Although the effect of increment values does not exceed the measurement error essentially (*Chapter 3.1.1.1*), this fact could correspond to specific peculiarities of the AB rock samples studied.

*Figure 15* shows curves that relate average thermal conductivity to temperature for the Bazhenov and Abalak samples in the 30-300 °C temperature range. Equations that relate thermal conductivity to temperature for each formation are shown in *Table 19*. The equation for sample 3BF is shown separately due to its unique behavior. Correction for change in the structure of the rock samples during heating (due to the appearance of cracks) was carried out using thermal conductivity data obtained with the TCS after heating. Considering that thermal conductivity changes are related to the appearance of cracks after heating the difference between thermal conductivity before and after heating obtained with TCS was included as correction for results (obtained with DTC-300) shown in *Figure 15*. Correction of experimental data at high temperatures using the TCS data was made by steps described in *Chapter 3.1.2*. The correction was applied to the curves for each formation (*Figure 15*, dashed line) by taking account of the average change in thermal conductivity ( $\lambda_{||}$ ) after heating (*Table 13*), as measured by the TCS.

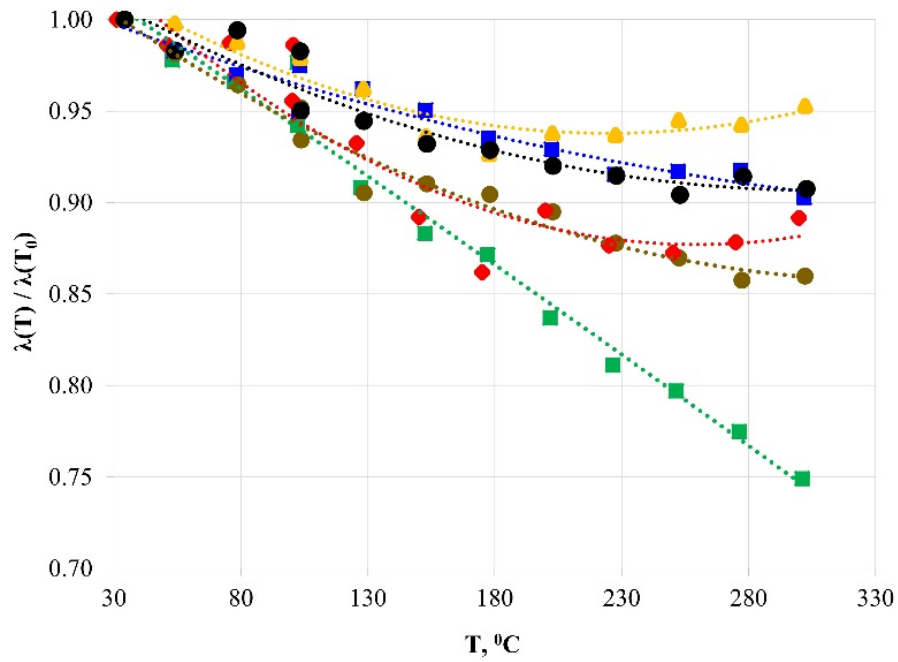


**Figure 14.** Thermal conductivity decrease for rock samples from the Bazhenov and Abalak formations in the 30-300 °C temperature range. Different colors refer to different rock samples:  $\blacklozenge$  – 1AB,  $\blacktriangle$  – 2AB,  $\bullet$  – 5AB,  $\blacksquare$  – 3BF,  $\blacksquare$  – 4BF,  $\bullet$  – 5BF.

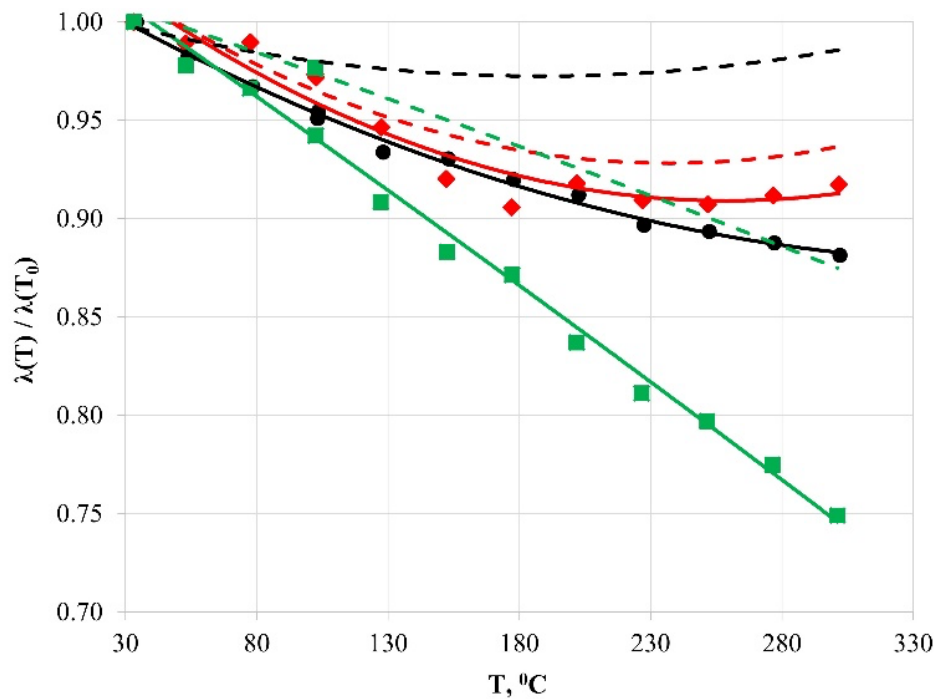


**Figure 15.** Curves drawn on a scatter diagram of average thermal conductivity change with temperature for rock samples from different formations:  $\blacklozenge$  – Abalak formation,  $\bullet$  – Bazhenov formation,  $\blacksquare$  – sample 3BF from the Bazhenov formation, - - correction for the Bazhenov formation, - - correction for the Abalak formation, - - correction for sample 3BF from the Bazhenov formation.

**Table 13.** TCS measurements of thermal properties of Bazhenov and Abalak samples at room temperature after heating to 300 °C and subsequent cooling.

No sample	$\lambda_{  }$ after heating, W/(m·K)	$\lambda_{\perp}$ after heating, W/(m·K)	Variations in $\lambda_{  }$ after heating to 300 °C, %	Variations in $\lambda_{\perp}$ after heating to 300 °C, %	K after heating to 300 °C	Variations in K after heating to 300 °C, %	$\beta_1$ after heating to 300 °C	$\beta_2$ after heating to 300 °C	Absolute difference in $\beta_1$ after heating to 300 °C	Absolute difference in $\beta_2$ after heating to 300 °C
Bazhenov formation										
3BF	1.93	1.87	-13.0	-15	1.03	2.2	0.55	0.12	0.01	0.03
4BF	1.87	1.14	-10.1	-14.3	1.64	5.2	0.19	0.11	0.06	-0.07
5BF	2.16	1.00	-10.7	-32.4	2.16	32.5	0.19	0.13	-0.01	0
Abalak formation										
1AB	2.29	1.18	0.4	-7.1	1.94	8.4	0.09	0.10	-	-
2AB	1.96	0.97	-11.7	-25.4	2.02	18.9	0.14	0.07	0.06	0
5AB	2.84	1.45	4.0	-6.5	1.96	10.7	0.08	0.06	0	0.03
Average	2.18	1.27	-6.9	-16.8	1.78	13.0	0.21	0.10	0.02	0.00

Analysis of the change in thermal conductivity of BF and AB rock samples after heating to 300 °C and subsequent cooling to room temperature was based on measurements using a TCS instrument (*Table 13*). After completion of measurements using the DTC-300, all samples were studied again with the TCS to determine thermal conductivity components for the same directions as were gauged before the high-temperature measurements. The comparison results presented in *Tables 12-13* show that thermal conductivity parallel to bedding decreases by 7% on average and changes in thermal conductivity perpendicular to bedding ( $\lambda_{\perp}$ ) are more pronounced, averaging 17%. The thermal anisotropy coefficient increases by 13% on average after heating to 300 °C for the Bazhenov and Abalak samples. This behavior is explained by the presence of additional microcracks after heating to 300 °C. All changes are related to loss of intergranular contact and thermal resistance during heating. The absolute difference in thermal heterogeneity of the rock samples after heating showed small changes of 0.07 on average. A slight increase of thermal conductivity after measurements at elevated temperatures is observed due to the displacement of the scanning line for heterogeneous rock samples relative to scanning before the high-temperature measurements.

## Oil field 2

The thermal conductivity of 8 rock samples from the Golchih (GF) and Abalak (AB) formations from Oil field 2 was measured with a TCS at room temperature and then with a DTC-300 instrument in a temperature range of 30-300 °C. The results of the measurements with the TCS are shown in *Table 14*. The GF and AB rocks have low variations in both thermal conductivity components: parallel to the bedding plane ( $\lambda_{||} = 1.39-1.49$  W/(m·K)) and perpendicular to the bedding plane ( $\lambda_{\perp} = 1.21-1.51$  W/(m·K)). A low range of values of the thermal anisotropy

coefficient (up to 1.05) and thermal heterogeneity factors ( $\beta_1 = 0.08-0.17$ ,  $\beta_2 = 0.09-0.17$ ) were established.

**Table 14.** Results of thermal property measurements of rock samples from Golchih and Abalak formations at room temperature with a TCS before measurements at elevated temperatures.

No sample	$\lambda_{  }$ , W/(m·K)	$\lambda_{\perp}$ , W/(m·K)	K	$\beta_1$	$\beta_2$
1G	1.39	1.36	1.02	0.16	0.17
2G	1.27	1.21	1.05	0.17	0.13
3G	1.23	1.21	1.01	0.09	0.12
4G	1.40	1.40	1.00	0.08	0.09
5A	1.41	1.39	1.02	0.15	0.10
6A	1.39	1.35	1.03	0.12	0.09
7A	1.49	1.51	1.00	0.09	0.12
8A	1.45	1.42	1.02	0.11	0.13

Thermal conductivity measurements in the 30-300 °C range show curvilinear dependences of thermal conductivity on temperature along bedding ( $\lambda_{||}$ ) of rock samples from the Golchih and Abalak formations (*Figure 16*). *Figure 17* shows the percentage decrease of thermal conductivity of corresponding rocks at a particular temperature relative to the initial temperature  $T_0 = 30$  °C. As the temperature increases, thermal conductivity decreases and the average value of thermal conductivity (for 8 studied samples) becomes lower than its value at 30 °C by 1-5% at 100 °C and 5-25% at 300 °C.

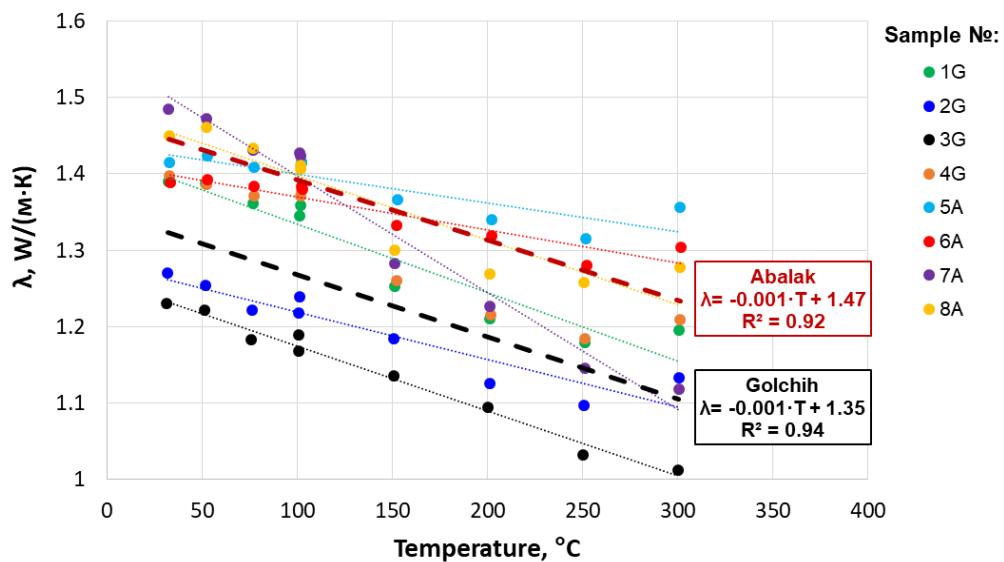


**Figure 16.** Changes in thermal conductivity for rock samples of the Golchih and Abalak formations of oil field 2 with increasing temperature. Black dotted line - curve obtained by averaging thermal conductivity over all rock samples of the Golchih formation; brown dotted line - curve obtained by averaging thermal conductivity over all rock samples of the Abalak formation.

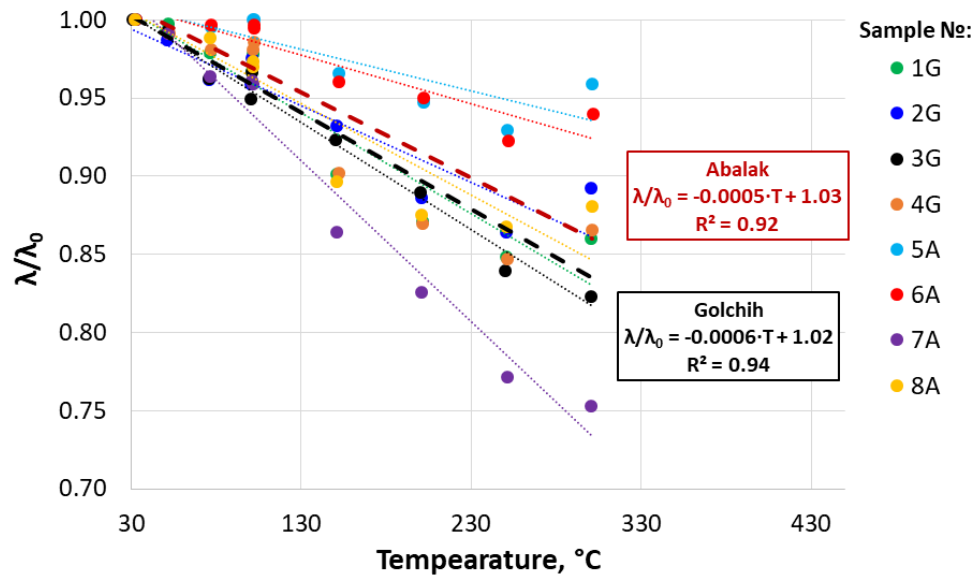


**Figure 17.** Relative change in thermal conductivity for rock samples from the Golchih and Abalak formations of oil field 2 with increasing temperature. Black dotted line - curve obtained by averaging the relative change in thermal conductivity for all rock samples of the Golchih formation; brown dotted line - curve obtained by averaging the relative change in thermal conductivity for all rock samples of the Abalak formation.

The comparison results presented in *Tables 14-15* show that thermal conductivity parallel and perpendicular to bedding decreases by 15% on average. The thermal anisotropy coefficient increases by 2% on average after heating to 300 °C for the Gochih and Abalak samples.

**Table 15.** TCS measurements of thermal properties of Golchih and Abalak samples at room temperature after heating to 300 °C and subsequent cooling.

№	$\lambda_{  }$ after heating, W/(m·K)	$\lambda_{\perp}$ after heating, W/(m·K)	Variations in $\lambda_{  }$ after heating to 300 °C, %	Variations in $\lambda_{\perp}$ after heating to 300 °C, %	K after heating to 300 °C	Variations in K after heating to 300 °C, %	$\beta_1$ after heating to 300 °C	$\beta_2$ after heating to 300 °C	Absolute difference in $\beta_1$ after heating to 300 °C	Absolute difference in $\beta_2$ after heating to 300 °C
1G	1.18	1.14	-15	-17	1.03	2	0.21	0.15	33	-11
2G	1.06	1.04	-17	-14	1.01	-3	0.23	0.16	33	20
3G	1.01	1.00	-17	-18	1.01	0	0.08	0.11	-18	-11
4G	1.24	1.19	-12	-15	1.04	4	0.14	0.09	63	6
5A	1.18	1.15	-17	-17	1.02	0	0.15	0.13	-1	29
6A	1.22	1.15	-12	-15	1.07	3	0.13	0.14	4	57
7A	1.32	1.24	-11	-18	1.07	8	0.08	0.13	-13	5
8A	1.28	1.27	-12	-11	1.00	-2	0.17	0.14	50	7

Thermal conductivity of the rock samples of the Golchih formation decreases by an average of 9% relative to the thermal conductivity at an initial temperature of 30 °C when the temperature rises to 150 °C; for the rocks of the Abalak formation, the decrease in thermal conductivity is 8%.

### Oil field 3

The thermal conductivity of 5 rock samples from the Bazhenov formation (BF) from Oil field 3 was measured with a TCS at room temperature and then with a DTC-300 instrument in a temperature range of 30-300 °C. The results of the measurements with the TCS before and after heating are shown in *Table 16*. The BF rocks have high variations in thermal conductivity perpendicular to the bedding plane ( $\lambda_{\perp}$  = 0.84-1.91 W/(m·K)).

**Table 16.** TCS measurements of thermal properties of Bazhenov formation samples at room temperature after heating to 300 °C and subsequent cooling.

No sample	$\lambda_{\perp}$ , W/(m·K)	$\lambda_{\perp}$ after heating, W/(m·K)	Variations in $\lambda_{\perp}$ after heating to 300 °C, %
1B	0.84	0.81	-4
2B	1.00	0.88	-11
3B	1.76	1.74	-1
4B	1.60	1.43	-1
5B	1.91	1.65	-13

Thermal conductivity measurements in the 30-300 °C range show curvilinear dependences of thermal conductivity on temperature perpendicular to bedding ( $\lambda_{\perp}$ ) of rock samples from the Bazhenov formations (*Figure 18*). *Figure 19* shows the percentage decrease of thermal conductivity of corresponding rocks at a particular temperature relative to the initial temperature  $T_0 = 30$  °C. As the temperature increases, thermal conductivity decreases and the average value of thermal conductivity (for 5 studied samples) becomes lower than its value at 30 °C by 0-2% at 100 °C and 5-20% at 300 °C.

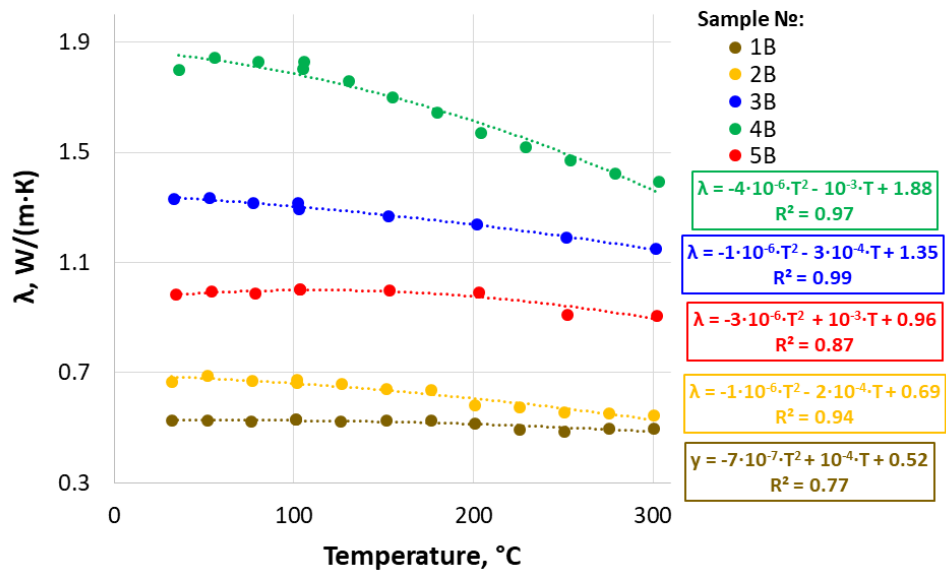


**Figure 18.** Changes in thermal conductivity for rock samples of Bazhenov formations of oil field 3 with increasing temperature.

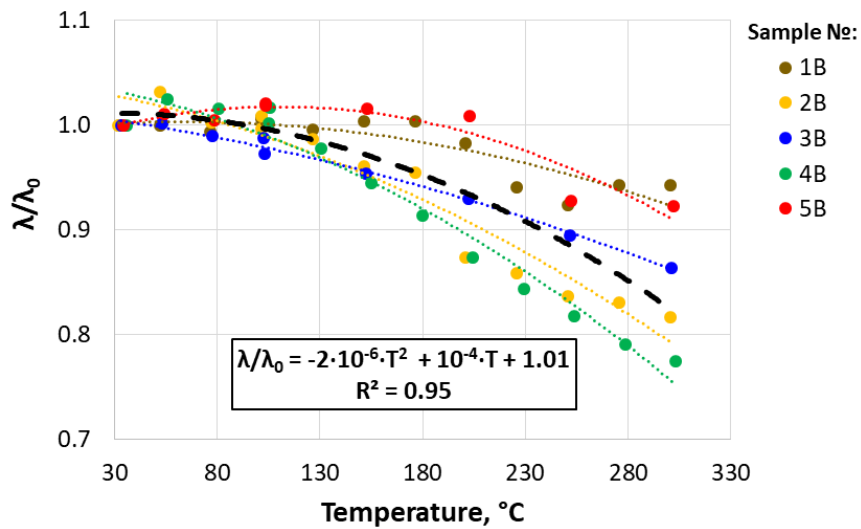


**Figure 19.** Relative change in thermal conductivity for rock samples from the Bazhenov formation of oil field 3 with increasing temperature. Black dotted line - curve obtained by averaging the relative change in thermal conductivity for all rock samples of the Bazhenov formation.

The comparison results presented in *Table 16* show that thermal conductivity perpendicular to bedding decreases by 6% on average after heating. The thermal conductivity of the rock samples of the Bzhenov formation decreases by an average of 13% relative to the thermal conductivity at an initial temperature of 30 °C when the temperature rises to 300 °C.

#### Oil field 4

The thermal conductivity of 12 rock samples from the Bazhenov formation from Oil field 4 was measured with a DTC-300 instrument in a temperature range of 30-300 °C. Thermal conductivity measurements in the 30-300 °C range show curvilinear dependences of thermal conductivity on temperature perpendicular to bedding ( $\lambda_{\perp}$ ) of rock samples from the Bazhenov formations (Figure 20). Figure 21 shows the percentage decrease of thermal conductivity of corresponding rocks at a particular temperature relative to the initial temperature  $T_0 = 30$  °C. As the temperature increases, thermal conductivity decreases and the average value of thermal conductivity (for 12 studied samples) becomes lower than its value at 30 °C by 0-5% at 100 °C and 1-6% at 300 °C.

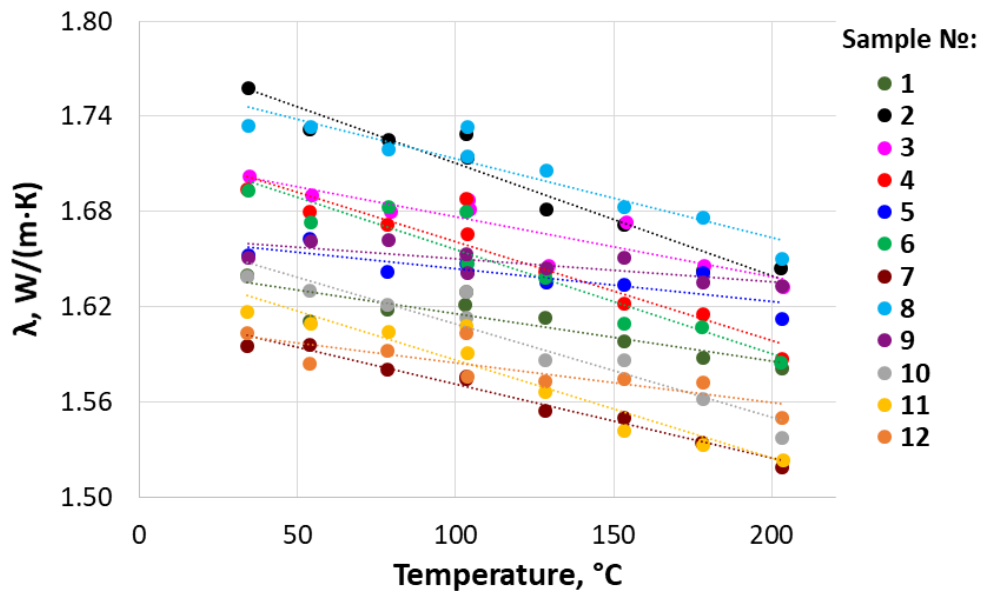


**Figure 20.** Changes in thermal conductivity for rock samples of Bazhenov formations of oil field 4 with increasing temperature.

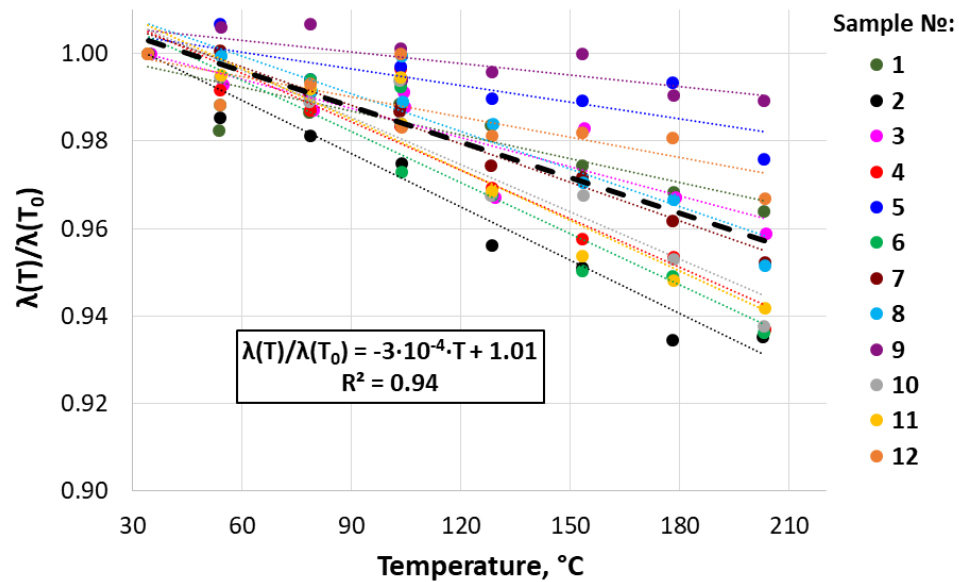


**Figure 21.** Relative change in thermal conductivity for rock samples from the Bazhenov formation of oil field 4 with increasing temperature. Black dotted line - curve obtained by averaging the relative change in thermal conductivity for all rock samples of the Bazhenov formation.

### Oil field 5

Thermal conductivity measurements on 22 rock samples from formations in Russia's Volga-Ural region were carried out using the DTC-300 instrument in a temperature range of 30-300 °C. Results of thermal property measurements with the TCS before heating of the samples (*Table 17*) showed significant variations of thermal conductivity of samples from the Mendym formation (2.30-3.74 W/(m·K)), which is related to the presence of dolomites (samples 1Md, 2Md). Thermal conductivity of dolomites is 1.2-1.4 times higher than that of limestones, due to the presence of rock-forming dolomite and calcite minerals with higher thermal conductivity (thermal conductivity of dolomite single crystal is 5.7-6.3 W/(m·K), the thermal conductivity of calcite single crystal is 3.35-3.50 W/(m·K)) (Popov et al., 1987). Variations of the thermal anisotropy coefficient were up to 1.20 for samples from the Mendym, Domanic, and Sargaev formations, and 1.53 for the sample from the Timan formation. Variations of the thermal heterogeneity coefficient were 0.07-0.22 for samples from the Mendym, Sargaev, and Timan formations and 0.08-0.48 for the Domanic samples. The high thermal heterogeneity coefficient of the Domanic rocks is related to essential lithological heterogeneity and significant variations of organic matter in the rock samples (from a few millimeters to tens of centimeters).

**Table 17.** TCS measurements of thermal properties of Mendym, Domanic, Sargaev, and Timan samples at room temperature before measurements at high temperatures.

№ sample	Rock type	$\lambda_{  }$ , W/(m·K)	$\lambda_{\perp}$ , W/(m·K)	K	$\beta_1$	$\beta_2$
Mendym formation						
1Md	Dolomite	3.74	3.13	1.20	0.12	0.16
2Md	Dolomite	3.40	3.16	1.07	0.11	0.09
3Md	Limestone	2.55	2.55	1.00	0.10	0.09
4Md	Clayey limestone	2.39	2.39	1.00	0.13	0.10
5Md	Limestone with fractures	2.40	2.40	1.00	0.21	0.13
6Md	Limestone	2.39	2.38	1.00	0.07	0.07
7Md	Limestone	2.45	2.43	1.00	0.11	0.14
8Md	Clayey limestone	2.37	2.20	1.08	0.09	0.09
9Md	Limestone with fractures	2.30	1.98	1.16	0.18	0.21
10Md	Limestone	2.44	2.42	1.00	0.08	0.06
Domanic formation						
1Dm	Clayey limestone	2.29	2.29	1.00	0.08	0.11
2Dm	Clayey limestone	2.39	2.39	1.00	0.15	0.10
3Dm	Limestone	2.58	2.58	1.00	0.30	0.14
4Dm	Calcareous argillite	2.69	2.28	1.18	0.16	0.48
5Dm	Calcareous argillite	2.31	2.21	1.05	0.30	0.30
6Dm	Limestone	2.42	2.36	1.03	0.13	0.12
7Dm	Limestone	2.48	2.32	1.07	0.12	0.12
Sargaev formation						
1S	Limestone with fractures	2.76	2.59	1.07	0.09	0.11
2S	Limestone with fractures	2.49	2.44	1.00	0.22	0.10
3S	Limestone	2.33	2.01	1.16	0.18	0.13
4S	Clayey limestone	2.34	2.00	1.17	0.15	0.11
Timan formation						
1Tm	Sandstone	3.40	2.23	1.53	0.15	0.15

Figures 22, 23, 24, 25 show a percentage decrease of thermal conductivity of rocks from the Mendym, Domanic, Sargaev, and Timan formations at a particular temperature relative to the initial temperature ( $T_0 = 30\text{ }^{\circ}\text{C}$ ). The average decrease of thermal conductivity for rock samples from the Mendym formation at 100 °C and 300 °C relative to room temperature is 9% and 23% respectively; for the Domanic rock samples it is 10% and 24%; for the Sargaev samples, 8% and 20%; and 10% and 27% for the Timan sample. The lowest decrease of thermal conductivity in the 30-300 °C temperature range is observed for the Sargaev sample 4S and Mendym sample 4Md and

is related to the high clay content in these samples. *Figures 26, 27* show curves of thermal conductivity change averaged for different lithotypes and formations in the 30-300 °C temperature range. *Figure 26, Table 19* show three curves with similar average thermal conductivity behavior at 30-300 °C for the following types: clayey limestones (determination coefficient  $R^2 = 0.92$ ); limestones and argillites ( $R^2 = 0.89$ ); and dolomites and sandstone ( $R^2 = 0.97$ ). Correction for changing structure of samples during heating was applied to the curves as described above for the Abalak and Bazhenov formations (*Figure 27*, dashed lines).

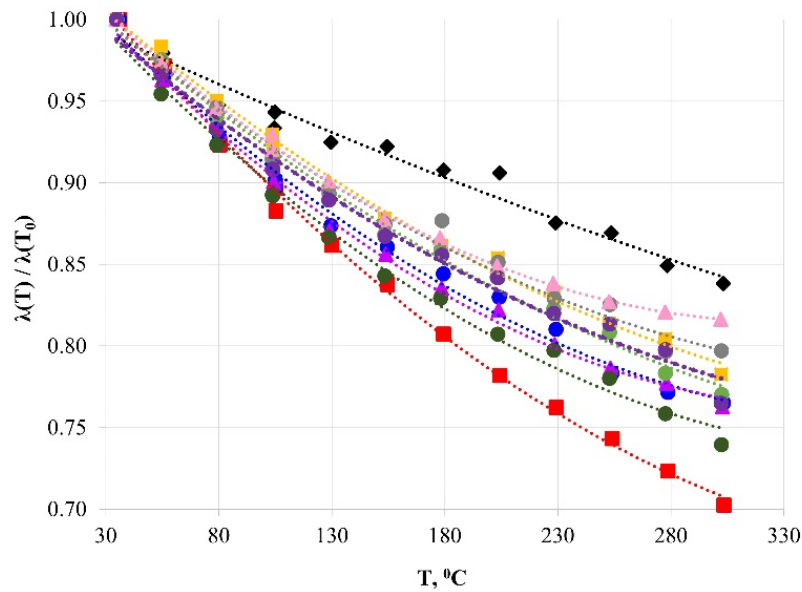


**Figure 22.** Curves drawn on the thermal conductivity-temperature scatter diagram for Mendym samples (■ – 1Md, ● – 2Md, ▲ – 3Md, ◆ – 4Md, ■ – 5Md, ● – 6Md, ● – 7Md, ● – 8Md, ▲ – 9Md, ● – 10Md) in the 30-300 °C temperature range.

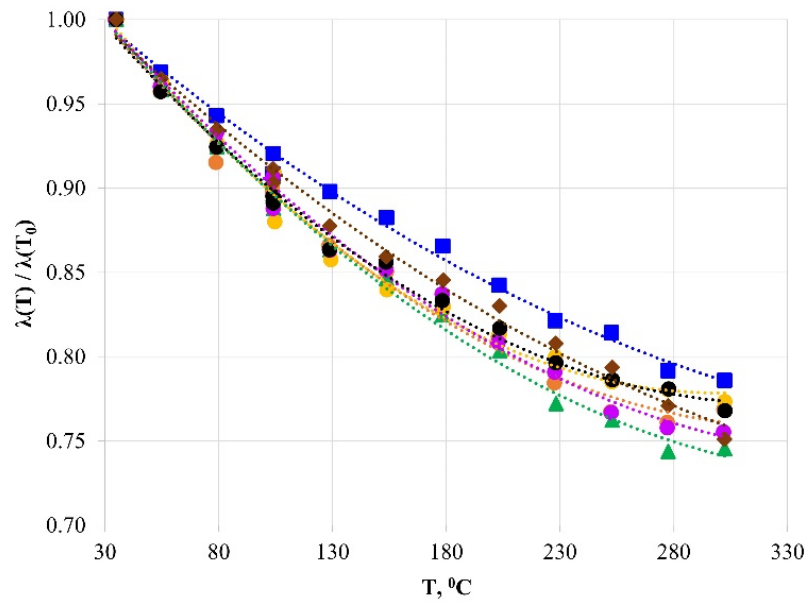


**Figure 23.** Curves lines drawn on the thermal conductivity-temperature scatter diagram for Domanic samples (■ – 1Dm, ○ – 2Dm, ▲ – 3Dm, ● – 4Dm, ● – 5Dm, ● – 6Dm, ◆ – 7Dm) in the 30-300 °C temperature range.

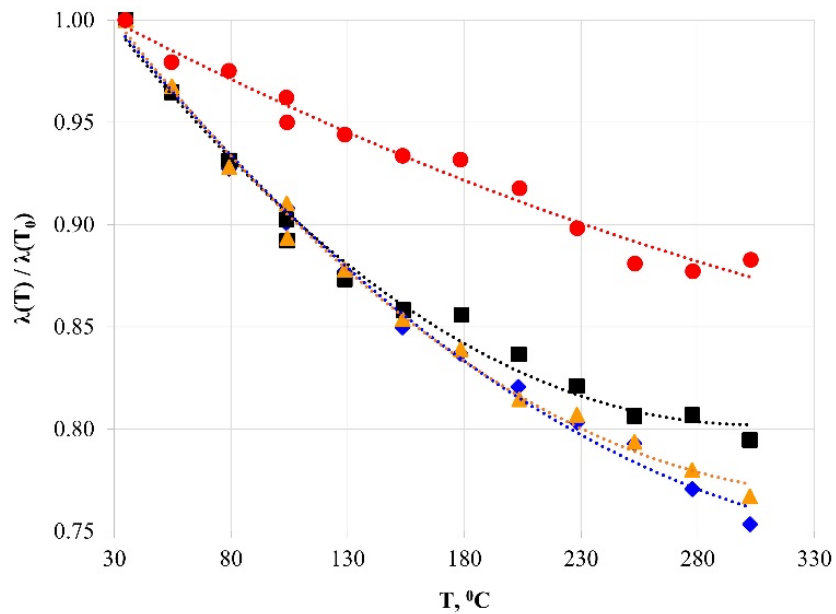


**Figure 24.** Curves lines drawn on the thermal conductivity-temperature scatter diagram for Sargaev samples (◆ – 1S, ■ – 2S, ▲ – 3S, ● – 4S) in the 30-300 °C temperature range.

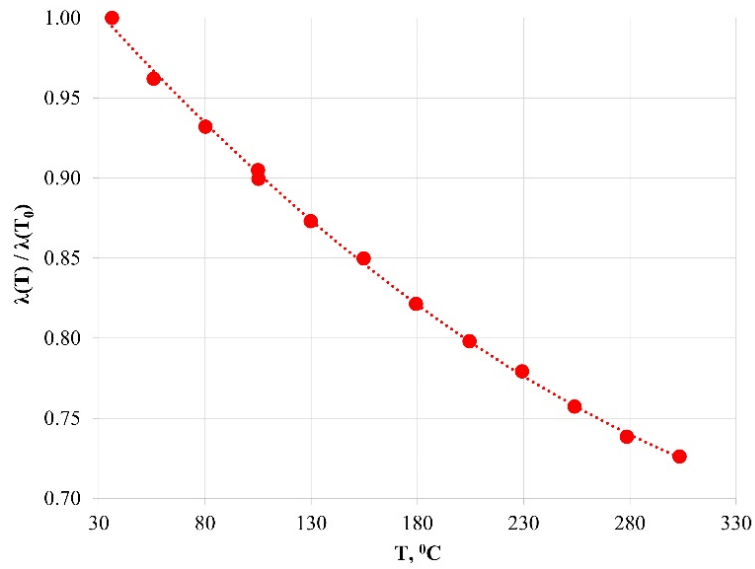


**Figure 25.** The curve drawn on the thermal conductivity-temperature scatter diagram for the Timan sample (Tm) in the 30-300 °C temperature range.

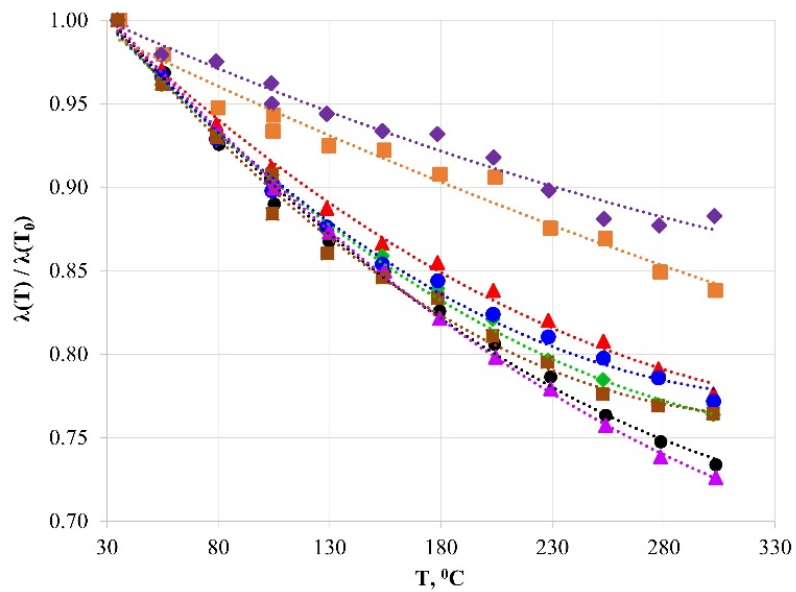


**Figure 26.** Curves drawn on the average thermal conductivity- temperature scatter diagram for lithotypes from different formations in the 30-300 °C temperature range. Different colors are related to different lithotypes: ● – dolomites (Mendym), ▲ – limestones (Mendym), ◆ – limestones (Domanic), ● – limestones (Sargaev), ▲ – sandstone (Timan), ■ – argillites (Domanic), ■ – clayey limestones (Mendym), ◆ – clayey limestones (Sargaev).

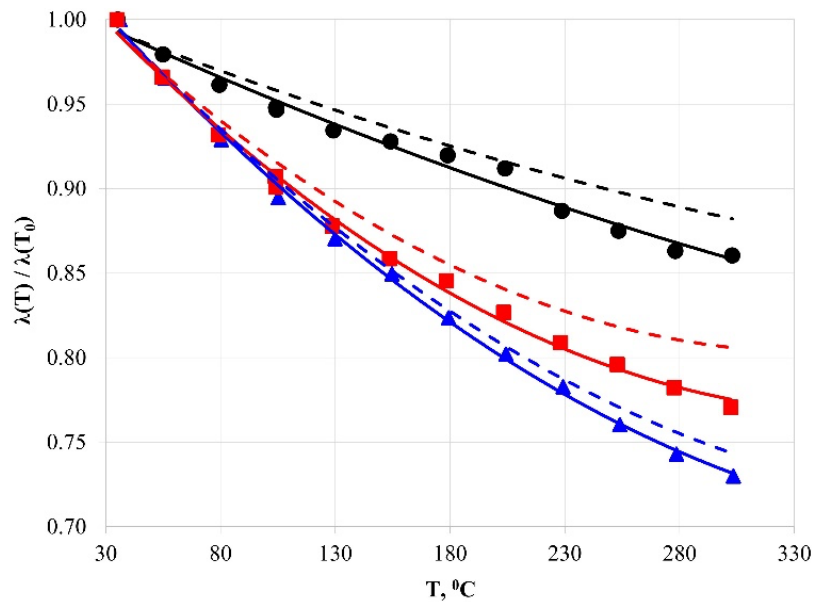


**Figure 27.** Curves drawn on the average thermal conductivity- temperature scatter diagram for different lithotypes from different formations (● – clayey limestones, ▲ – dolomites and sandstones, ■ – limestones and argillites, - - clayey limestones with correction, - - dolomites and sandstones with correction, - - limestones and argillites with correction) in the 30-300 °C temperature range.

After thermal conductivity measurements with the DTC-300 instrument at high temperatures, all samples from the Mendym, Domanic, Sargaev, and Timan formations were studied again with the TCDS to gauge thermal conductivity components for the same directions as had been studied before the high-temperature measurements (*Table 18*). The comparison results in *Tables 17 and 18* show that the thermal conductivity components ( $\lambda_{\parallel}$ ,  $\lambda_{\perp}$ ) decrease by 2-3% on average and that the thermal anisotropy coefficient was almost unchanged (~1%) after heating to 300 °C. Significant change of thermal properties after heating for samples 9Md and 10Md from the Mendym formation, 3Dm and 6Dm from the Domanic formation, and 4S from the Sargaev formation is related to the presence of numerous fractures in these samples. *Figures 28a, b* show photographs of one of the Bazhenov samples before and after heating to 300 °C. The cracks oriented along the bedding are a change induced by the high temperatures.



**Figure 28.** A Bazhenov sample before heating (a) and after heating to 300 °C (b).

**Table 18.** TCS measurements of thermal properties after heating to 300 °C and subsequent cooling of Mendym, Domanic, Sargaev, and Timan samples.

№	$\lambda_{  }$ after heating, W/(m·K)	$\lambda_{\perp}$ after heating, W/(m·K)	Variations in $\lambda_{  }$ after heating to 300 °C, %	Variations in $\lambda_{\perp}$ after heating to 300 °C, %	K after heating to 300 °C, room temperature	Variations in K after heating to 300 °C, %	$\beta_1$ after heating to 300 °C	$\beta_2$ after heating to 300 °C	Absolute difference in $\beta_1$ after heating to 300 °C	Absolute difference in $\beta_2$ after heating to 300 °C
Mendym formation										
1Md	3.60	3.14	-3.7	0.3	1.15	-4.2	0.15	0.12	0.03	-0.04
2Md	3.24	3.02	-4.7	-4.4	1.07	0.0	0.15	0.12	0.04	0.03
3Md	2.62	2.57	2.7	0.8	1.00	0.0	0.10	0.11	0	0.02
4Md	2.46	2.43	2.9	1.7	1.00	0.0	0.09	0.10	-0.04	0
5Md	2.39	2.29	-0.4	-4.6	1.04	4.0	0.21	0.12	0	-0.01
6Md	2.35	2.28	-1.7	-4.2	1.03	3.0	0.08	0.10	0.01	0.03
7Md	2.26	2.20	-7.8	-9.5	1.03	2.0	0.12	0.15	0.01	0.01
8Md	2.25	2.13	-5.1	-3.2	1.06	-1.9	0.10	0.11	0.01	0.02
9Md	2.34	1.90	1.7	-4.0	1.23	6.2	0.19	0.12	0.01	-0.09
10Md	2.39	2.08	-2.0	-14.0	1.15	13.9	0.12	0.10	0.04	0.04
Domanic formation										
1Dm	2.19	2.19	-4.4	-4.4	1.00	0.0	0.11	0.09	0.03	-0.02
2Dm	2.21	2.21	-7.5	-7.5	1.00	0.0	0.12	0.11	-0.03	0.01
3Dm	2.56	2.56	-0.8	-0.8	1.00	0.0	0.23	0.15	-0.07	0.01
4Dm	2.58	2.20	-4.1	-3.5	1.17	-0.6	0.41	0.11	0.25	-0.37
5Dm	2.14	2.03	-7.4	-8.1	1.05	0.0	0.38	0.23	0.08	-0.07
6Dm	2.40	2.40	-0.8	1.7	1.00	-2.9	0.10	0.12	-0.03	0
7Dm	2.19	2.19	-11.7	-5.6	1.00	-6.5	0.19	0.11	0.07	-0.01
Sargaev formation										
1S	2.68	2.46	-2.9	-5.0	1.09	1.9	0.09	0.09	0	-0.02
2S	2.37	2.31	-4.8	-5.3	1.03	1.0	0.16	0.12	-0.06	0.02
3S	2.43	2.11	4.3	5.0	1.15	-0.9	0.17	0.13	-0.01	0
4S	2.16	2.02	-7.7	1.0	1.07	-8.5	0.15	0.12	0	0.01
Timan formation										
1Tm	3.56	2.31	4.7	3.6	1.54	0.7	0.16	0.22	0.01	0.07
Average	2.52	2.35	-2.8	-1.5	1.07	-1.3	0.16	0.13	0.02	-0.02

### 4.2.3 Equations that relate thermal conductivity to temperature for unconventional reservoir rocks

Comparison of thermal conductivity behavior with temperature for organic-rich samples from different formations shows that equations vary with formations and lithotypes. All of the equations with determination coefficients, root mean square error (RMSE), and the number of studied samples are shown in *Table 19*. It should be noted that these equations are correct only for the studied temperature range (30-300 °C) and their extrapolation to predict the thermal conductivity of oil shales, in general, could lead to serious error (Rajeshwar et al., 1979).

**Table 19.** Equations which relate average thermal conductivity to temperature in the 30-300 °C temperature range for studied lithotypes from different formations.

Formation	Lithotype	Equations	R <sup>2</sup>	RMSE	Number of studied samples
Bazhenov	Clayey-siliceous with lentils siltstone	$\lambda(T)/\lambda(T_0) = -10^{-7} \cdot T^2 - 4 \cdot 10^{-4} \cdot T + 1.02$	0.98	0.01	1
	Clayey-siliceous	$\lambda(T)/\lambda(T_0) = 10^{-6} \cdot T^2 - 4 \cdot 10^{-4} \cdot T + 1.01$	0.75	0.02	2
		$\lambda(T)/\lambda(T_0) = -2 \cdot 10^{-6} \cdot T^2 + 10^{-4} \cdot T + 1.01$	0.95	0.01	5
	Bituminous argillite	$\lambda(T)/\lambda(T_0) = -3 \cdot 10^{-4} \cdot T + 1.01$	0.94	0.01	12
Golchih	Bituminous argillite	$\lambda(T)/\lambda(T_0) = -6 \cdot 10^{-4} \cdot T + 1.02$	0.94	0.01	4
Abalak	Silty argillite	$\lambda(T)/\lambda(T_0) = 2 \cdot 10^{-6} \cdot T^2 - 10^{-3} \cdot T + 1.05$	0.69	0.02	3
	Bituminous argillite	$\lambda(T)/\lambda(T_0) = -5 \cdot 10^{-4} \cdot T + 1.03$	0.92	0.01	4
Mendym, Domanic, Sargaev, Timan	Clayey limestone	$\lambda(T)/\lambda(T_0) = 4 \cdot 10^{-7} \cdot T^2 - 6 \cdot 10^{-4} \cdot T + 1.01$	0.92	0.01	2
	Argillite, limestone	$\lambda(T)/\lambda(T_0) = 2 \cdot 10^{-6} \cdot T^2 - 15 \cdot 10^{-4} \cdot T + 1.04$	0.89	0.02	16
	Dolomite, sandstone	$\lambda(T)/\lambda(T_0) = 2 \cdot 10^{-6} \cdot T^2 - 16 \cdot 10^{-4} \cdot T + 1.05$	0.97	0.02	3

### 4.2.4 Changes in thermal conductivity of unconventional reservoir rocks during heating and cooling

For determining the temperature range on which changes in samples structure appeared a number of experiments were provided on 5 samples from oil field 2. The thermal conductivity of 5 samples was measured in the temperature range 30-300 °C during heating and cooling. The results are shown in *Figure 29*. The thermal conductivity of rock samples during a cooling cycle is decreasing in the temperature range of 150-200 °C that is related to structural changes in the sample.

Changes in thermal properties of unconventional reservoir rocks from 5 oil fields before and after heating are shown in *Table 20*. The decrease of thermal conductivity parallel to bedding

after heating is 2-15%, the decrease of thermal conductivity perpendicular to bedding after heating is 1-20%. Variations in thermal conductivity anisotropy can reach 13%.

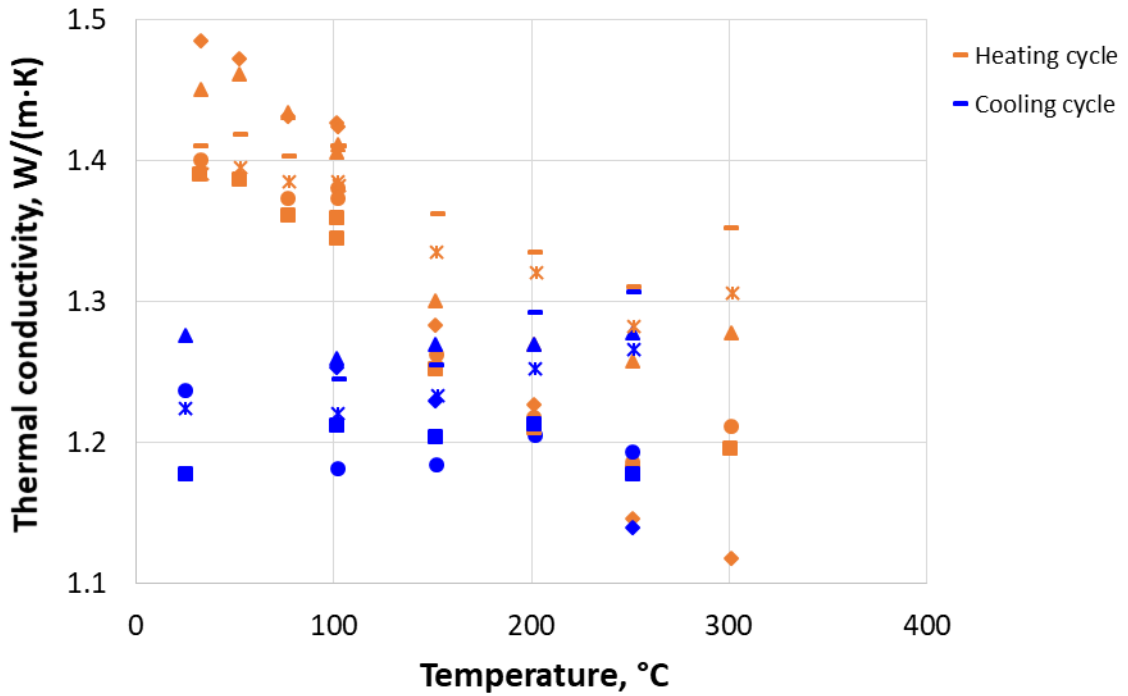


**Figure 29.** Thermal conductivity values of Golchih and Abalak formations rocks measured with the DTC-300 instrument during heating and cooling.

**Table 20.** Changes in thermal properties of unconventional reservoir rocks from 5 oil fields before and after heating.

Oil field	Formation	$\delta\lambda_{  }$ , %	$\delta\lambda_{\perp}$ , %	$\delta K$ , %
1	Bazhenov	-11	-20	13
	Abalak	-5	-14	13
2	Golchih	-15	-16	1
	Abalak	-15	-15	2
3	Bazhenov	-	-6	-
5	Mendym	-2	-4	2
	Domanic	-5	-4	-1
	Sargaev	-3	-1	-2
	Timan	5	4	1

#### **4.1.1 Analysis of thermal conductivity with temperature characteristic of unconventional reservoir rocks in comparison with other sedimentary rocks**

The results of thermal conductivity measurements of unconventional reservoir rocks at elevated temperatures showed that the percentage of thermal conductivity decreasing is much lower than for other sedimentary rocks (*Figure 30*). These results agree with the experimental data for bituminous argillites from Bazhenov formations obtained earlier by Sokolova et al. (1986) where average thermal conductivity at 100-130 °C was found to be 10% lower than its value at room temperature. The decrease in thermal conductivity of Bazhenov rocks is much lower than in other sedimentary rock samples (sandstones, sands, siltstones), which show 10-15% reduction of thermal conductivity at 100 °C (Popov et al., 2013). This anomalously low decrease of thermal conductivity of organic-rich samples was also observed for other formations (Green River, Devonian) shown in *Table 1* (Prats and O'Brien, 1975; Rajeshwar et al., 1980). The effect is related to the presence of organic matter in the studied rock samples. Organic matter is an amorphous substance, the thermal conductivity of which increases with temperature (Chudnovsky, 1962; Yudin et al., 2015). So, the presence of organic matter in a sample limits the decrease of thermal conductivity as temperature increases. This was also demonstrated by measurements of thermal conductivity when temperature increases in shale samples with various oil yields from the Green River formation. The greater the oil yield in a shale sample, the less the decrease of thermal conductivity with temperature, and thermal conductivity even become constant for samples with high oil yield (27-82 gal/t) (Rajeshwar et al., 1980).

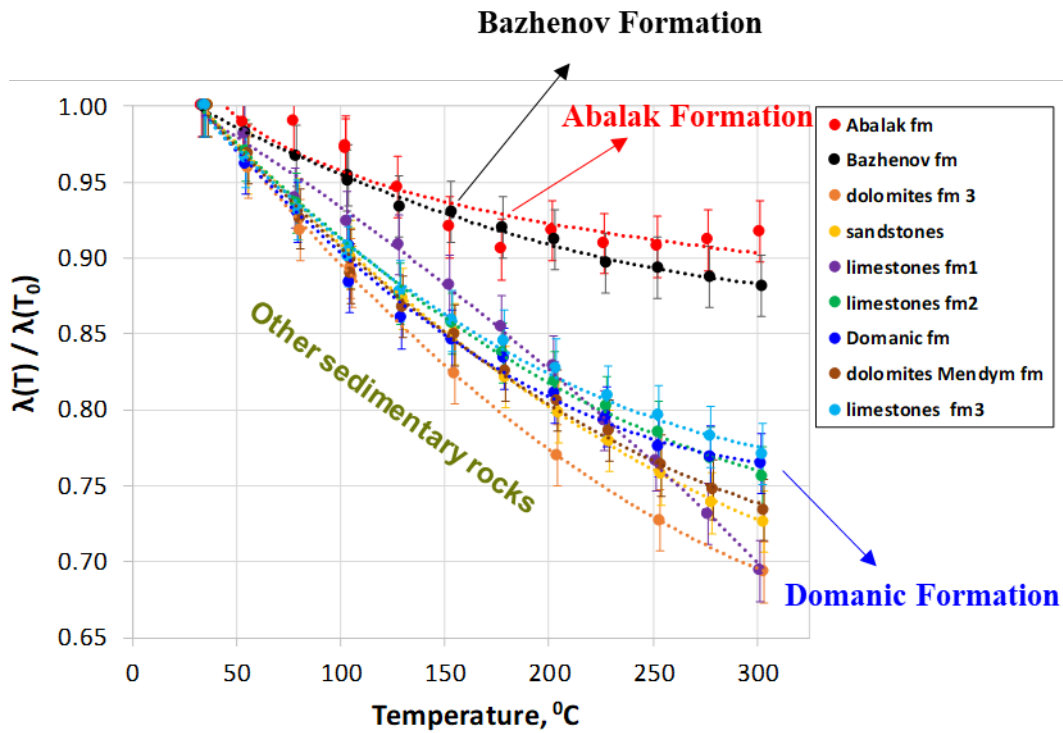


**Figure 30.** Relative change in thermal conductivity for unconventional and other sedimentary rock samples with increasing temperature.

#### 4.2.5 Measurements on kerogen sample

For determining the thermal conductivity of kerogen at elevated temperatures a synthetic sample was made (*Figure 31*). The kerogen was received by the dissolution of all rock minerals, as kerogen has maximum chemical resistance (Bugaev et al, 2014). Then kerogen particles were pressed by a press machine (PP 25, Retsch) to the tablet with a diameter of 40 mm (*Figure 31*). TOC is 31% that was measured by the HAWK pyrolysis instrument. Thermal conductivity values of the kerogen sample at elevated temperature measured with the DTC-300 instrument are shown in *Figure 32*. The results are shown after correction with TCS instrument measurements. It is observed that the thermal conductivity of kerogen is increasing with the temperature that is in agreement with the theoretical background: organic matter is an amorphous substance, the thermal conductivity of which increases with temperature (Chudnovsky, 1962; Yudin et al., 2015).

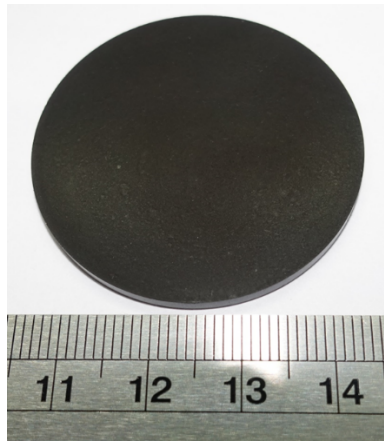


**Figure 31.** A synthetic sample of kerogen.

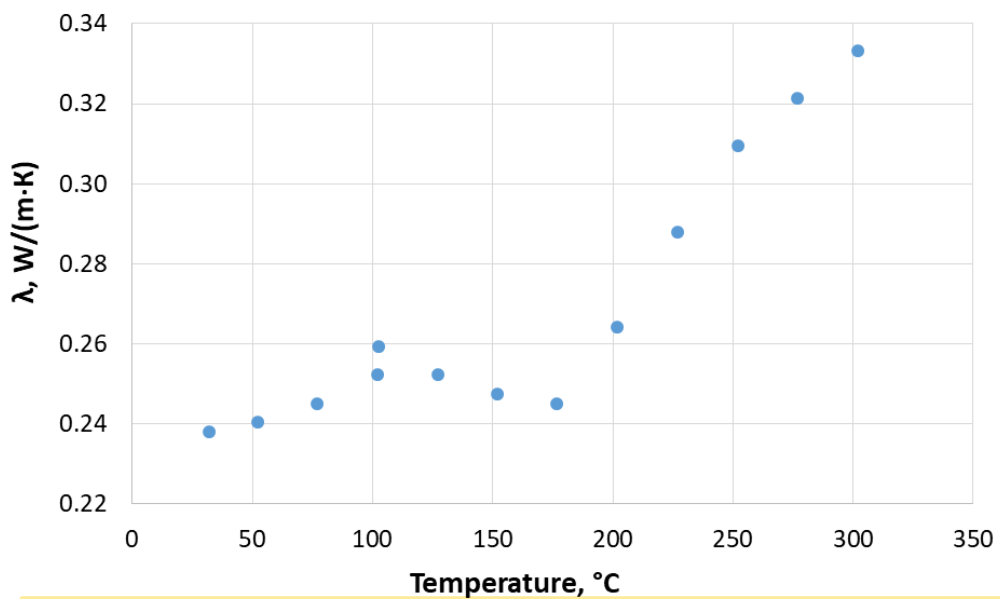


**Figure 32.** Thermal conductivity of kerogen sample at elevated temperatures measured with DTC-300 instrument.

### 4.3 CLTE investigations for unconventional reservoir rocks

#### 4.3.1 Rock collections for studying CLTE

Rock collection for CLTE at elevated temperatures includes 6 oil fields of the West-Siberian oil and gas basin.

##### Oil field 1

The collection of 15 rock samples (30×30 mm) of Oil field 1 are from Bazhenov and Abalak formations and were all drilled along a single well (see *Table 21*). Bazhenov formation (BF) samples are presented by high-carbonaceous shales that are composed of clayey, carbonate,

and siliceous minerals in different proportions. Pyrite is presented as globules, finely disseminated inclusions, and nodules. Pyrite replaces organogenic remains tend to organic matter. The texture of shales is pelitic; the structure is silty-pelitic and straticulate thin-bedded, lightly massive. Abalak formation (AF) samples are presented by shales that are composed of argillites, silty argillites with glauconite inclusions, and siltstones. TOC range of studied rock samples is 1.3-8.3%, the density range is 2.21-2.70 g/cm<sup>3</sup>.

**Table 21.** Characteristics of studied rock samples from oil field 1.

Sample №	Formation	Brief geological description
10	Bazhenov	Shale (Carbonate - Clayey-Siliceous rock, pelitic, thin-bedded, carbonaceous)
11-14		Shale (Clayey-Siliceous rock, silty-pelitic, thin-bedded, carbonaceous)
15-17		Shale (Clayey-Siliceous rock, thin-bedded, pelitic, carbonaceous)
18		Shale (Clayey-Siliceous rock, silty-pelitic, thin-bedded, carbonaceous with glauconite inclusions)
19-21	Abalak	Silty argillites with glauconite inclusions, thin-bedded
22		Clayey siltstone, thin-bedded
23		Silty argillites with pyrite nodules

## Oil field 2

The collection of 8 rock samples (30×30 mm) of Oil field 2 are from Golchih and Abalak formations and were all drilled along a single well (see *Table 22*). Golchih and Abalak formation rock samples are presented by bituminous argillites. TOC range of studied rock samples is 1.6-10.9%, the density range is 2.31-2.70 g/cm<sup>3</sup>.

**Table 22.** Characteristics of studied rock samples from oil field 2.

№ of sample	Formation	Lithology
1GF	Golchih	bituminous argillite
2GF	Golchih	bituminous argillite
3GF	Golchih	bituminous argillite
4GF	Golchih	bituminous argillite
5GF	Golchih	bituminous argillite
6GF	Golchih	bituminous argillite
7GF	Golchih	bituminous argillite
8AF	Abalak	bituminous argillite

### Oil field 3

The collection of 12 rock samples (30×30 mm) of Oil field 3 are from Bazhenov formation and were all drilled along a single well (see *Table 23*). Bazhenov formation rock samples are presented by bituminous argillites. The density range of studied rock samples is 2.34-2.54 g/cm<sup>3</sup>.

**Table 23.** Characteristics of studied rock samples from oil field 3.

№ of sample	Formation	Lithology
1BF	Bazhenov	bituminous argillite
2BF	Bazhenov	bituminous argillite
3BF	Bazhenov	bituminous argillite
4BF	Bazhenov	bituminous argillite
5BF	Bazhenov	bituminous argillite
6BF	Bazhenov	bituminous argillite
7BF	Bazhenov	bituminous argillite
8BF	Bazhenov	bituminous argillite
9BF	Bazhenov	bituminous argillite
10BF	Bazhenov	bituminous argillite
11BF	Bazhenov	bituminous argillite
12BF	Bazhenov	bituminous argillite

### Oil field 4

The collection of 4 rock samples (30×30 mm) of Oil field 4 are from Bazhenov formation and were all drilled along a single well. Bazhenov formation rock samples are presented by high-carbonaceous shales that are composed of clayey, carbonate, and siliceous minerals in different proportions. TOC range of studied rock samples is 7.5-17.2%, the density range is 2.08-2.28 g/cm<sup>3</sup>.

### Oil field 5

The collection of 5 rock samples (30×30 mm) of Oil field 5 are from Bazhenov formation and were all drilled along a single well. Bazhenov formation rock samples are presented by high-carbonaceous shales that are composed of clayey, carbonate, and siliceous minerals in different proportions. TOC range of studied rock samples is 6.8-11.9%, the density range is 2.18-2.34 g/cm<sup>3</sup>.

#### 4.3.2 CLTE and thermal conductivity measurements at room temperature

CLTE values for temperature range 25-50 °C for core plugs drilled from the full-size core samples of the BF and AF in the direction perpendicular to bedding are shown in *Table 24*. The data demonstrate that CLTE values perpendicular to the bedding plane are twice higher than CLTE values along the bedding plane. The BF rocks have high CLTE anisotropy coefficients (up to 2.2).

*Table 24* also shows that CLTE measurement data for the shales are much higher (by 5-10 times) than for other sedimentary rocks as, for example, CLTE range is  $(3.5\div 10.2)\cdot 10^{-6} \text{ K}^{-1}$  for limestones, and  $(7.8\div 10.1)\cdot 10^{-6} \text{ K}^{-1}$  for sandstones (Popov et al, 2008). Such high CLTE values for the BF rocks are related to the presence of organic matter in studied rock samples as the CLTE of organic matter is much higher ( $\sim 3.4\cdot 10^{-4} \text{ K}^{-1}$  (Smith and Johnson, 1976)) than for mineral components of rocks. For example, CLTE of bitumen is  $200\cdot 10^{-6} \text{ K}^{-1}$  (Yarzev and Erofeev, 2004) and CLTE of kerogen was estimated as  $115\cdot 10^{-6} \text{ K}^{-1}$  (Kaevand and Lille, 2005) that is by 5-10 times higher than for CLTE of rock-forming minerals  $(16\div 50)\cdot 10^{-6} \text{ K}^{-1}$  (Anderson, 1989)). Average CLTE variations along bedding for the BF rocks from oil fields 5 ( $\text{CLTE}_{\text{average}} = 16.8\cdot 10^{-6} \text{ K}^{-1}$ ), 4 ( $\text{CLTE}_{\text{average}} = 21.1\cdot 10^{-6} \text{ K}^{-1}$ ) are higher than for the BF and GF (Golchih formation) rocks from oil fields 1 ( $\text{CLTE}_{\text{average}} = 10.2\cdot 10^{-6} \text{ K}^{-1}$ ), 2 ( $\text{CLTE}_{\text{average}} = 9.0\cdot 10^{-6} \text{ K}^{-1}$ ) that is related to different range of TOC along wells.

Results of the thermal conductivity measurements on core plugs of shale formations are presented in *Table 24*. The thermal conductivity component parallel to the bedding plane ( $\lambda_{\parallel}$ ) ranges within 1.63-3.58 W/(m·K) for BF, 1.67-2.09 W/(m·K) for GF and 2.05-3.74 W/(m·K) for AF. The thermal conductivity component perpendicular to the bedding plane ( $\lambda_{\perp}$ ) ranges within 0.95-2.15 W/(m·K) for BF, 1.14-1.52 W/(m·K) for GF and 1.35-2.55 W/(m·K) for AF. All formations are characterized by high variations of thermal anisotropy coefficient (K), which ranges within 1.06-3.74 for BF, 1.38-1.52 for GF, and 1.31-1.90 for AF (*Table 24*). Thermal heterogeneity factors inferred from the thermal conductivity profiles are also given in *Table 24*. The data in *Table 24* show that high values of thermal conductivity and thermal heterogeneity factors are related to samples that have pyrite inclusions (samples №11, 14). For most shale samples (№15-22) heterogeneity factor,  $\beta_1$  is larger than  $\beta_2$  and average values of  $\beta_1$  exceed average values of  $\beta_2$  essentially (correspondingly 0.19 and 0.11).

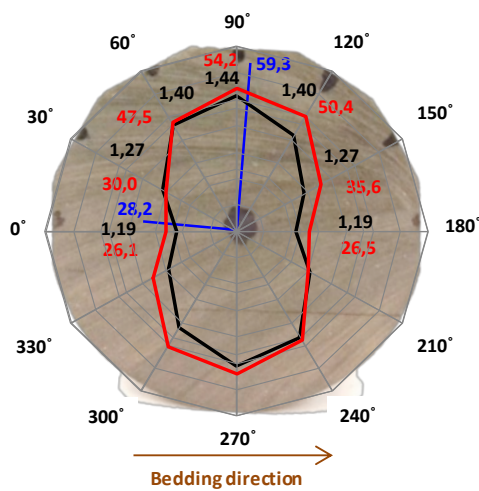
**Table 24.** Results of CLTE, CLTE anisotropy coefficient, density, TOC and thermal properties measurements

Sample №	Oil field	Formation	CLTE at 25-50 °C, 10 <sup>-6</sup> K <sup>-1</sup>		CLTE anisotropy coefficient	CLTE range at 25-300 °C, 10 <sup>-6</sup> K <sup>-1</sup>	Density, g/cm <sup>3</sup>	TOC, %	Thermal conductivity, W/(m·K)		Thermal conductivity anisotropy coefficient	Thermal heterogeneity factor		
			Along bedding	Perpendicular to bedding					λ <sub>  </sub>	λ <sub>⊥</sub>		β <sub>1</sub>	β <sub>2</sub>	
1	5	Bazhenov	11.6	-	-	11.6-16.8 <sup>a</sup>	2.34	6.57	-	-	-	-	-	
2			20.3	42.2	2.1	18.0-20.3 <sup>a</sup>	2.18	9.19	1.73	1.42	1.22	0.16	0.07	
3			19.4	41.7	2.2	16.6-18.8 <sup>a</sup>	2.18	11.50	1.73	1.44	1.20	0.11	0.07	
4			-	51.3	-	40.0-140 <sup>b</sup>	2.25	11.85	-	-	-	-	-	
5			15.9	29.9	1.9	21.1-54.8 <sup>b</sup>	2.27	6.80	1.97	1.65	1.19	0.10	0.06	
6	4	Bazhenov	14.9	18.5	1.2	14.4-18.4 <sup>b</sup>	2.28	16.39	2.28	2.15	1.06	0.08	0.06	
7			-	27.7	-	19.6-27.7 <sup>b</sup>	2.26	7.50	-	-	-	-	-	
8			26.0	54.2	2.1	16.5-143 <sup>b</sup>	2.08	15.43	1.44	1.19	1.21	0.08	0.08	
9			22.3	41.0	1.8	4.4-22.8 <sup>a</sup>	2.20	17.19	1.63	1.48	1.10	0.09	0.07	
10	1	Bazhenov	10.5	-	-	6.9-11.3 <sup>a</sup>	2.42	6.19	2.17	1.81	1.20	0.13	0.09	
11			6.7	-	-	5.4-12.9 <sup>a</sup>	2.34	7.47	2.83	1.91	1.48	0.57	0.41	
12			11.7	-	-	4.5-11.7 <sup>a</sup>	2.35	7.73	2.05	1.58	1.30	0.10	0.11	
13			11.9	-	-	8.7-12.7 <sup>a</sup>	2.34	7.47	2.20	1.76	1.25	0.11	0.11	
14			12.5	-	-	7.5-13.2 <sup>a</sup>	2.35	8.34	3.58	0.95	3.74	0.97	0.11	
15			8.3	-	-	3.3-10.8 <sup>a</sup>	2.38	7.69	2.21	1.60	1.38	0.12	0.09	
16			10.6	-	-	8.8-14.9 <sup>a</sup>	2.40	6.19	2.37	1.78	1.33	0.12	0.10	
17			9.2	-	-	7.4-15.9 <sup>a</sup>	2.52	3.19	2.36	1.95	1.21	0.13	0.14	
18			10.1	-	-	6.7-12.7 <sup>a</sup>	2.52	2.98	2.57	2.15	1.20	0.16	0.09	
19		Abalak		7.4	-	-	2.9-10.1 <sup>a</sup>	-	2.06	2.43	1.84	1.31	0.14	0.13
20				8.6	-	-	2.9-9.9 <sup>a</sup>	-	1.90	2.63	1.70	1.55	0.14	0.13
21				5.3	-	-	2.07-9.3 <sup>a</sup>	-	2.38	-	-	-	-	-
22				8.2	-	-	1.4-9.3 <sup>a</sup>	-	1.64	2.92	1.53	1.90	0.13	0.11
23	6.8			-	-	4.7-9.2 <sup>a</sup>	-	2.35	2.82	1.93	1.46	0.18	0.12	
1GF	2	Golchih	7.0	-	-	3.1-7.5 <sup>a</sup>	2.69	2.03	2.09	1.38	1.52	0.23	0.13	
2GF			7.5	-	-	3.6-8.4 <sup>a</sup>	2.65	1.60	1.97	1.52	1.30	0.36	0.25	
3GF			8.1	-	-	7.9-8.5 <sup>a</sup>	2.63	3.45	2.07	1.39	1.50	0.19	0.16	
4GF			9.6	-	-	5.1-9.6 <sup>a</sup>	2.70	2.99	2.08	1.41	1.47	0.19	0.17	
5GF			10.3	-	-	1.8-10.3 <sup>a</sup>	2.37	7.40	1.67	1.14	1.47	0.12	0.14	
6GF			10.0	-	-	3.0-10.0 <sup>a</sup>	2.46	4.28	1.77	1.24	1.43	0.32	0.20	
7GF			10.3	-	-	9.8-11.6 <sup>a</sup>	2.31	10.90	1.71	1.24	1.38	0.19	0.13	
1AF		Abalak		6.3	-	-	3.4-7.3 <sup>a</sup>	2.65	1.80	2.05	1.35	1.52	0.18	0.27

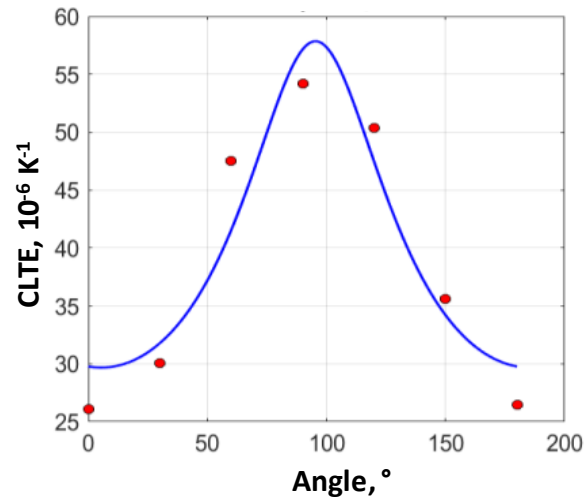
<sup>a</sup> Minimum-maximum CLTE values parallel to bedding at 25-300 °C range; <sup>b</sup> Minimum-maximum CLTE values perpendicular to bedding at 25-300 °C range.

### 4.3.3 CLTE anisotropy at room temperature

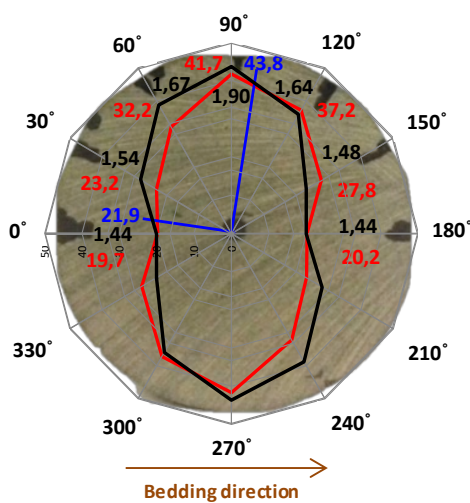
Measurements of CLTE anisotropy were carried out for six core plugs from Bazhenov formation in a reduced temperature range (25-50 °C) to prevent any changes of physical parameters of studied core plugs. Results of CLTE measurements on rock samples at different directions relative to the bedding plane are shown in *Figures 33a, c, e, g, i, k* by red lines and values, the measurement unit is  $10^{-6} \text{ K}^{-1}$ . Thermal conductivity measurements were provided with TCS on the core plugs in the same directions. Results are shown by black lines and values in *Figures 33 a, c, e, g, i, k*; measurement unit is  $\text{W}/(\text{m}\cdot\text{K})$ . Detection of main axes directions and CLTE values was provided by the application of ellipse with unknown semiaxes and rotation angle on experimental results and determination of unknown values by the least square method. The result of solving the optimization problem by the ellipse parameters method (blue line) is shown in *Figures 33 b, d, f, h, j, l*. Results of experimental measurements are presented by red markers.



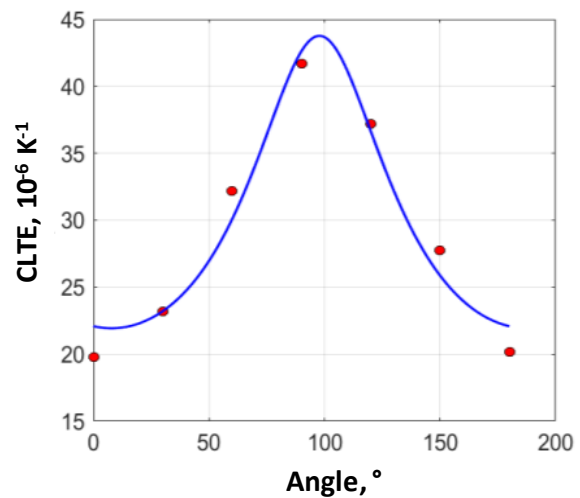
a



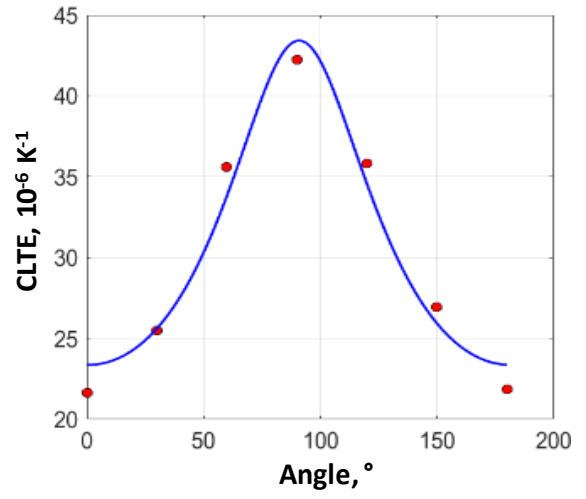
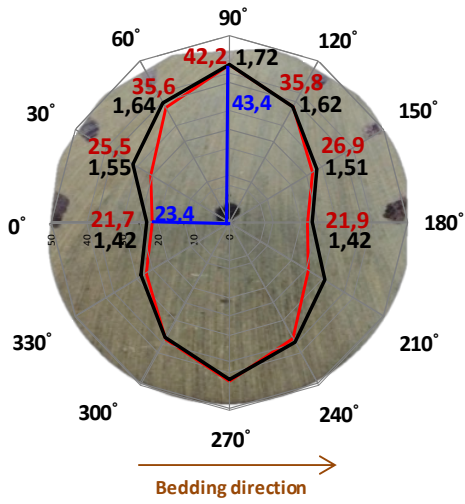
b



c

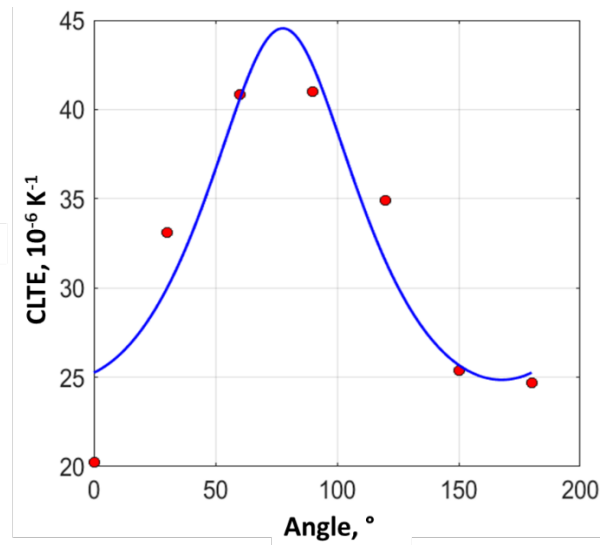
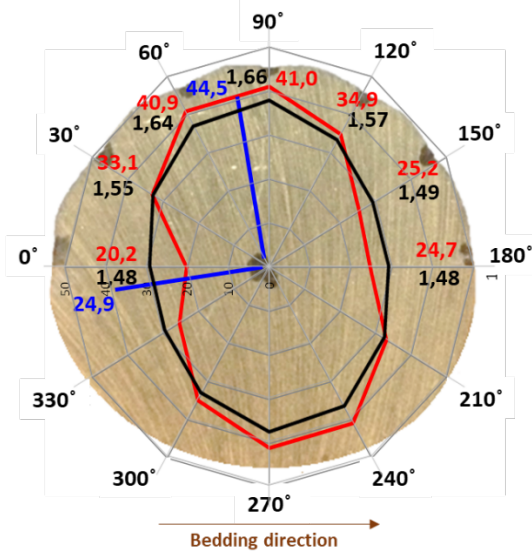


d



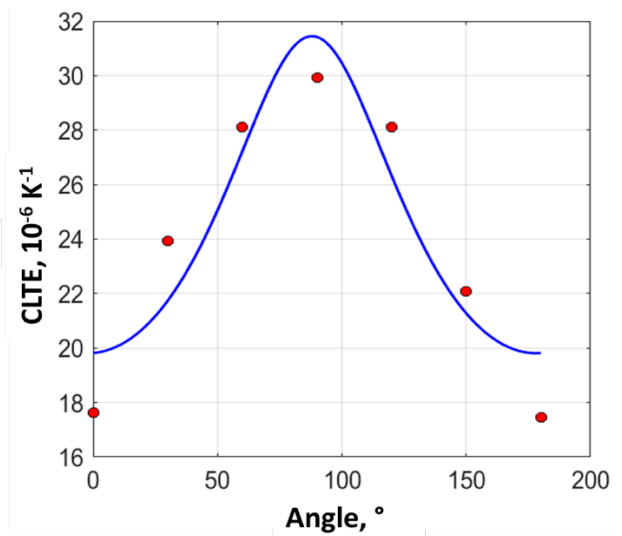
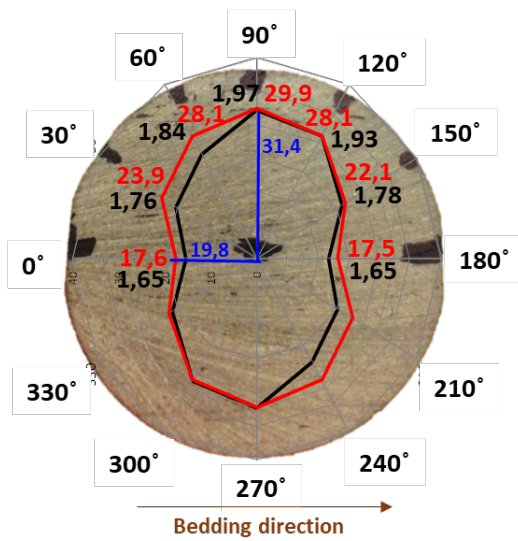
e

f



g

h



i

j

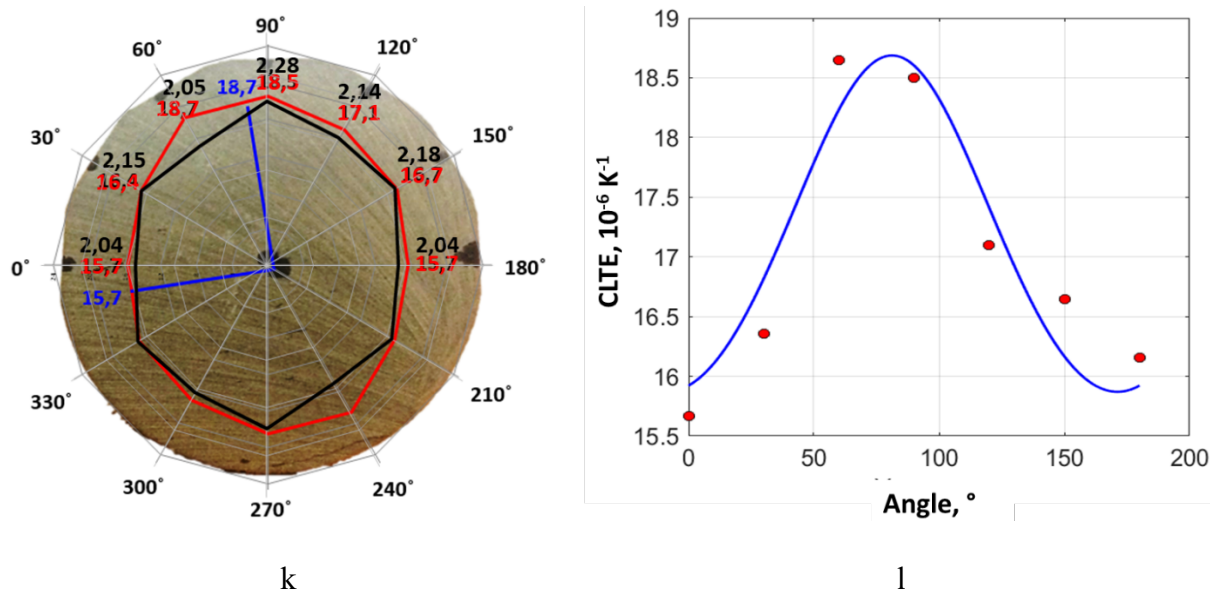


**Figure 33.** Results of CLTE (measurement unit is  $10^{-6} \text{ K}^{-1}$ , the data are shown by red lines and numbers) and thermal conductivity (measurement unit is  $\text{W}/(\text{m}\cdot\text{K})$ , black line and numbers) measurements of BF core plugs at different directions to the bedding plane (a, c, e, g, i, k). The results of solving the optimization problem by the ellipse parameters method (blue lines) and the CLTE measurement results (red markers) are shown in corresponding figures b, d, f, h, j, l.

The results given in *Figure 33* show that for the core plugs from BF main axes of CLTE anisotropy coincide with the main axes of thermal conductivity anisotropy. Though there is not enough data for fixing a reliable correlation dependence for CLTE anisotropy coefficient vs thermal conductivity anisotropy coefficient, the results showed the following tendency – the higher the thermal conductivity anisotropy coefficient is, the higher CLTE anisotropy coefficient is. It opens the possibility to predict CLTE anisotropy through the thermal conductivity anisotropy and vice versa.

#### 4.3.4 Integrated analysis and core state control

Comparison results of thermal profiling before and after CLTE measurements showed no significant changes in thermal conductivity parallel perpendicular to bedding (less than the uncertainty of thermal conductivity measurements) for most core plugs. As thermal conductivity is sensitive to any changes in rocks (Popov et al, 2017), it shows that there are no essential changes in rocks structure after high-temperature measurements for core plugs.

Integration of CLTE (parallel to bedding at temperature range 25-50 °C) and thermal conductivity measurements on core plugs allows us obtaining new correlation thermal conductivity vs CLTE (*Figures 34*):  $\lambda = 6.64 \cdot \alpha^{-0.45}$ , determination coefficient  $R^2 = 0.88$ , root

mean square error (RMSE) = 0.18 W/(m·K). The reason for such correlation is the sensitivity of thermal conductivity and CLTE of rock samples to the presence of organic matter (Popov et al, 2017). CLTE of organic matter is much higher (5-10 times) than for other sedimentary rock minerals. Similar correlation was obtained between CLTE (parallel to bedding at temperature range 25-50 °C) and mineral density of studied core plugs at room temperature:  $\rho = 3.38 \cdot \alpha^{0.15}$ ,  $R^2 = 0.85$ , RMSE = 0.05 g/cm<sup>3</sup> (Figures 35a). Also, close correlations between density, TOC, and thermal conductivity measured at room temperature were observed (Figures 35 b, c).

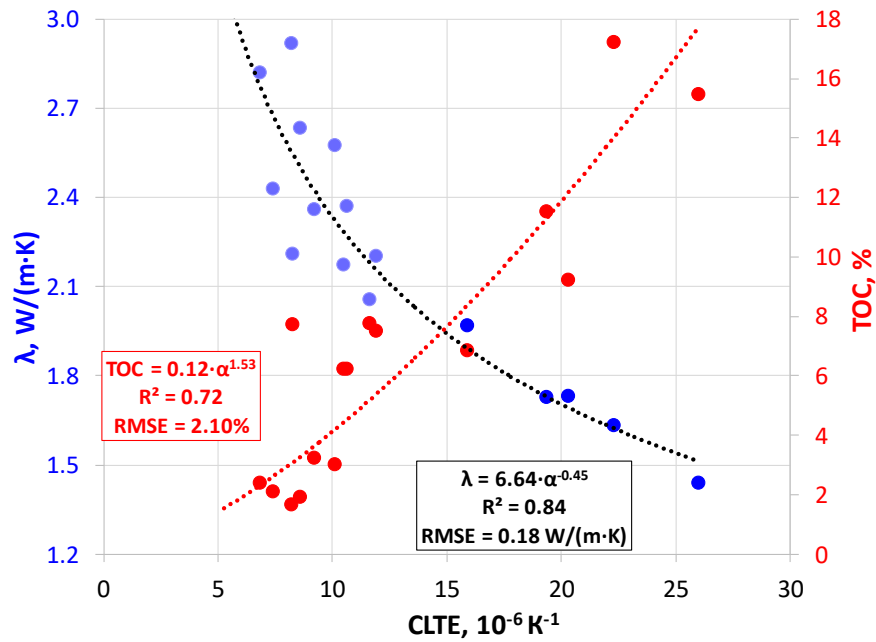


**Figure 34.** Correlation TC vs CLTE for core plugs from BF from 3 oil fields.

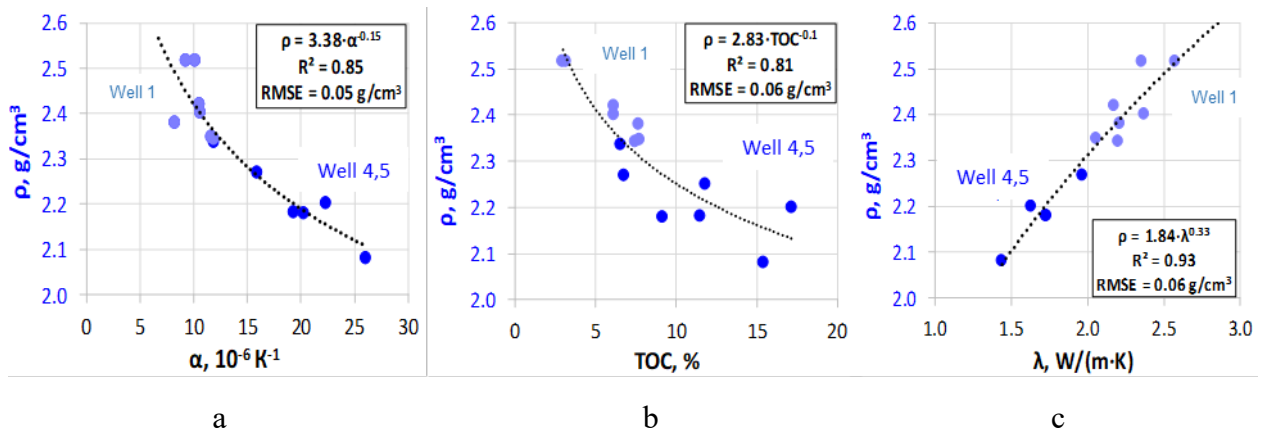


**Figure 35.** Correlations density vs CLTE (parallel to bedding at temperature range 25-50 °C) (a), density vs TOC (b), and density vs TC (c) for core plugs from BF from 3 oil fields.

Obtained correlations allow us to predict CLTE of BF rocks using density and thermal conductivity data. The observed correlation thermal conductivity vs CLTE for studied core plugs

( $\alpha = 52.82 \cdot \lambda^{-1.94}$ ,  $R^2 = 0.88$ ) gives the possibility to obtain a detailed CLTE profile (parallel to bedding at temperature range 25-50 °C) for wells 1, 4 and 5 (Figure 36) using the high resolution (1 mm) profiles of the thermal conductivity obtained from the continuous thermal core profiling performed on all full-size cores with the optical scanner. TOC for each well was obtained with the HAWK pyrolysis instrument and matched with CLTE profile along wells (Figure 36). Generalized correlation CLTE vs TOC for three studied wells was specified by CLTE profiles averaged in every 10 cm interval and pyrolysis data (Figure 37):  $\alpha = 0.09 \cdot \text{TOC}^2 + 0.34 \cdot \text{TOC} + 7.88$  ( $R^2 = 0.79$ ,  $\text{RMSE} = 6.34 \cdot 10^{-6} \text{ K}^{-1}$ ).

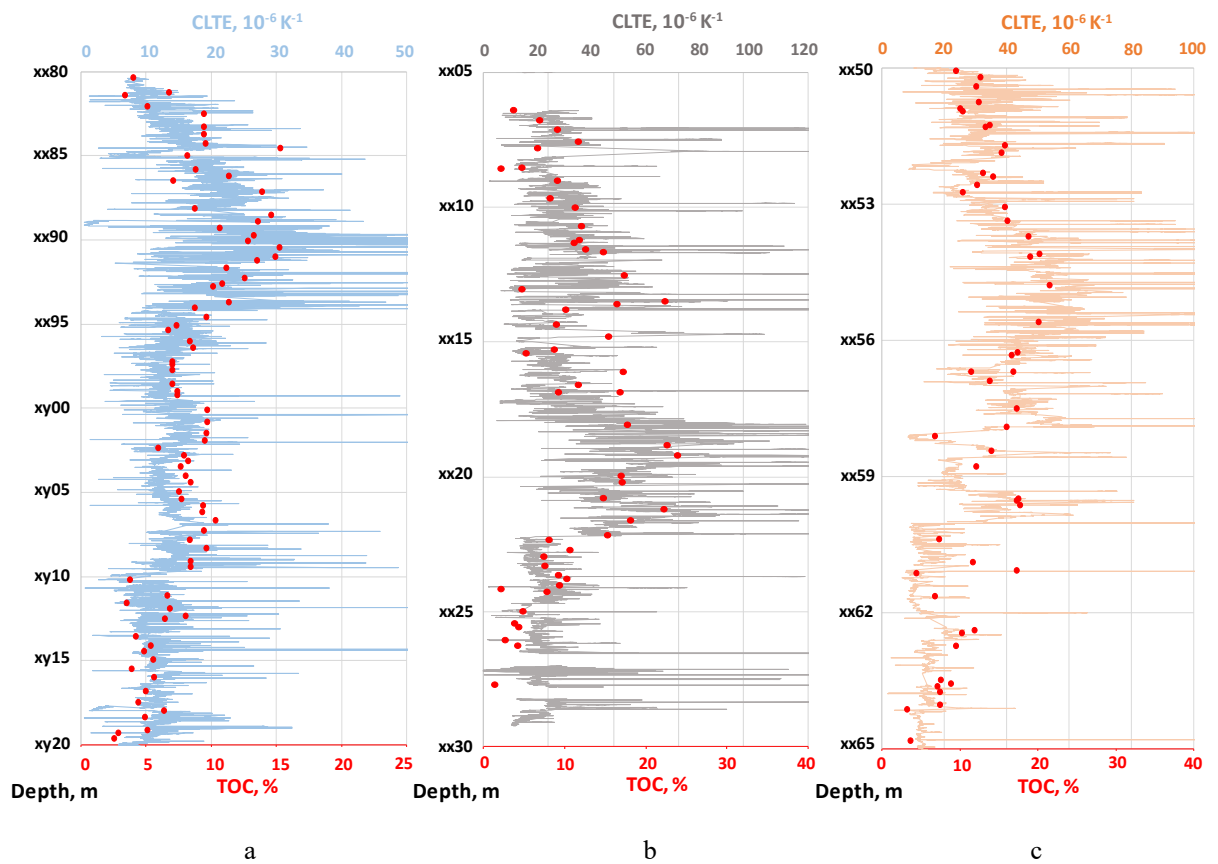


**Figure 36.** Detailed profile of CLTE and pyrolysis data (red markers) for BF rocks from well 4 (c), well 5 (b) and well 1 (a).

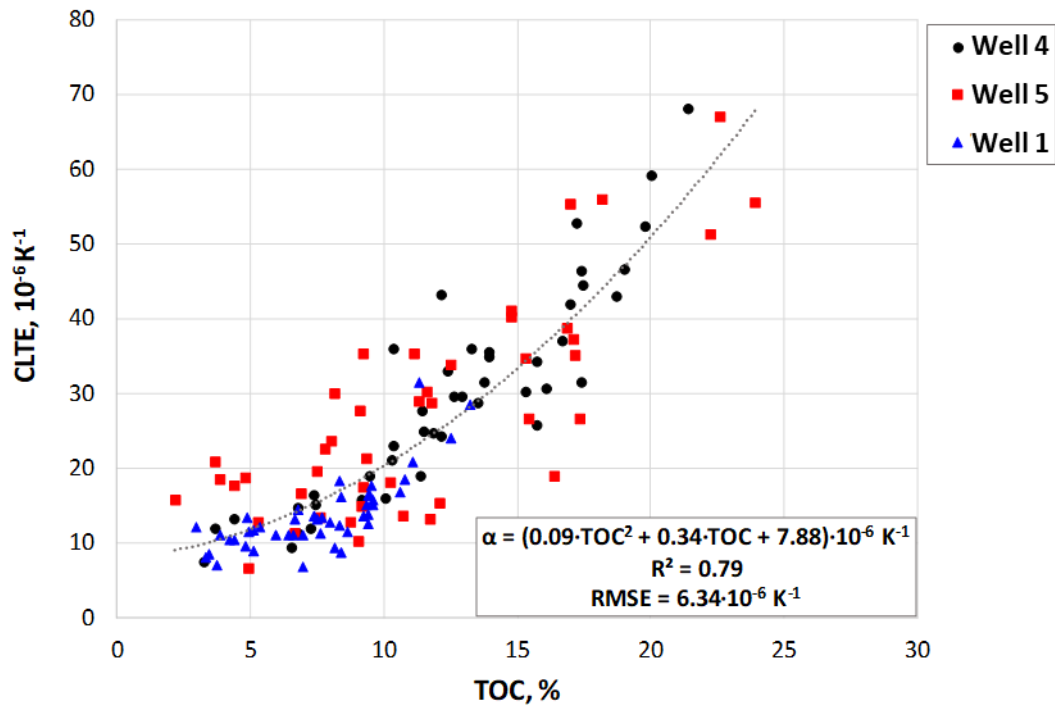


**Figure 37.** Correlation CLTE vs TOC for BF rocks form 3 wells.

#### 4.3.5 CLTE measurements at elevated temperatures

CLTE measurements at high temperatures (25-300 °C) were performed for each studied core plug. The measurement results are shown in *Figures 38-41*. The CLTE measurements at high temperatures were conducted for different directions – parallel and perpendicular to the bedding plane. The decrease of CLTE values within the temperature range of 25-140 °C for studied core plugs is probably related to the dehydration of water during heating. Clay minerals are very sensitive to temperature increase as they contain interlayer and physically adsorbed water. Dehydration of water during heating causes the decrease of interlayer spacing and thermal expansion of clay minerals. So, smectites lose interlayer water in the temperature range 100-200 °C and interlayer spacing decreases from 15-12 Å to 10-9.4 Å (Weaver, 1976). DTA curves of samples composed of illite-rich clay minerals were observed to have endothermic peaks within the temperature range of 98-114 °C that was related to dehydration of adsorbed water (Alver et al, 2016). It is demonstrated by the strong correlation of CLTE variations with a mass change of studied core plugs during the heating (*Figure 42*). Rock mass for each studied core plug was measured before, and after heating to 300 °C, CLTE variations were calculated as  $(\text{CLTE}_{\text{max}} - \text{CLTE}_{\text{min}}) / \text{CLTE}_{\text{average}}$ ,  $\text{CLTE}_{\text{max}}$ ,  $\text{CLTE}_{\text{min}}$ ,  $\text{CLTE}_{\text{average}}$  – maximum, minimum and average CLTE values correspondingly for each core plug within a temperature range of 25-300 °C. *Figure 42* demonstrates that more core plugs mass loss results in higher CLTE variations with

temperature. Moreover, for sample №1 evaporation of bitumen was observed after heating to 300 °C (Figure 43). The CLTE measurements on core plugs from the Bazhenov and Abalak formations at high temperatures showed that CLTE at high temperatures is 2.0-2.7 times higher than CLTE at initial temperature  $T_0$ . CLTE values measured for the directions perpendicular to the bedding plane reach  $(133\div 143)\cdot 10^{-6} \text{ K}^{-1}$  at temperature 160-200 °C (samples № 4 and 8, Figure 39).

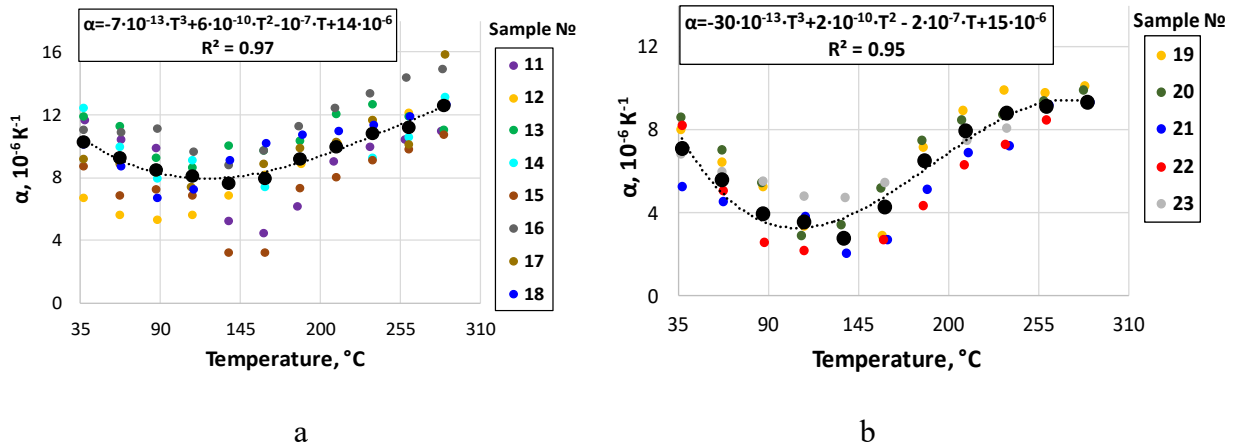


Figure 38. CLTE variations with a temperature increase for core plugs from the BF (a) and the AF (b) (well 1).

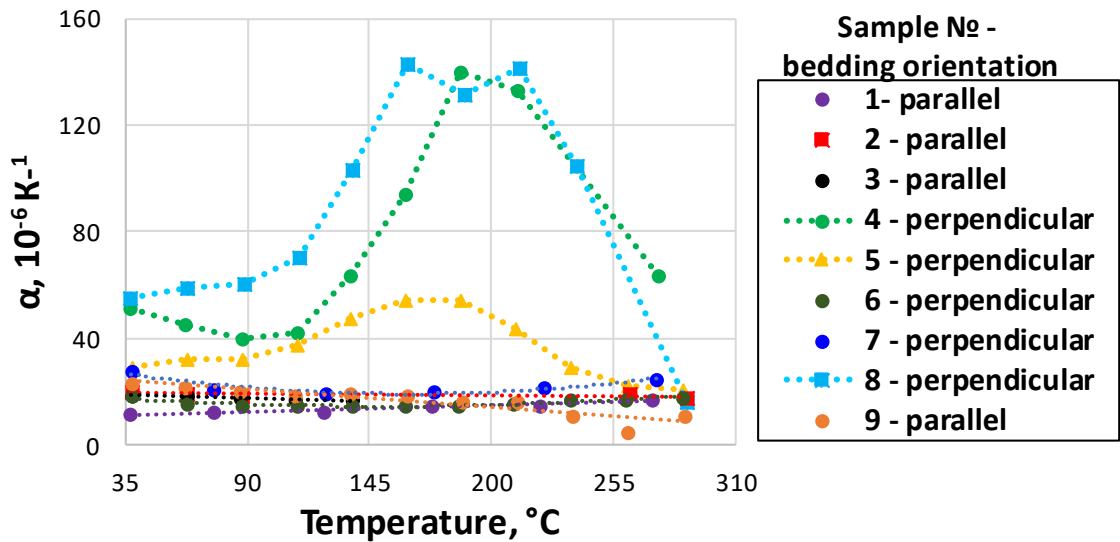
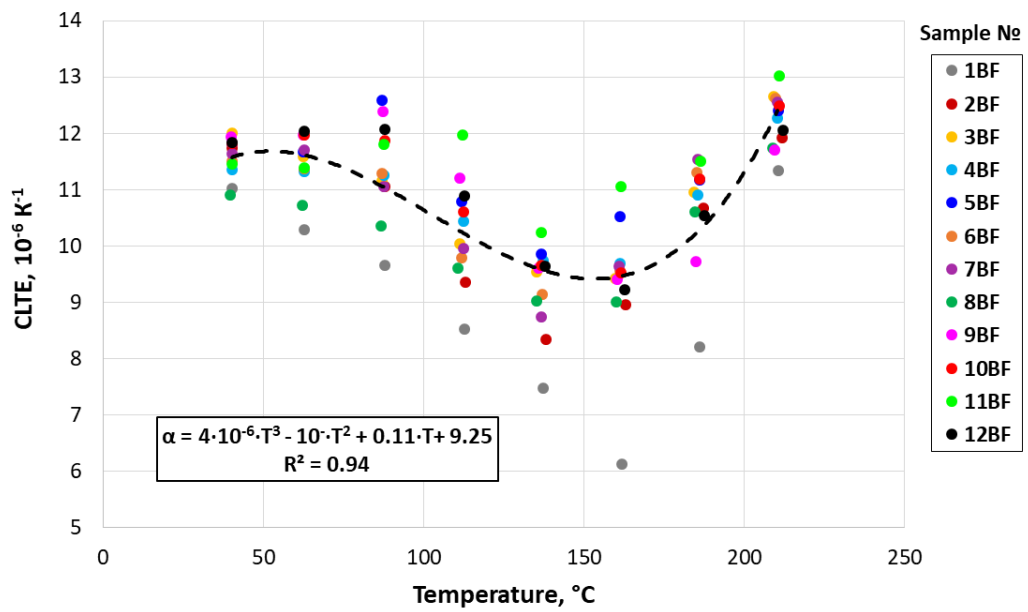
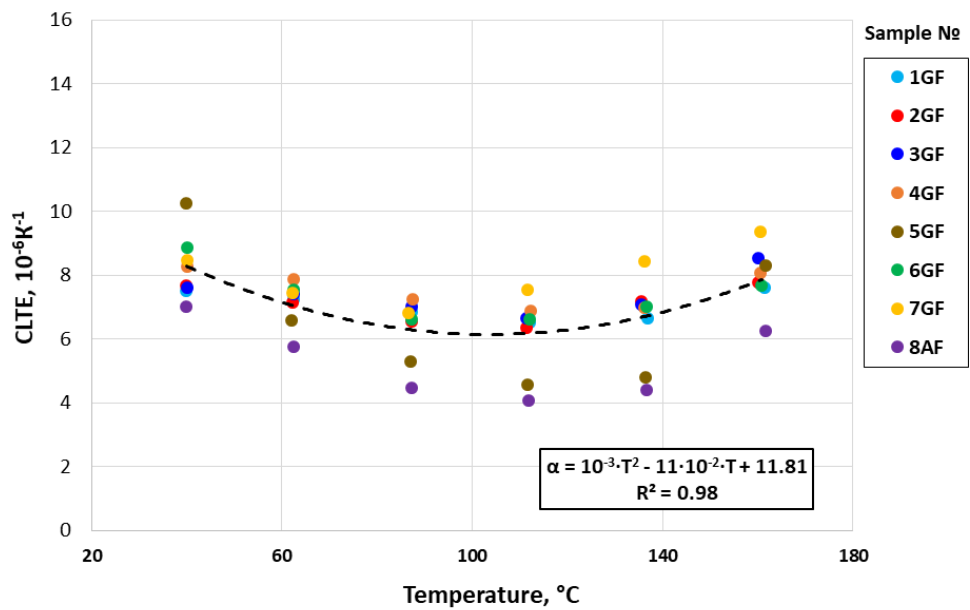


Figure 39. CLTE values change with temperature for core plugs from the BF (wells 4, 5).



**Figure 40.** CLTE variations with a temperature increase for core plugs from the BF (well 3).



**Figure 41.** CLTE variations with a temperature increase for core plugs from the GF and AF (well 2).

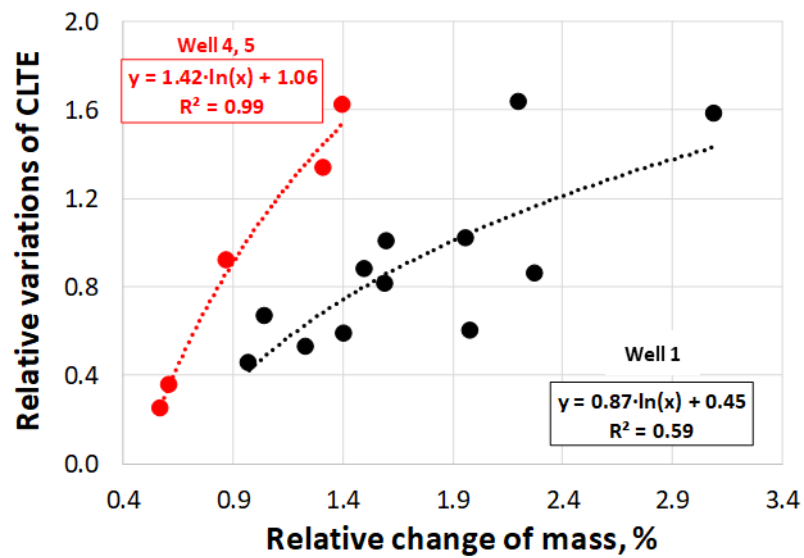


**Figure 42.** Variations of CLTE with a relative change of core plug mass after measurements at 300 °C for BF rocks (Samples №4, 5, 6, 7, 8, 10, 12-13, 15-23).



**Figure 43.** Photo of sample №1 before (a) and after high-temperature measurements with a zoomed area of bitumen exudation (b).

#### 4.4 Volumetric heat capacity of unconventional reservoir rocks at elevated temperatures

##### 4.4.1 Rock collection for studying volumetric heat capacity at elevated temperatures

Rock collection for studying volumetric heat capacity (VHC) at elevated temperatures includes 4 oil fields of the West-Siberian oil and gas basin.

###### Oil field 1

The collection of 11 rock samples (~15 g) of Oil field 1 are from Bazhenov and Abalak formations (see *Table 25*). Bazhenov formation (BF) samples are presented by argillites and siltstones, Abalak formation (AF) samples are presented by argillites.

**Table 25.** Characteristics of studied rock samples from oil field 1.

№ of sample	Formation	Lithology
1	Bazhenov	Argillite with quartz lenses
2	Bazhenov	Argillite with sand admixture
3	Bazhenov	Siltstone
4	Bazhenov	Silt-rich argillite
5	Bazhenov	Argillite with silty admixture
6	Bazhenov	Siltstone with fine-grained sand admixture
7	Bazhenov	Argillite with silty admixture and detritus
8	Bazhenov	Argillite
9	Abalak	Argillite with silty admixture
10	Abalak	argillite
11	Abalak	argillite

###### Oil field 2

The collection of 8 rock samples (~15 g) of Oil field 2 are from Bazhenov and Abalak formations (see *Table 26*). Bazhenov and Abalak formation samples are presented by bituminous argillites.

**Table 26.** Characteristics of studied rock samples from oil field 2.

№ of sample	Formation	Lithology
1	Bazhenov	bituminous argillite
2	Bazhenov	bituminous argillite
3	Bazhenov	bituminous argillite
4	Bazhenov	bituminous argillite
5	Bazhenov	bituminous argillite
6	Bazhenov	bituminous argillite
7	Bazhenov	bituminous argillite
8	Abalak	bituminous argillite

### **Oil field 3**

The collection of 12 rock samples (~15 g) of Oil field 3 are from Bazhenov formation that is presented by bituminous argillites.

#### **4.4.2 Results of measurements for unconventional reservoir rocks**

### **Oil field 1**

Volumetric heat capacity measurements in the temperature range of 25-200 °C were carried out on 11 non-extracted samples with a mass of 15 g from the most representative samples of full-sized core samples, selected based on the results of thermophysical profiling and geological description of the core. The determination of the volumetric heat was based on measurements of the specific heat capacity in the temperature range 25-200 °C on 11 non-extracted samples weighing 15 g, measurements of the density of rocks, estimates of changes in the density of rocks with a temperature in the temperature range of 25-200 °C according to the results of measurements of the coefficient of linear thermal expansion in a given temperature range with the subsequent determination of the volumetric heat capacity by the ratio (16). To measure the specific heat capacity, tablets (4 mm in diameter) were prepared, which were obtained using a manual hydraulic press at a pressure of 8 MPa. *Tables 27-36* provide summary information on the results of measurements of the specific heat capacity of samples 1 - 11 at temperatures of 25, 50, 100, 150, and 200 °C. For rock samples, No. 1 - 5 and No. 9 - 11, the values of specific heat capacity obtained in the first and second experiments are in satisfactory agreement with each other within the error of the DSC method (according to ASTM E 1269-05, on average, the relative error of the method is 5-7%). For samples 6-8, the specific heat capacity is in poor agreement according to the results of the first and second experiments. In the case of sample No. 7, this may be due to the fact that measurements were carried out on a rock powder, and not on a tablet; therefore, an increased error in measurements on the powder could arise due to the fact that the condition of good and reproducible thermal contact between the crucible bottom was not met and a sample. The second reason for the discrepancy between the results can be associated with the high hygroscopicity of the samples - as a result of this, the error in determining the mass of the dried preparations could be increased.

**Table 27.** The results of measurements of the specific heat capacity of sample №1.

Sample №1					
$T, ^\circ\text{C}$	$c_p, \text{J}/(\text{g}\cdot\text{K})$			Standard deviation, $\text{J}/(\text{g}\cdot\text{K})$	Student's confidence interval ( $\alpha= 0.05$ ), $\text{J}/(\text{g}\cdot\text{K})$
	Tablet 2	Tablet 3	Average		
25	0.830	0.796	0.813	0.02	0.2
50	0.879	0.840	0.859	0.03	0.2
100	0.976	0.918	0.947	0.04	0.4
150	1.055	0.988	1.021	0.05	0.4
200	1.098	1.048	1.073	0.03	0.3

**Table 28.** The results of measurements of the specific heat capacity of sample №3.

Sample №3					
$T, ^\circ\text{C}$	$c_p, \text{J}/(\text{g}\cdot\text{K})$			Standard deviation, $\text{J}/(\text{g}\cdot\text{K})$	Student's confidence interval ( $\alpha= 0.05$ ), $\text{J}/(\text{g}\cdot\text{K})$
	Tablet 2	Tablet 3	Average		
25	0.860	0.781	0.820	0.06	0.5
50	0.905	0.824	0.865	0.06	0.5
100	1.033	0.917	0.975	0.08	0.7
150	1.159	1.031	1.095	0.09	0.8
200	1.259	1.189	1.224	0.05	0.4

**Table 29.** The results of measurements of the specific heat capacity of sample №4.

Sample №4					
$T, ^\circ\text{C}$	$c_p, \text{J}/(\text{g}\cdot\text{K})$			Standard deviation, $\text{J}/(\text{g}\cdot\text{K})$	Student's confidence interval ( $\alpha= 0.05$ ), $\text{J}/(\text{g}\cdot\text{K})$
	Tablet 2	Tablet 3	Average		
25	0.867	0.836	0.852	0.02	0.2
50	0.936	0.877	0.907	0.04	0.4
100	1.035	0.968	1.002	0.05	0.4
150	1.111	1.069	1.090	0.03	0.3
200	1.192	1.177	1.185	0.01	0.1

**Table 30.** The results of measurements of the specific heat capacity of sample №5.

Sample №5					
$T, ^\circ\text{C}$	$c_p, \text{J}/(\text{g}\cdot\text{K})$			Standard deviation, $\text{J}/(\text{g}\cdot\text{K})$	Student's confidence interval ( $\alpha= 0.05$ ), $\text{J}/(\text{g}\cdot\text{K})$
	Tablet 2	Tablet 3	Average		
25	0.816	0.803	0.810	0.01	0.1
50	0.875	0.847	0.861	0.02	0.2
100	0.951	0.922	0.937	0.02	0.2
150	0.995	0.971	0.983	0.02	0.2
200	1.029	1.053	1.041	0.02	0.2

**Table 31.** The results of measurements of the specific heat capacity of sample №6.

Sample №6					
$T, ^\circ\text{C}$	$c_p, \text{J}/(\text{g}\cdot\text{K})$			Standard deviation, $\text{J}/(\text{g}\cdot\text{K})$	Student's confidence interval ( $\alpha= 0.05$ ), $\text{J}/(\text{g}\cdot\text{K})$
	Tablet 2	Tablet 3	Average		

25	0.723	0.871	0.797	0.1	0.9
50	0.773	0.916	0.845	0.1	0.9
100	0.859	1.003	0.931	0.1	0.9
150	0.927	1.074	1.001	0.1	0.9
200	0.979	1.124	1.051	0.1	0.9

**Table 32.** The results of measurements of the specific heat capacity of sample №7.

Sample №7					
$T, ^\circ\text{C}$	$c_p, \text{J}/(\text{g}\cdot\text{K})$			Standard deviation, $\text{J}/(\text{g}\cdot\text{K})$	Student's confidence interval ( $\alpha=0.05$ ), $\text{J}/(\text{g}\cdot\text{K})$
	Tablet 2	Tablet 3	Average		
25	0.954	0.774	0.864	0.1	1
50	1.000	0.822	0.911	0.1	1
100	1.067	0.898	0.982	0.1	1
150	1.113	0.960	1.036	0.1	1
200	1.178	1.023	1.101	0.1	1

**Table 33.** The results of measurements of the specific heat capacity of sample №8.

Sample №8					
$T, ^\circ\text{C}$	$c_p, \text{J}/(\text{g}\cdot\text{K})$			Standard deviation, $\text{J}/(\text{g}\cdot\text{K})$	Student's confidence interval ( $\alpha=0.05$ ), $\text{J}/(\text{g}\cdot\text{K})$
	Tablet 2	Tablet 3	Average		
25	0.821	0.738	0.779	0.06	0.5
50	0.892	0.784	0.838	0.08	0.7
100	0.983	0.867	0.925	0.08	0.7
150	1.030	0.942	0.986	0.06	0.6
200	1.069	0.994	1.031	0.05	0.5

**Table 34.** The results of measurements of the specific heat capacity of sample №9.

Sample №9					
$T, ^\circ\text{C}$	$c_p, \text{J}/(\text{g}\cdot\text{K})$			Standard deviation, $\text{J}/(\text{g}\cdot\text{K})$	Student's confidence interval ( $\alpha=0.05$ ), $\text{J}/(\text{g}\cdot\text{K})$
	Tablet 2	Tablet 3	Average		
25	0.820	0.784	0.802	0.03	0.2
50	0.859	0.830	0.844	0.02	0.2
100	0.932	0.912	0.922	0.01	0.1
150	0.998	0.984	0.991	0.01	0.1
200	1.043	1.023	1.033	0.01	0.1

**Table 35.** The results of measurements of the specific heat capacity of sample №10.

Sample №10					
$T, ^\circ\text{C}$	$c_p, \text{J}/(\text{g}\cdot\text{K})$			Standard deviation, $\text{J}/(\text{g}\cdot\text{K})$	Student's confidence interval ( $\alpha=0.05$ ), $\text{J}/(\text{g}\cdot\text{K})$
	Tablet 2	Tablet 3	Average		
25	0.836	0.797	0.817	0.03	0.2
50	0.879	0.837	0.858	0.03	0.3
100	0.958	0.912	0.935	0.03	0.3
150	1.018	0.975	0.996	0.03	0.3
200	1.074	1.026	1.050	0.03	0.3

**Table 36.** The results of measurements of the specific heat capacity of sample №11.

Sample №11					
$T, \text{ }^\circ\text{C}$	$c_p, \text{ J}/(\text{g}\cdot\text{K})$			Standard deviation, $\text{J}/(\text{g}\cdot\text{K})$	Student's confidence interval ( $\alpha= 0.05$ ), $\text{J}/(\text{g}\cdot\text{K})$
	Tablet 2	Tablet 3	Average		
25	0.728	0.751	0.739	0.02	0.1
50	0.764	0.791	0.777	0.02	0.2
100	0.835	0.862	0.849	0.02	0.2
150	0.884	0.918	0.901	0.02	0.2
200	0.918	0.960	0.939	0.03	0.3

The dependence of density on temperature can be taken into account using the equation (15). According to the results of the measurements of the CLTE (*Chapter 4.3*) and the results of density measurements (measurements were carried out laboratory by the method of hydrostatic weighing, see *Table 37*), it was found that for this collection of samples the density of the samples is practically independent of temperature: the difference in density at 25 °C and 200 °C when calculating by formula (15) is less than 0.5% (*Figure 44*). In this regard, for this collection of samples, it is quite correct to assume that  $\rho(T) \approx \rho_0$ . Taking into account this assumption, formula (16) for calculating the volumetric heat capacity takes the form:

$$C_p(T) = c_p(T) \cdot \rho_0 \quad (19)$$

**Table 37.** Density measurement results by the hydrostatic weighing method.

Sample No.	$\rho, \text{ g}/\text{cm}^3$
1	2.46
3	2.27
4	2.25
5	2.50
6	2.41
7	2.42
8	2.43
9	2.67
10	2.01
11	2.89

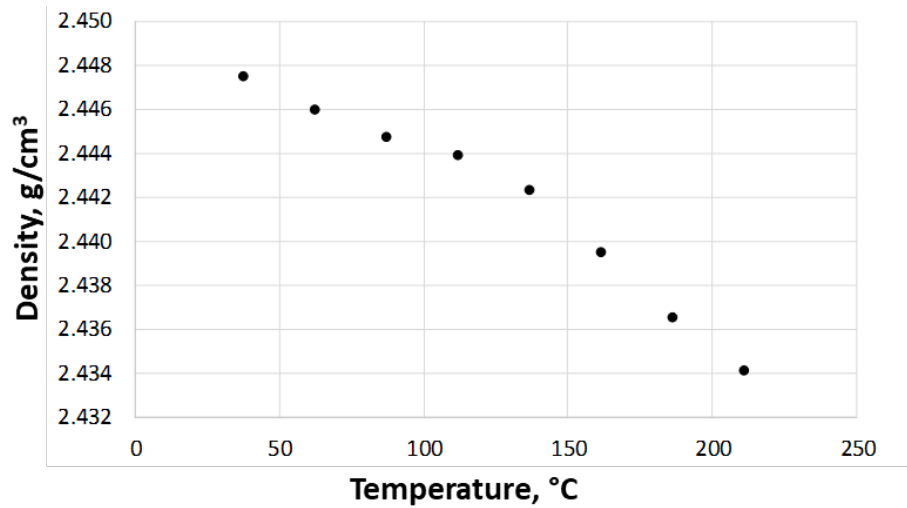


**Figure 44.** The dependence of the density on temperature, calculated by the formula (15), for a sample from the studied collection of rocks, which has the maximum CLTE ( $\alpha = 15.9 \cdot 10^{-6} \text{ K}^{-1}$ ).

Figures 45 and 46 show the dependence of the volumetric heat capacity on temperature for the collection of the studied samples, calculated by the formula (19). The range of volumetric heat capacity variations for Bazhenov formation rocks in the temperature range 25-200 °C is 1.86-2.78 MJ/(m<sup>3</sup>·K), for Abalak formation rocks - 1.64-2.74 MJ/(m<sup>3</sup>·K). The average percentage of volumetric heat capacity increasing with temperature relative to initial volumetric heat capacity (T = 25 °C) for Bazhenov formation rocks is 34%, for Abalak formation rocks – 27% (Figure 47 and 48).

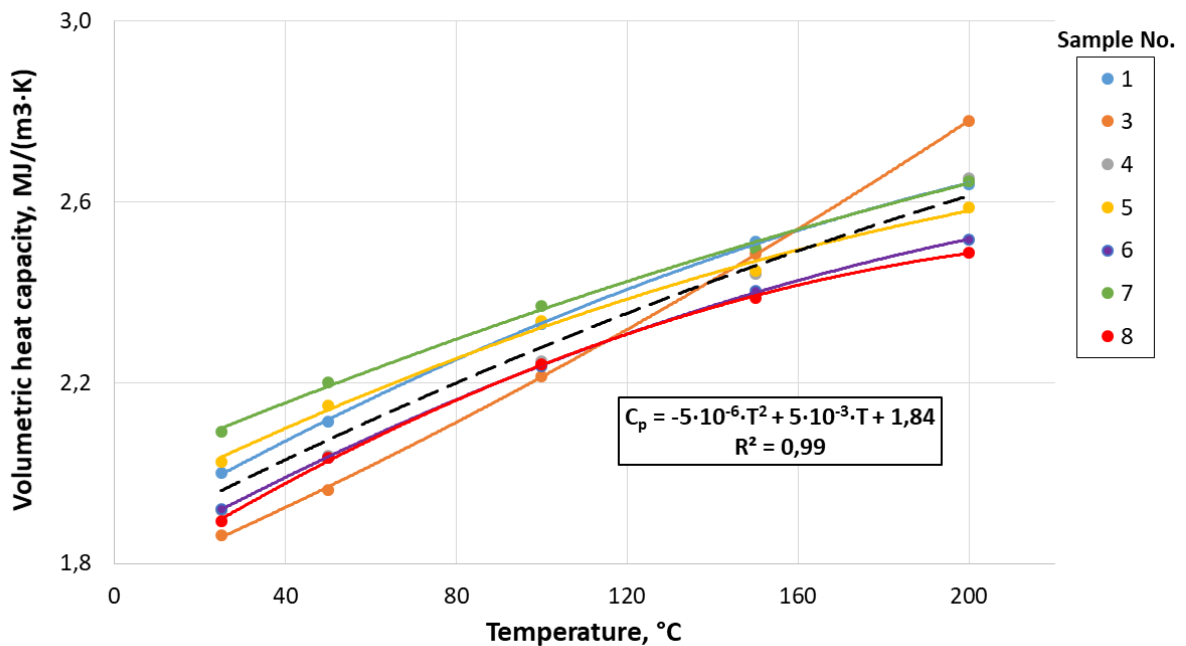


**Figure 45.** The dependence of the volumetric heat capacity on temperature for Bazhenov formation rock samples from oil field 1.

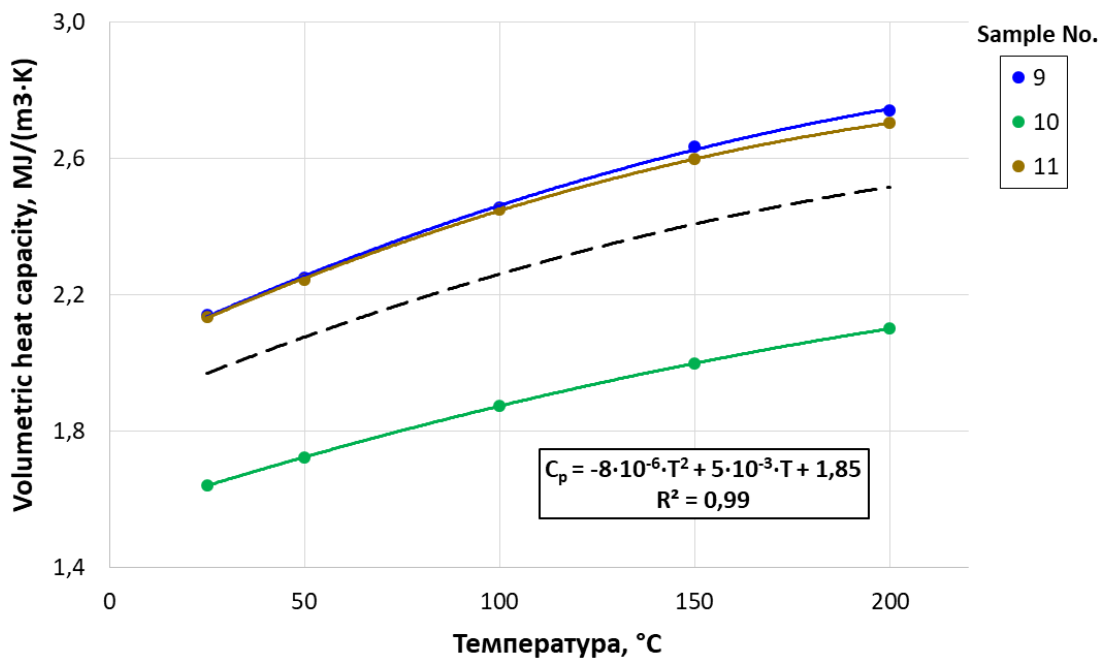


**Figure 46.** The dependence of the volumetric heat capacity on temperature for Abalak formation rock samples from oil field 1.

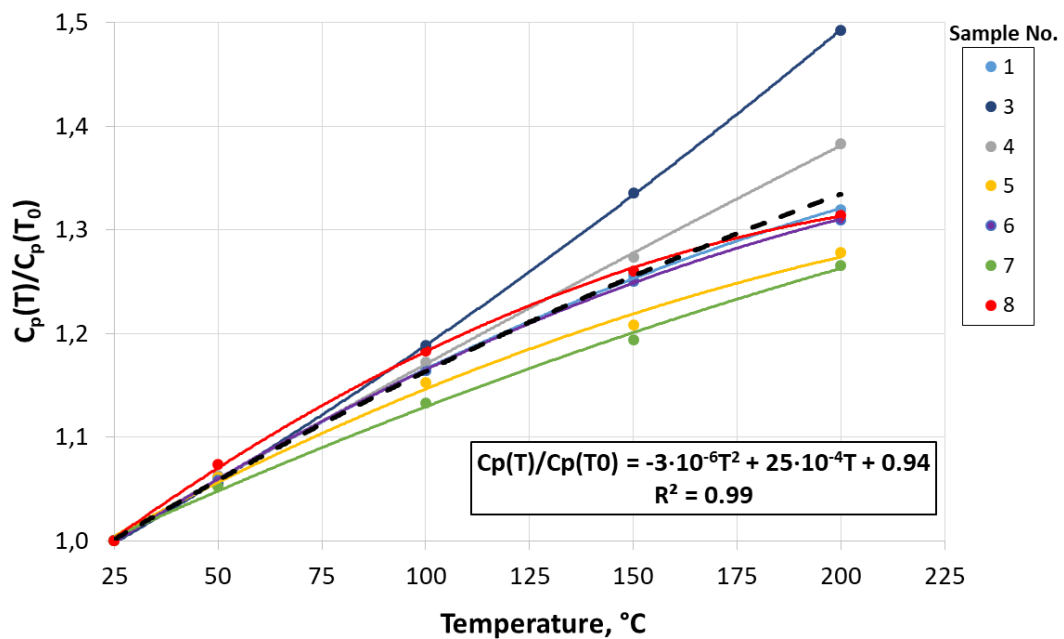


**Figure 47.** The percentage of volumetric heat capacity increasing relatively to initial volumetric heat capacity ( $T = 25$  °C) for Bazhenov formation rocks.

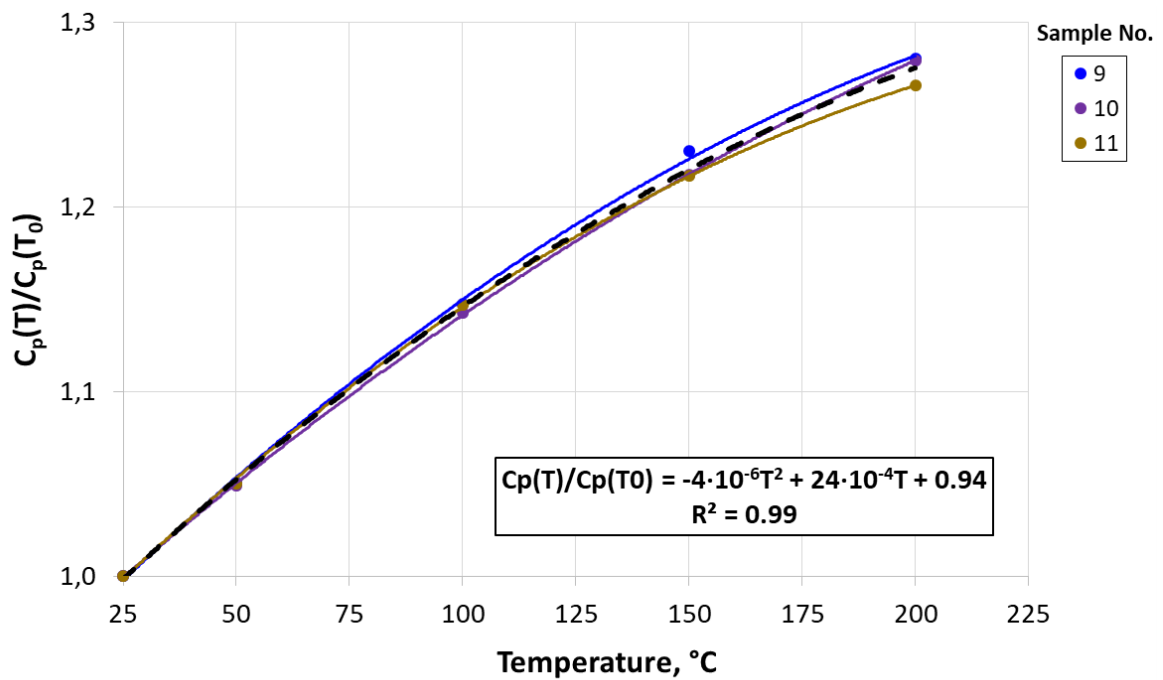


**Figure 48.** The percentage of volumetric heat capacity increasing relatively to initial volumetric heat capacity ( $T = 25\text{ }^{\circ}\text{C}$ ) for Abalak formation rocks.

## Oil field 2

Specific heat measurements were carried out on 8 rock samples of the Golchih and Abalak formations. The measurements were carried out on disc-shaped samples 4.2 mm in diameter, no more than 1 mm thick and weighing 20-40 mg on a NETZSCH-DSC 214 Polyma device in the temperature range 50-300 ° C. During measurements, the mass of the samples changed by no more than 0.15%, which indicates the absence of significant possible phase transitions of pore fluids and the reliability of the results obtained. The measurement results are shown in *Figure 49*.

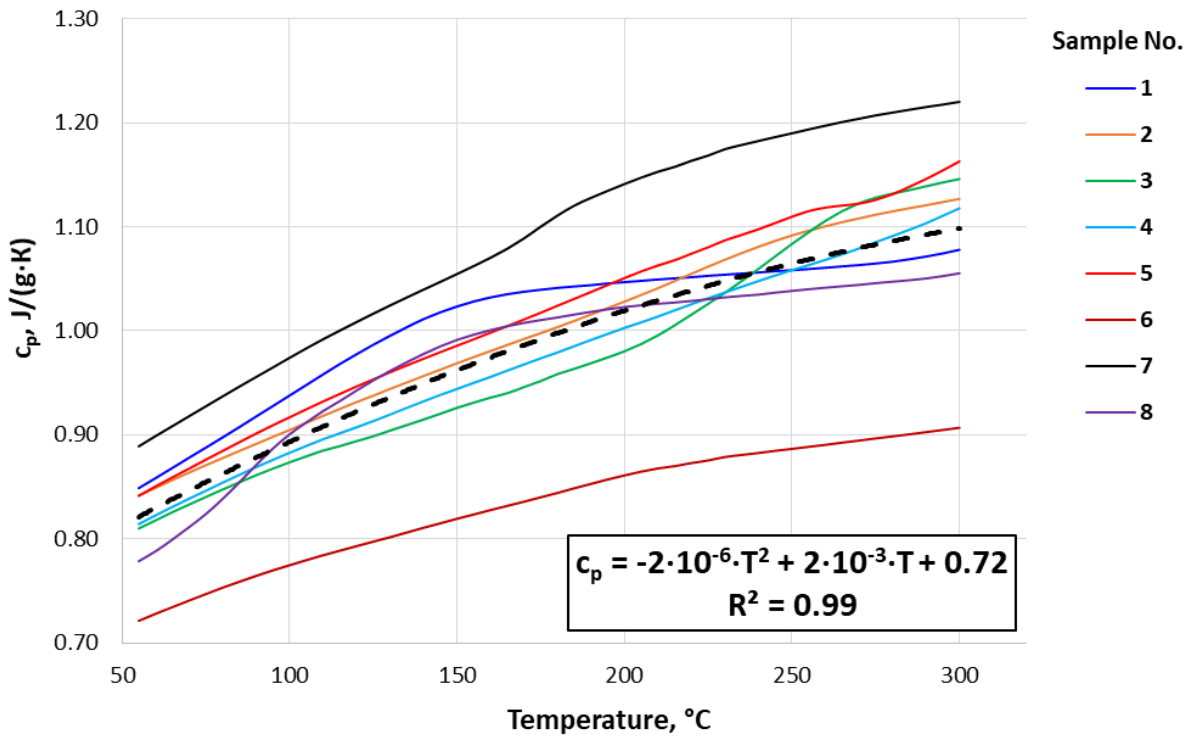


**Figure 49.** Experimental data on the change in the specific heat capacity of rock samples from the Golchih and Abalak formations (Oil field 2) with temperature increasing. The black dotted line is the curve obtained by averaging the specific heat capacity for all samples.

According to the results of the CLTE measurements (*Chapter 4.3*) and the results of density measurements (measurements were carried out by the method of hydrostatic weighing (GOST 25281-82, 1982)) (*Table 38*), it was found that for this collection of rock samples, the density of samples practically does not depend on temperature: the difference in density at 25 °C and 150 °C when calculating by formula (15) is less than 1% (*Figure 50*). In this regard, for this collection of samples, it is quite correct to assume that  $\rho(T) \approx \rho_0$  in the temperature range 25-300 °C. Taking into account this assumption, formula (16) for calculating the volumetric heat capacity takes the form (19).

**Table 38.** The density of the studied rock samples of the Golchih and Abalak formations.

Sample No.	Density, g/cm <sup>3</sup>	Porosity, %
1	2.70	3.8
2	2.69	4.4
3	2.65	3.9
4	2.46	4.2
5	2.31	2.0
6	2.63	3.6
7	2.37	6.0
8	2.65	8.0

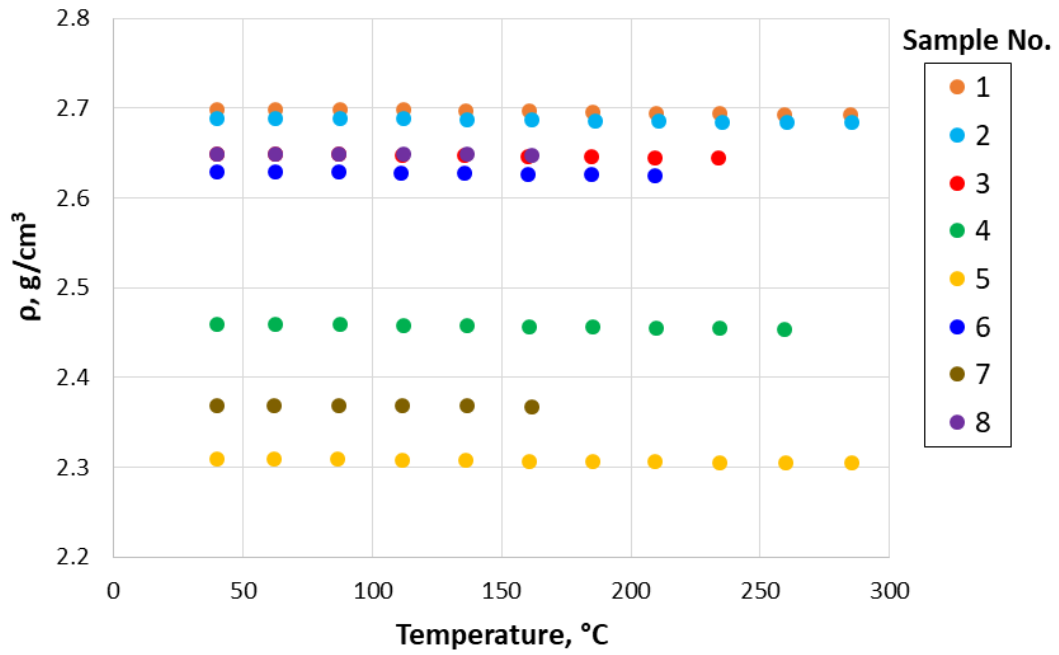


**Figure 50.** Dependence of density on temperature for rock samples of the Golchih and Abalak formations (Oil field 2).

The additivity of the volumetric heat capacity and the fact that the measurements were carried out on porous samples (i.e., consisting of two phases - a matrix and air) make it possible to write formula (16) in the form:

$$C_{\rho}(T) = C_{\rho}^M(T) \cdot (1-x) + c^a(T) \cdot \rho^a(T) \cdot x \quad (20)$$

$$C_{\rho}(T) = c^{\text{meas}}(T) \cdot \rho_0 \quad (21)$$

$C_{\rho}^M$  – volumetric heat capacity of the matrix;  $c^a$ ,  $\rho^a$  – specific heat capacity and density of air;  $c^{\text{meas}}$ ,  $\rho_0$  – measured specific heat capacity and density of a sample at room temperature;  $x$  – air fraction in the sample.

Then,

$$C_{\rho}^M(T) = (c^{\text{meas}}(T) \cdot \rho_0 - c^a(T) \cdot \rho^a(T) \cdot x) / (1-x) \quad (22)$$

Neglecting the volumetric heat capacity of air, we obtain:

$$C_{\rho}^M(T) = (c^{\text{meas}}(T) \cdot \rho_0) / (1-x) \quad (23)$$

Expression (23) was used to determine the matrix values of the volumetric heat capacity as a function of temperature. *Figure 51* shows the general relationships and equations for VHC vs temperature for the rocks of the Golchih and Abalak formations, constructed from the results of measurements for all studied samples. The specific and volumetric heat capacities of the

studied rocks of the Golchih and Abalak formations at 300 °C increase by an average of 35% relative to the specific and volumetric heat capacities at 25 °C.

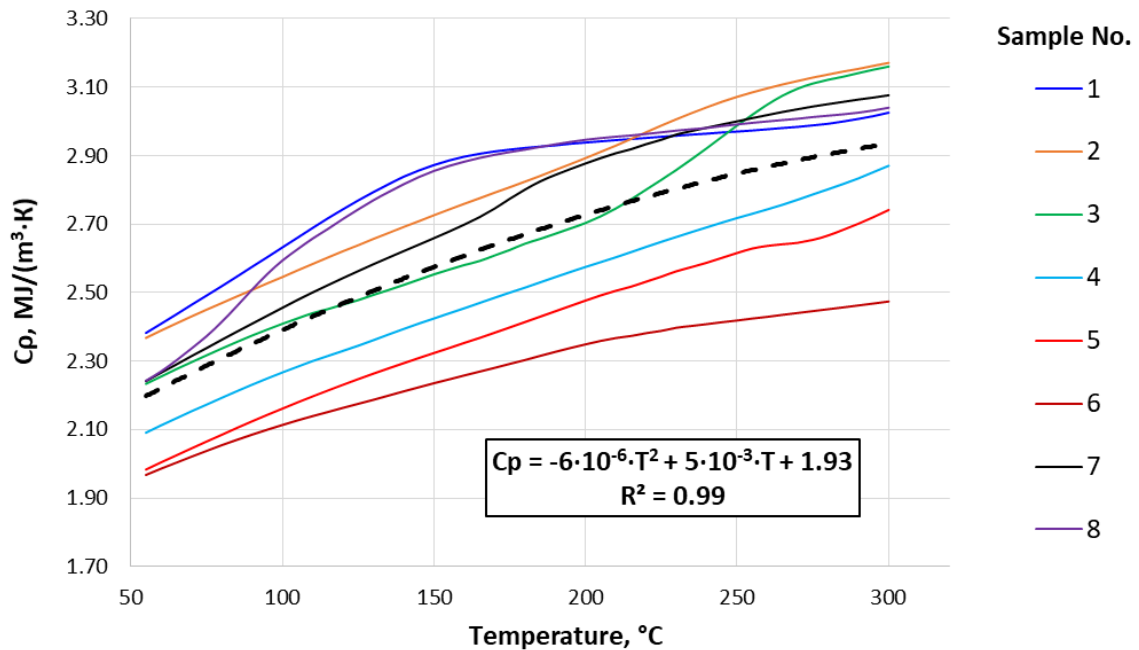


**Figure 51.** The dependence of the volumetric heat capacity of the matrix for all rock samples of the Golchih and Abalak formations (Oil field 2) on temperature. The dashed line is the curve obtained by averaging the volumetric heat capacity of the matrix over all samples.

### Oil field 3

Specific heat measurements were carried out on 12 rock samples of the Bazhenov formation. Measurements were carried out on disk-shaped samples 4.2 mm in diameter, no more than 1 mm thick and weighing 20-40 mg on a NETZSCH-DSC 214 Polyma device in the temperature range 25-200 ° C. During measurements, the mass of the samples changed by no more than 0.15%, which indicates the absence of significant possible phase transitions of pore fluids and the reliability of the results obtained. The measurement results are shown in *Figure 52*.

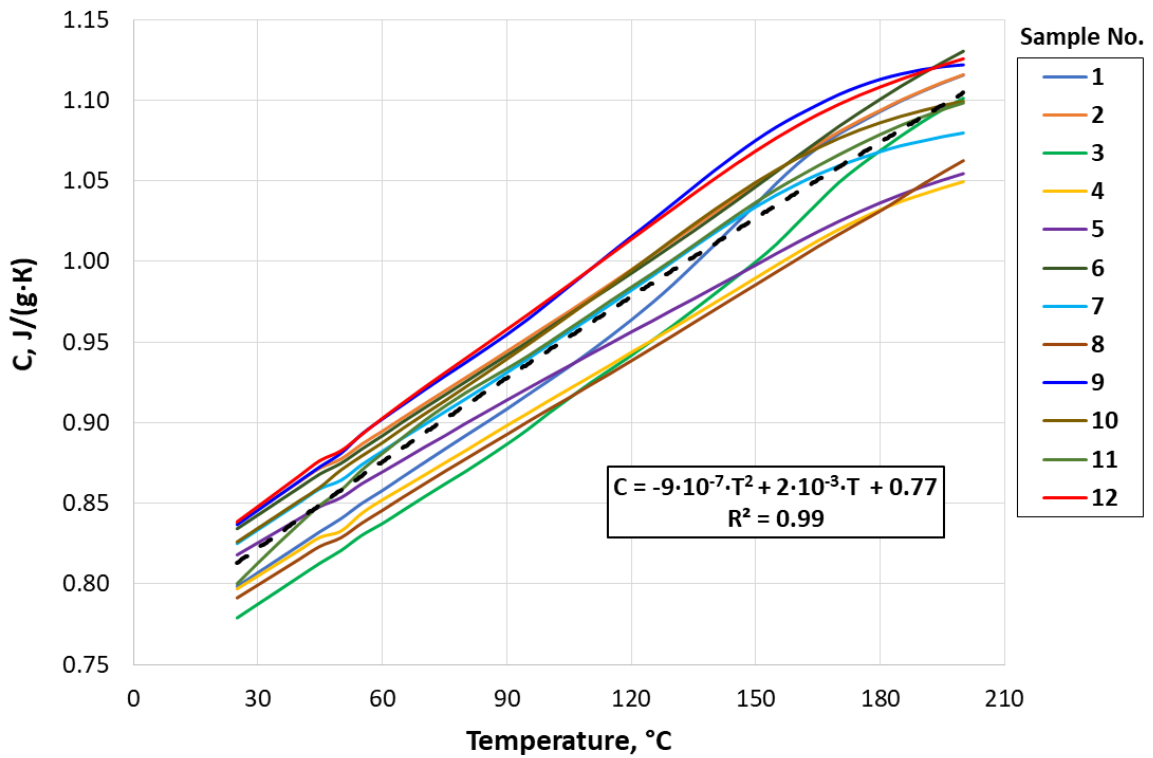


**Figure 52.** Experimental data on the change in the specific heat capacity of rock samples of the Bazhenov formation with an increase in temperature. The black dotted line is the curve obtained by averaging the specific heat capacity for all samples.

According to the results of the measurements of the CLTE (*Chapter 4.3*) and the results of density measurements (the density was determined on the basis of measurements of sample volumes obtained using a PIK-PP porosimeter (Geologika) and measurements of sample masses (*Table 39*), it was found that for this collection of rock samples, the density of the samples is practically independent of temperature: the difference in density at 25 °C and 200 °C when calculating by formula (15) is less than 1%. In this regard, for this collection of samples, it is permissible to assume that  $\rho(T) \approx \rho_0$  in the temperature range 25-200 °C. Formula (16) for calculating the volumetric heat capacity takes the form (19).

**Table 39.** Density of the studied rock samples of the Bazhenov Formation.

№	Density, g/cm <sup>3</sup>
1	2,37
2	2,38
3	2,42
4	2,40
5	2,46
6	2,40
7	2,39
8	2,54
9	2,47
10	2,40
11	2,34
12	2,39

Figure 53 shows the general relationships and equations for the rocks of the Bazhenov Formation, constructed from the results of measurements for all studied samples. The specific and volumetric heat capacities of the studied rocks of the Bazhenov formation at 200 °C increase by an average of 34% relative to the specific and volumetric heat capacities at 25 °C. The range of volumetric heat capacity values is 1.87-2.71 MJ/(m<sup>3</sup>·K).

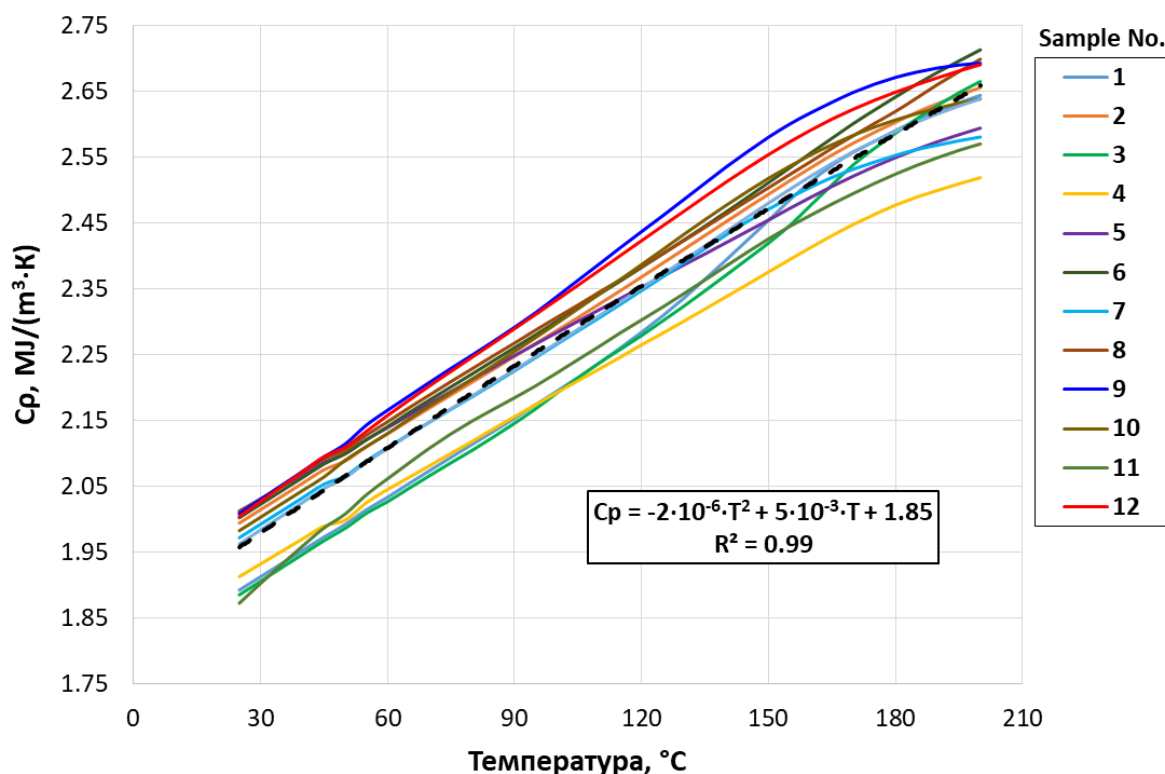


**Figure 53.** The dependence of the volumetric heat capacity, averaged over all rock samples of the Bazhenov formation (Oil field 4), on temperature. The dashed line is the curve obtained by averaging the volumetric heat capacity of all samples.

#### 4.4.3 Equations that relate volumetric heat capacity to temperature for unconventional reservoir rocks

The developed methodology of volumetric heat capacity measurements allows us to establish new equations of VHC vs temperature for unconventional reservoir rocks in the temperature range 25-300 °C (*Table 40*). Volumetric heat capacity range 1.64-3.16 MJ/(m<sup>3</sup>·K). The average percentage of volumetric heat capacity increasing is 27-34%.

**Table 40.** Equations of VHC vs temperature for studied unconventional reservoir rocks

Oil field	Formation	Number of samples	Temperature range, °C	VHC range, MJ/(m <sup>3</sup> ·K)	Equations	Average percentage of VHC increasing, %
1	Bazhenov	7	25-200	1.86-2.78	$C_p = -5 \cdot 10^{-6} \cdot T^2 + 5 \cdot 10^{-3} \cdot T + 1.84$	34
	Abalak	3			$C_p = -8 \cdot 10^{-6} \cdot T^2 + 5 \cdot 10^{-3} \cdot T + 1.85$	27
2	Golchih	7	50-300	1.97-3.16	$C_p = -6 \cdot 10^{-6} \cdot T^2 + 5 \cdot 10^{-3} \cdot T + 1.93$	35
	Abalak	1				
3	Bazhenov	12	25-200	1.87-2.71	$C_p = -2 \cdot 10^{-6} \cdot T^2 + 5 \cdot 10^{-3} \cdot T + 1.85$	34

#### 4.4.4 Analysis of volumetric heat capacity with temperature characteristic of unconventional reservoir rocks in comparison with other sedimentary rocks

*Figure 54* shows the percentage of volumetric heat capacity increasing relatively to initial volumetric heat capacity ( $T = 25$  °C) for Bazhenov formation and other sedimentary rocks. The percentage of volumetric heat capacity increasing for unconventional reservoir rocks with temperature is higher (1.5-1.7 times) than for other sedimentary rocks (limestones, sandstones).

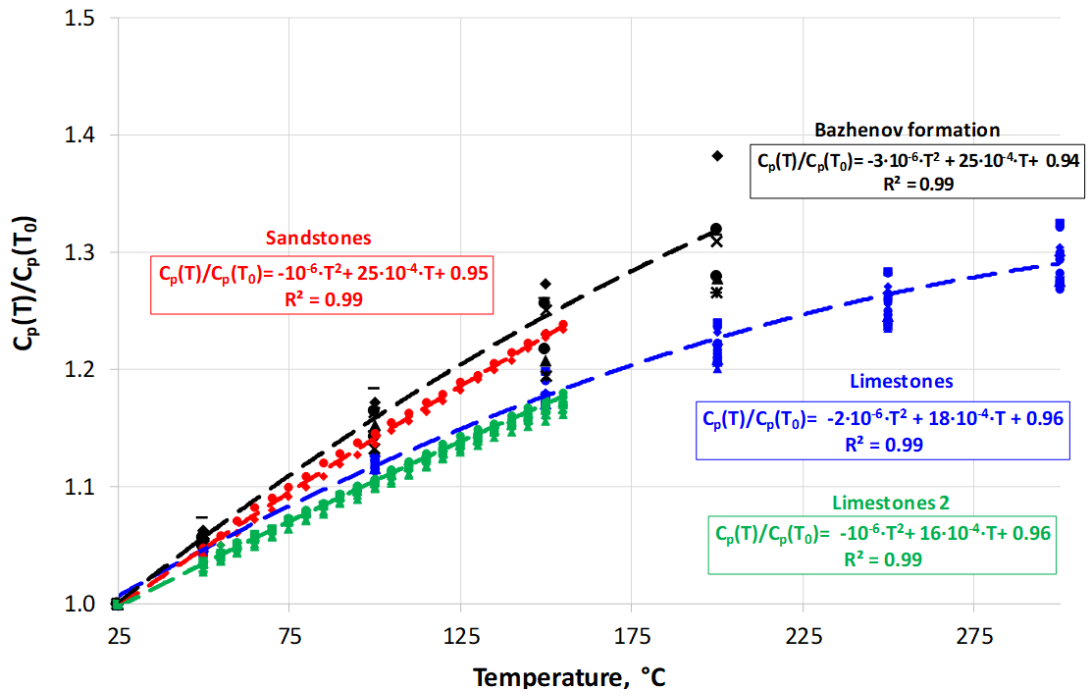


**Figure 54.** The percentage of volumetric heat capacity increasing relatively to initial volumetric heat capacity ( $T = 25 \text{ }^{\circ}\text{C}$ ) for Bazhenov formation and other sedimentary rocks.

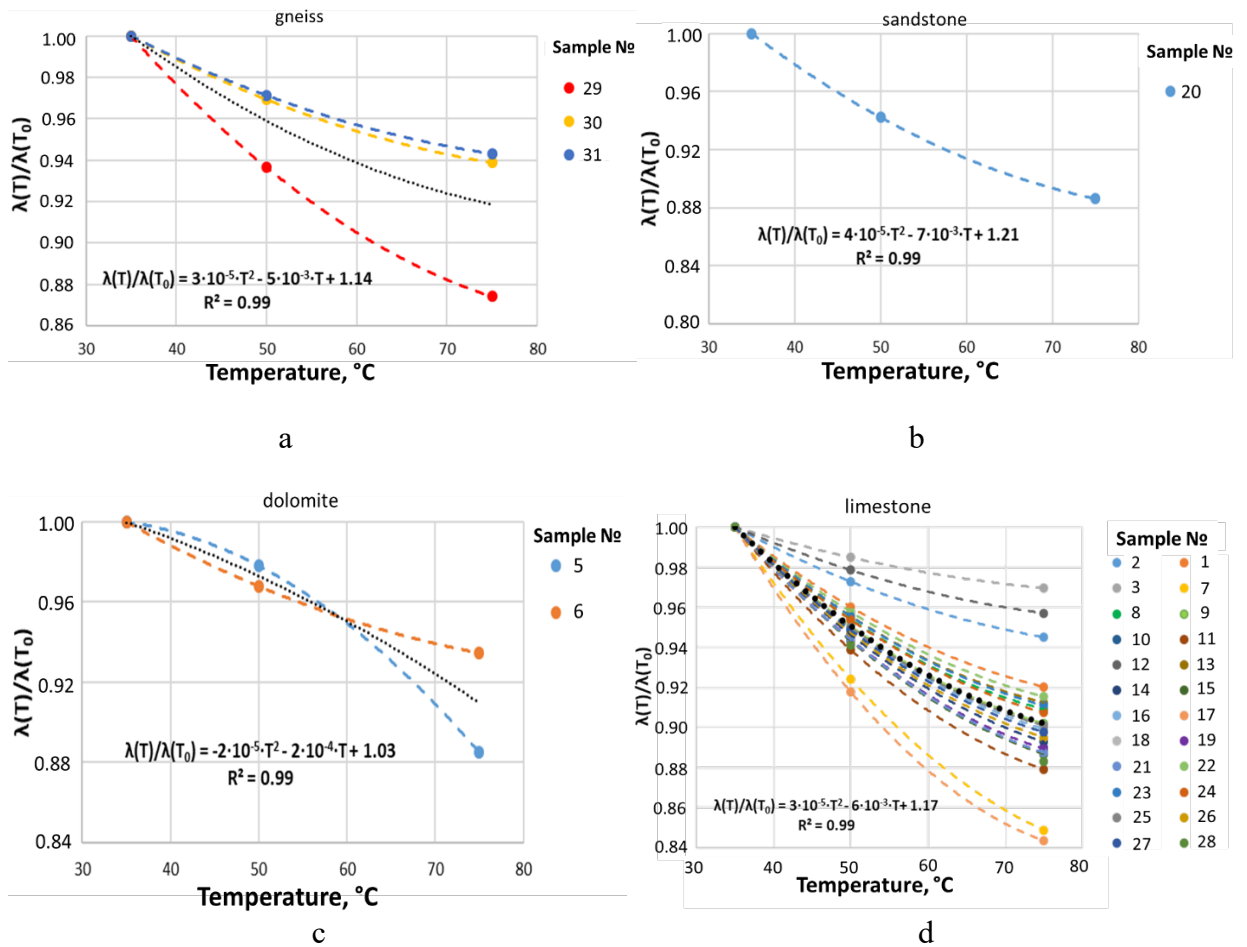
#### 4.5 Experimental investigations of thermal conductivity on rock cuttings and non-consolidated rocks at elevated temperatures

Developed methodology of thermal conductivity measurements on rock cuttings and non-consolidated rocks (*Chapter 3.2*) at elevated temperatures allows us to obtain thermal conductivity of matrix for rock cuttings. *Table 41* shows the results of determining the thermal conductivity and volumetric heat capacity of the matrix for 31 rock-cuttings samples of Domanic formation in the temperature range  $25\text{-}75 \text{ }^{\circ}\text{C}$ . *Figures 55a, b, c, d* show the temperature dependence of the thermal conductivity of the rock matrix for the studied lithotypes.

**Table 41.** The results of determining the thermal conductivity of the matrix (at 25, 50, and 75 °C) and the volumetric heat capacity of the matrix (at 25 °C) based on the results of measurements on rock-cuttings.

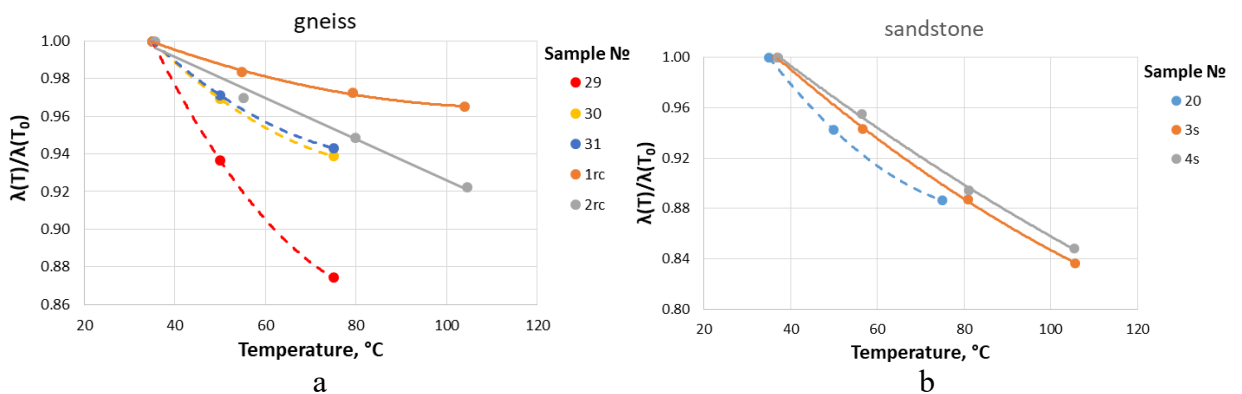
Sample №	Lithotype	T, °C	$\lambda_{\text{matrix}}$ , W/(m·K)	$C_{\text{matrix}}$ , MJ/(m <sup>3</sup> ·K) (T = 25°C)
1	limestone	25	2.09	2.22
		50	2.01	
		75	1.92	
2	limestone	25	3.86	2.44
		50	3.75	
		75	3.64	
3	limestone	25	3.48	2.48
		50	3.43	
		75	3.38	
4	dolomitic limestone	25	4.68	2.40
		50	4.56	
		75	4.43	
5	dolomite	25	5.18	2.52
		50	5.07	
		75	4.59	
6	dolomite	25	5.10	2.44
		50	4.94	
		75	4.77	
7	limestone	25	2.55	2.46
		50	2.35	
		75	2.16	
8	argillite	25	2.90	2.33
		50	2.77	
		75	2.64	
9	argillitic limestone	25	2.64	2.20
		50	2.51	
		75	2.39	
10	limestone	25	2.88	2.22
		50	2.72	
		75	2.57	
11	limestone	25	2.46	2.17
		50	2.31	
		75	2.17	
12	argillite	25	2.38	2.01
		50	2.33	
		75	2.28	
13	argillite	25	2.76	2.14
		50	2.64	
		75	2.52	
14	argillitic limestone	25	2.41	2.25
		50	2.28	
		75	2.16	
15	limestone	25	2.24	2.35
		50	2.12	
		75	1.99	
16	limestone	25	2.54	2.26
		50	2.42	
		75	2.29	
17	argillite	25	3.17	2.03
		50	2.91	
		75	2.67	

18	argillite	25	2.10	2.04
		50	1.99	
		75	1.87	
19	argillite	25	2.48	2.03
		50	2.34	
		75	2.20	
20	argillitic limestone	25	2.54	1.81
		50	2.39	
		75	2.25	
21	argillitic limestone	25	1.95	2.68
		50	1.84	
		75	1.73	
22	argillite	25	1.93	2.26
		50	1.85	
		75	1.76	
23	argillite	25	2.00	2.27
		50	1.91	
		75	1.82	
24	argillite	25	1.98	2.42
		50	1.88	
		75	1.79	
25	argillite	25	2.58	2.39
		50	2.45	
		75	2.32	
26	limestone	25	2.23	2.37
		50	2.11	
		75	1.99	
27	limestone	25	2.22	2.46
		50	2.11	
		75	1.99	
28	limestone	25	2.30	2.39
		50	2.17	
		75	2.03	
29	gneiss	25	2.14	2.16
		50	2.01	
		75	1.87	
30	gneiss	25	2.03	2.12
		50	1.97	
		75	1.91	
31	gneiss	25	2.03	2.25
		50	1.97	
		75	1.91	



**Figure 55.** The results of determining the dependences of the thermal conductivity of the matrix on temperature from the results of measuring the thermal properties on rock cuttings. The equations show the average decreasing of thermal conductivity for the corresponding lithotype.

Figure 56 shows the results of comparing the dependences of the relative decrease in the thermal conductivity of rocks on temperature, obtained by measurements on standard rock samples, with the dependences of the relative decrease in the thermal conductivity of the matrix on temperature, obtained by measurements on rock cuttings.



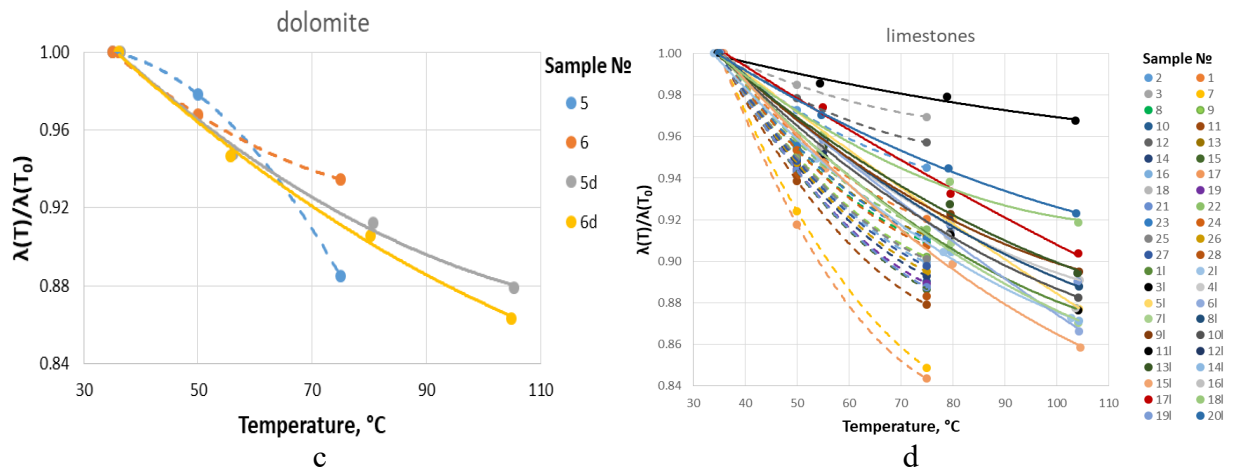


**Figure 56.** Comparison of the results of determining the dependences of the thermal conductivity of the matrix on temperature (according to the results of measurements on rock cuttings) with the results of determining the dependences of the thermal conductivity of rocks on temperature (according to the results of measurements on standard samples). The dashed lines represent the dependences obtained from the results of measurements on rock cuttings, the solid lines represent the dependences obtained from the results of measurements on standard rock samples.

Based on the results of comparing the results of determining the dependences of the thermal conductivity of the matrix on temperature (according to the results of measurements on rock cuttings) with the results of determining the dependences of the thermal conductivity of rocks on temperature (according to the results of measurements on standard samples) (Figure ), the following conclusions can be drawn:

- The behavior of the relative decrease in the thermal conductivity of rocks with increasing temperature is similar to the behavior of the relative decrease in the thermal conductivity of the rock matrix with increasing temperature.
- The average percentage of decrease in the thermal conductivity of the matrix at 75 ° C for the “limestone” lithotype was 10%, for the “dolomite” lithotype - 9%, for the “sandstone” lithotype - 11%, and for the “gneiss” lithotype - 8%.
- For each of the studied lithotypes, averaged equations are obtained, which show the dependence of the thermal conductivity of the matrix on temperature.

**Table 42.** The results of determining the dependences of the thermal conductivity of the matrix on temperature from the results of measurements on rock cuttings.

Lithotype	Number of samples	Equations
limestone	25	$\lambda(T)/\lambda(T_0) = 3 \cdot 10^{-5} \cdot T^2 - 6 \cdot 10^{-3} \cdot T + 1.17$
dolomite	2	$\lambda(T)/\lambda(T_0) = -2 \cdot 10^{-5} \cdot T^2 - 2 \cdot 10^{-4} \cdot T + 1.03$
sandstone	1	$\lambda(T)/\lambda(T_0) = 4 \cdot 10^{-5} \cdot T^2 - 7 \cdot 10^{-3} \cdot T + 1.21$
gneiss	3	$\lambda(T)/\lambda(T_0) = 3 \cdot 10^{-5} \cdot T^2 - 5 \cdot 10^{-3} \cdot T + 1.14$

## Chapter 5. Conclusion

### 5.1 Summary

The research work has produced new experimental data on variations of thermal conductivity in a 30-300 °C temperature range for 39 rock samples from Bazhenov and Abalak formations in the West-Siberian oil basin and Mendym, Domanic, Sargaev, and Timan formations in the Volga-Ural oil basin. The new approach to the measurement of rock thermal conductivity at elevated temperatures, combining two methods (divided-bar and optical scanning) was developed. The approach was applied to organic-rich rocks from unconventional reservoirs. It allows us to control changes in the rock samples during their heating to 300 °C, making a separate definition of changes in thermal conductivity components along the bedding plane and perpendicular to it and correcting the experimental data for variations of rock thermal conductivity with temperature increase, which are due to changes in the rock samples (the appearance of cracks) during heating of the samples.

Comparison of thermal conductivity behavior with temperature for two different regions (West Siberia and Volga-Ural) showed different variations of rock thermal conductivity with temperature and equations with different constants. The results demonstrate that the extrapolation of equations for organic-rich samples from different formations can lead to significant uncertainties due to major differences in the minerals and organic matter contained in the samples.

Quartz dilatometer allowed us to obtain CLTE values of Bazhenov and Abalak formations rocks in a temperature range of 25-300 °C. It is important as reliable information on thermal expansion of particular shale formation could not be obtained from literature data and requires experimental investigation of CLTE on particular representative rock samples collection with advanced equipment and methodology, accounting for rock anisotropy. The total amount of studied samples is 44. Integration of quartz dilatometer and TCS gave the possibility to establish relations between CLTE and thermal conductivity of Bazhenov and Abalak formations rocks.

Directions of CLTE anisotropy main axes were obtained for each rocks sample by multiple measurements in different directions in a short temperature window with following using the least square method. CLTE profiles along wells of unconventional reservoirs were provided as well.

The new methodology of determining the volumetric heat capacity of rocks at elevated temperatures allowed us to obtain new data on the volumetric heat capacity of unconventional reservoir rocks (31 samples) within a temperature range of 25-300 °C. New equations of VHC vs temperature for Bazhenov and Abalak formations were obtained.

Using original techniques for measuring the thermal properties of rocks on rock cuttings for well intervals drilled without core sampling, the thermal conductivity of the rock matrix was measured and the dependence of thermal conductivity on temperature was obtained for 31 rock cutting samples. Based on the results of measurements on rock cuttings, equations were obtained that characterize the dependence of the thermal conductivity of the matrix on temperature for four lithotypes. For each of the studied lithotypes, averaged equations were obtained, which show the dependence of the thermal conductivity of the matrix of the selected lithotypes on temperature.

## 5.2 Conclusions

Unconventional reservoir rocks require new approaches to experimental investigation of thermal properties at elevated temperatures as their properties are different from other sedimentary rocks due to the presence of fractures, organic matter, etc. Experimental investigation of thermal properties of unconventional reservoir rocks at elevated temperatures provided in this research allowed us to make the following conclusions:

- The new approach to the measurement of rock thermal conductivity at elevated temperatures improves the quality of thermal conductivity measurement: (1) the uncertainty up to 20% in DTC-300 thermal conductivity measurement results caused by nonparallelism of studied rock samples was removed, and (2) systematic decrease in thermal conductivity up to 12% caused by rock sample fracturing was accounted for;
- After high-temperature measurements (once the samples have cooled down to room temperature) thermal conductivity components of Bazhenov, Abalak, and Domanic formations rocks decrease up to 20%, a thermal anisotropy coefficient increases up to 13%. The increase of the thermal anisotropy coefficient is caused by the creation of microcracks during heating when the microcracks explain the reduction of thermal conductivity component perpendicular to the bedding plane.

- The effect of temperature on thermal conductivity of the Bazhenov and Abalak formations rocks was found to be much lower (by 2-3 times) than for other sedimentary rocks that is explained by a high content of organic matter in rock samples, which thermal conductivity increases with temperature.
- Bazhenov and Abalak formation rocks have a high degree of CLTE anisotropy. The range of thermal expansion values of the Bazhenov rocks is much higher than values of carbonates, limestones, and clay minerals that is caused by high TOC in studied rock samples (while the thermal expansion of organic matter is much higher than the thermal expansion of rock mineral matrix). Directions of CLTE anisotropy main axes correspond closely to the direction of the main axes of thermal conductivity tensor, that can be used in practice (e.g., for express evaluation of main CLTE directions with optical scanning and correct positioning of a sample before performing time-consuming CLTE measurements).
- New close correlations between CLTE, thermal conductivity, TOC, and density were explained by the high sensitivity of these parameters to the presence of organic matter in studied rock samples. Correlation CLTE vs thermal conductivity showed that core plugs for CLTE investigations should be sampled according to the results of continuous thermal profiling on full-size core samples.
- The temperature behavior of thermal expansion coefficient of the Bazhenov and Abalak formations rocks turned out to have non-monotonic behavior. It agrees with previous observations and differs from the CLTE behavior of other sedimentary rocks (demonstrating a monotonous increase of thermal expansion with temperature). The non-monotonic behavior is, probably, related to bitumen exudation and evaporation of volatile components during heating or non-linear behavior of CLTE of organic matter with temperature. New experimental data showed that the investigation of thermal expansion of organic-rich shales requires an integrated approach to explain observed features like anisotropy and non-monotonic behavior with temperature.
- The average percentage of volumetric heat capacity increase for Bazhenov and Abalak formations rocks is 30%. The results showed that the percentage of volumetric heat capacity increase for unconventional reservoir rocks with temperature is 2 times higher than for other sedimentary rocks.
- The behavior of the relative decrease in the thermal conductivity of the matrix with increasing temperature coincides quite well with the behavior of the relative decrease in the effective thermal conductivity of rocks with increasing temperature. The relative

decrease in the thermal conductivity of the matrix and the thermal conductivity of rocks at a temperature of 75 ° C varies from 8 to 11% for the studied four lithotypes.

## Bibliography

1. Abdulagatova, Z.Z., Abdulagatov, I.M., Emirov, V.N., 2009. Effect of temperature and pressure on the thermal conductivity of sandstone. *Int. J. Rock Mech. Min. Sci.* 46, 1055–1071.
2. Alver B., Gökhan D., Alver Ö. Investigation of the influence of heat treatment on the structural properties of illite-rich clay mineral using FT-IR, <sup>29</sup>SiMAS NMR, TG, and DTA methods. *Anadolu Univ J Sc Tech.* 2016;17(5):823-829. <https://doi.org/10.18038/aubtda.279851>
3. Anderson D.L. Theory of the Earth. *Boston, Blackwell Scientific Publications*;1989.
4. Bauer S.J., Handin J. Thermal expansion and cracking of three confined water-saturated igneous rocks to 800°C. *Rock Mech Rock Eng.* 1983;16:181-198. <https://doi.org/10.1007/BF01033279>
5. Asaad Y. A study of the thermal conductivity of fluid-bearing porous rocks. *Ph.D. Dissertation (Univ. of Calif. Berkeley)*, 1995.
6. Chekhonin, E., Popov, E., Popov, Y., Gabova, A., Romushkevich, R., Spasennykh, M., Zagranovskaya, D., 2018. High-resolution evaluation of elastic properties and anisotropy of unconventional reservoir rocks via thermal core logging. *Rock Mech. Rock Eng.* 51, 2747-2759. <https://doi.org/10.1007/s00603-018-1496-z>
7. Chekhonin E., Parshin A., Pissarenko D., Popov Y., Romushkevich R., Safonov S., Spasennykh M., Chertenkov M., Stenin V. When rocks get hot: thermal properties of reservoir rocks. *Oilfield Review*, 2012; 24(3):20-37. <https://www.slb.com/-/media/files/oilfield-review/2-rocks-hot-2-english>
8. Chudnovsky A., 1962. Thermophysical characteristics of dispersive materials, *first ed. Physmatgiz, Moscow* (in Russian).
9. Clauser, C., 2006. Types of geothermal energy use, in: Heinloth, K. (Ed.), *Renewable Energy, Springer-Verlag Berlin Heidelberg*. pp. 551-565. <https://doi.org/10.1007/b83039>
10. Clauser, C., Huenges, E., 1995. Thermal conductivity of rocks and minerals, in: Ahrens, T. J. (Ed.), *Rock Physics & Phase Relations: A Handbook of Physical Constants, AGU Ref. Shelf*, pp. 105-126. <http://dx.doi.org/10.1029/RF003p0105>
11. Cooper H.W., Simmons G. The effect of cracks on the thermal expansion of rocks. *Earth Planet Sc Lett.* 1977;36:404-412. [https://doi.org/10.1016/0012-821X\(77\)90065-6](https://doi.org/10.1016/0012-821X(77)90065-6)
12. Delage P. Thermal issues in shales and clay rocks. *Proceedings of International Symposium on Energy Geotechnics (SEG) - SEG 2015, Barcelona.* 2015.

<http://citeseerx.ist.psu.edu/viewdoc/download?doi=10.1.1.861.6953&rep=rep1&type=pdf>

13. Dobrynin V.M., Vendelstein B.Yu., Kozhevnikov D.A. *Petrophysics (Physics of rocks)*. Moscow: Oil and Gas, Russian State University of Oil and Gas, 2004.
14. DuBow, J., Nottenburg, R., Collins, G., 1976. Thermal and electrical conductivities of Green River oil shales. *J. Am. Chem. Soc.* 21, 77-86.
15. Durham, W. B., Abey A. E., 1981. The effect of pressure and temperature on the thermal properties of salt and quartz monzonite. *Proceedings of the 22nd US symposium on rock mechanics, Cambridge, MA, USA*. <https://www.osti.gov/servlets/purl/6791312>
16. Duvall FEW, Sohn HY, Pitt CH, Bronson MC. Physical behavior of oil shale at various temperatures and compressive loads: 1. Free thermal expansion. *Fuel*. 1983;62:1455-1461. [https://doi.org/10.1016/0016-2361\(83\)90114-X](https://doi.org/10.1016/0016-2361(83)90114-X)
17. Edvabnik V.G. Modern problems of science and education. On the theory of generalized conductivity of mixtures. *Issue 1 (Part 2)*, 2015
18. Gabova A, Chekhonin E, Popov E, Savelev E, Popov Y, Kozlova E, Karpov I. Investigation of coefficient of linear thermal expansion of Bazhenov formation rocks. *Proceedings of the 19th conference "Geomodel-2017", Gelendzhik, Russia, 2017* (in Russian). <https://doi.org/10.3997/2214-4609.201702219>
19. Garitte B., Gens A., Vaunat J., Armand G., 2014. Thermal conductivity of argillaceous rocks: determination methodology using in situ heating tests. *Rock Mech. Rock Eng.* 47, 111-129. <https://doi.org/10.1007/s00603-012-0335-x>
20. Gilliam T., Morgan I., 1987. Shale: Measurement of thermal properties. *Technical Report, Oak Ridge National Laboratory, United States*. <https://doi.org/10.2172/6163318>
21. Grebowicz J., 2014. Understanding thermal properties of oil shales at high temperature toward the application of nuclear energy in the extraction of natural hydrocarbons. *J. Therm. Anal. Calorim.* 116, 1481–1490. <https://doi.org/10.1007/s10973-014-3822-3>
22. Hantschel T., Kauerauf A.I., 2009. Fundamentals of basin and petroleum systems modeling. *Springer-Verlag Berlin Heidelberg*. <https://doi.org/10.1007/978-3-540-72318-9>
23. Harvey R.D. Thermal expansion of certain Illinois limestones and dolomites. *Illinois State Geol Surv.* 1967;415:1-33. <https://core.ac.uk/download/pdf/17355277.pdf>
24. Heard H.C., Page L. Elastic Moduli, Thermal Expansion, and Inferred Permeability of Two Granites to 350°C and 55 Megapascals. *J Geophys Res.* 1982;87:9340–9348. <https://doi.org/10.1029/JB087iB11p09340>

25. Hillel D. *Fundamentals of Soil Physics*, 1980.
26. Horai K., Susaki G., 1989. The effect of pressure on the thermal conductivity of silicate rocks up to 12 kbar. *Phys. Earth Planet. Inter.* 55, 292-305. [https://doi.org/10.1016/0031-9201\(89\)90077-0](https://doi.org/10.1016/0031-9201(89)90077-0)
27. Huotari T., Kukkonen I. Thermal expansion properties of rocks: literature survey and estimation of thermal expansion coefficient for Olkiluoto mica gneiss. *Working Report, Geological Survey of Finland, Finland*. 2004. [http://www.posiva.fi/files/2259/POSIVA-2004-04\\_Working-report\\_web.pdf](http://www.posiva.fi/files/2259/POSIVA-2004-04_Working-report_web.pdf)
28. Ilozobhie A., George A., Asuquo O., Yahaya I., 2016. Determination of thermal conductivity of some shale samples in Awi formation and its geophysical implications, Cross River State, Nigeria. *Journal of Environment and Earth Science. Environ Earth Sci.* 6(8), 102-111.
29. Irani M., Cokar M., 2016. Discussion on the effects of temperature on thermal properties in the steam-assisted-gravity-drainage (SAGD) process. *Part 1: Thermal Conductivity*. 21, SPE 178426. <https://doi.org/10.2118/178426-PA>
30. Jha M., Verma A., Maheshwar S., Chauhan A., 2016. Study of temperature effect on thermal conductivity of Jhiri shale from Upper Vindhyan, India. *Bull Eng Geol Environ.* 75, 1657–1668. <https://doi.org/10.1007/s10064-015-0829-3>
31. Kaevand T., Lille U. Atomistic molecular simulation of thermal volume expansion of Estonian kukersite kerogen. *Oil Shale*. 2005;22(3):291–303.
32. Kasenov B.K., Ermagambet, Bekturganov N.S., Nabiev M.A., Kasenova Sh.B., Sagintaeva Zh.I., Kuanyshbekov E.E., Seisenova A.A. Chemical composition and Heat Capacity of Shale from the Kendyrlyk and Shubarkol Deposits // *Solid Fuel Chemistry*. - 2016. - Vol. 50. - №.3 - P. 149-151.
33. Khan L., Maqsood A., 2007. Prediction of effective thermal conductivity of porous consolidated media as a function of temperature: a test example of limestones. *J. Phys. D: Appl. Phys.* 40, 4953–4958. <https://doi.org/10.1088/0022-3727/40/16/030>
34. Kukkonen, I., Suppala I., 1999. Measurement of thermal conductivity and diffusivity in-situ: Literature survey and theoretical modeling of measurements. *Report POSIVA 99-1, Geological Survey of Finland, Helsinki*.
35. Lemenager A., O'Neill C., Zhang S., Evans M. The effect of temperature-dependent thermal conductivity on the geothermal structure of the Sydney Basin., *Geothermal Energy*, 6: 1-27, 2018.

36. Luque A., Leiss B., Álvarez-Lloret P., Cultrone G., Siegesmund S., Sebastian E., Cardell C. Potential thermal expansion of calcitic and dolomitic marbles from Andalusia (Spain). *J Appl Cryst.* 2011;44:1227-1237. <https://doi.org/10.1107/S0021889811036910>
37. MacGillivray D.A., Dusseault M.B. Thermal conduction and expansion of saturated quartz-illitic and smectitic shales as a function of stress, temperature, and bedding anisotropy. *Int J Rock Mech Min Sci.* 1998;35:613. [https://doi.org/10.1016/S0148-9062\(98\)00051-5](https://doi.org/10.1016/S0148-9062(98)00051-5)
38. McKinstrey H.A. Thermal expansion of clay minerals. *American Mineralogist.* 1965;50(1-2): 212-222.
39. Merriman J., Whittington A., Hofmeister A., 2017. Re-evaluating thermal conductivity from the top down: thermal transport properties of crustal rocks as a function of temperature, mineralogy, and texture. *Proceedings of 42nd Workshop on Geothermal Reservoir Engineering, Stanford University, Stanford, California.* 1, 1180-1191.
40. Miklashevsky D. Development and application of an instrumental and methodological complex for measuring the thermal properties of rocks at elevated temperature and pressure conditions. *Ph.D. dissertation.* 2007
41. Miklashevsky D., Popov Yu., Vertogradsky V., Bayuk I., 2006. Measurements of components of thermal conductivity and thermal diffusivity tensors of rocks at reservoir thermobaric conditions. *Geology and Exploration.* 6, 38-42 (in Russian).
42. Milner, H.B., 1962. *Sedimentary petrography, volume II, Principles and Applications.* MacMillan Company, NY, 715 pp.
43. Nottenburg R., Rajeshwar K., Rosenvold R., DuBow J., 1978. Measurement of thermal conductivity of Green River oil shales by a thermal comparator technique. *Fuel.* 57(12), 789-795. [https://doi.org/10.1016/0016-2361\(78\)90141-2](https://doi.org/10.1016/0016-2361(78)90141-2)
44. Novikov S.V., Popov Yu.A., Tertychnyi V.V., Shako V.V., Pimenov V.P., 2008. The potentialities and problems of modern thermal logging. *Geology and Exploration.* 3, 54–57 (in Russian).
45. Pitts M. Thermal properties of the Cobourg limestone. *Master Thesis. Queen's University, Kingston, Ontario, Canada.* 2017. <https://qspace.library.queensu.ca/handle/1974/15339>
46. Popov E., Chekhonin E., Popov Y., Romushkevich R., Gabova A., Zhukov V., 2016a. Novel approach of Bazhenov formation investigation through thermal core profiling. *Nedropolzovanie XXI vek,* 6, 52-61 (in Russian).

47. Popov E., A. Trofimov, A. Goncharov, S. Abaimov, E. Chekhonin, Yu. Popov, I. Sevostianov. Technique of rock thermal conductivity evaluation on core cuttings and nonconsolidated rocks. *International Journal of Rock Mechanics and Mining Sciences*, 108, 15–22, 2018.
48. Popov E., Popov Y., Romushkevich R., Spasennykh M., Kozlova E. Detailed Profiling Organic Carbon Content of Oil Shales with Thermal Core Logging Technique. *Proceedings of the Sixth EAGE Shale Workshop, Bordeaux, France*. 2019. <https://doi.org/10.3997/2214-4609.201900305>
49. Popov Yu., Beardsmore G., Clauser C., Roy S., 2016b. ISRM Suggested methods for determining thermal properties of rocks from laboratory tests at atmospheric pressure. *Rock Mech. Rock Eng.* 49(10), 4179-4207. <https://doi.org/10.1007/s00603-016-1070-5>
50. Popov Yu., Chekhonin E., Parshin A., Law D.H.-S., Pissarenko D., Miklashevskiy D., Popov E., Spasennykh M., Safonov S., Romushkevich R., Bayuk I., Danilenko A., Gerasimov I., Ursegov S., Konoplev Yu., Taraskin E., 2013. Experimental investigations of spatial and temporal variations in rock thermal properties as necessary stage in thermal EOR. *SPE Heavy Oil Conference, Calgary, Alberta, Canada*, SPE-165474-MS. <https://doi.org/10.2118/165474-MS>.
51. Popov Yu.A., Popov E.Yu., Chekhonin E.M., Gabova A.V., Romushkevich R.A., Spasennykh M.Yu., Zagranovskaya D.E., 2017. Investigation of Bazhenov formation using thermal core logging technique. *Oil Industry*. 3, 23-27. <https://doi.org/10.24887/0028-2448-2017-3-22-27>
52. Popov Yu., Tertychnyi V., Romushkevich R., Korobkov D., Pohl J., 2003. Interrelations between thermal conductivity and other physical properties of rocks: experimental data. *Pure Appl. Geophys.* 160, 1137–1161. <https://doi.org/10.1007/PL00012565>
53. Popov Yu., Berezin V., Solov'ev G., Romushkevich R., Korostelev V., Kosturin A., 1987. Thermal conductivity of minerals. *Izvestiya, Physics of the Solid Earth*. 3, 83-92 (in Russian).
54. Popov Yu., Parshin A., Al-Hinai S., Miklashevskiy D., Popov E., Dyshlyuk E., Chekhonin, E., Safonov S., Khan R., 2014. Experimental investigations of reservoir thermal properties for heavy oil field in Oman with new methods and equipment. *World Heavy Oil Congress, New Orleans, Louisiana, USA*, WHOC14 – 258.
55. Popov Y.A., Miklashevsky D.Y., Vertogradsky V.A., Shuvalov V.I., Korobkov D.A., Lazarenko A.P. Improvement of instrumental and methodical base for measuring the

- coefficient of linear thermal expansion of rocks and minerals. *Geol Explor.* 2008;6:63-68.
56. Popov Y., Parshin A., Miklashevskiy D., Abashkin V. Instrument for Measurements of Linear Thermal Expansion Coefficient of Rocks. *Proceedings of 46th US Rock Mechanics/Geomechanics Symposium, Chicago, IL, USA.* ARMA-2012-510. 2012.
  57. Popov E., Romushkevich R., Popov Y. Measurement of thermal properties on standard core samples as necessary step for thermophysical investigation of hydrocarbon reservoirs. *Geol Explor.* 2017; 2:56-70.
  58. Prats M., O'Brien, S., 1975. Thermal conductivity and diffusivity of Green River Oil Shale, *J. Pet. Technol.* 27, 97-106. <https://doi.org/10.2118/4884-PA>
  59. Pribnow D., Sass J.H. Determination of thermal conductivity from deep boreholes, *Journal of Geophysical Research*, 100, 9981–9994, 1995.
  60. Ramazanov A., Magdiev A., 2014. Influence of pressure and temperature on thermal conductivity of limestone. *Izvestiya MGTU "MAMP".* 1(19), 91-95 (in Russian).
  61. Rajeshwar, K., Nottenburg, J., Dubow, J., 1979. Thermophysical properties of oil shales. *J. Mater. Sci.* 14(9), 2025–2052. <https://doi.org/10.1007/BF00688409>
  62. Rajeshwar, K., DuBow, J., 1980. Thermophysical properties of Devonian shales. *Fuel.* 59(11), 790-794. [https://doi.org/10.1016/0016-2361\(80\)90257-4](https://doi.org/10.1016/0016-2361(80)90257-4)
  63. Rajeshwar, K., DuBow, J., Rosenvold, R., 1980. Dependence of thermal conductivity on organic content for Green River oil shales. *Ind. Eng. Chem. Prod. Res. Dev.* 19(4), 629–632. <https://doi.org/10.1021/i360076a029>
  64. Savest N., Oja V. Heat capacity of kukersite oil shale: literature overview. *Oil Shale*, 2013, Vol. 30, No. 2, pp. 184–192.
  65. Seipold U., 1998. Temperature dependence of thermal transport properties of crystalline rocks - a general law. *Tectonophysics.* 291, 161-171. [https://doi.org/10.1016/S0040-1951\(98\)00037-7](https://doi.org/10.1016/S0040-1951(98)00037-7)
  66. Sekiguchi K., 1984. A method for determining terrestrial heat flow in oil basinal areas. *Tectonophysics.* 103, 67–79. [https://doi.org/10.1016/0040-1951\(84\)90075-1](https://doi.org/10.1016/0040-1951(84)90075-1)
  67. Siegesmund S., Ullemeyer K., Weiss T., Tschegg E.K. *Int J Earth Sci.* 2000;89:170. <https://doi.org/10.1007/s005310050324>
  68. Siratovich P.A., Aulock F.W., Lavallée Y., Cole J.W., Kennedy B.M., Villeneuve M.C. Thermoelastic properties of the Rotokawa andesite: a geothermal reservoir constraint. *J Volcanol Geotherm Res.* 2015;301:1-13. <https://doi.org/10.1016/j.jvolgeores.2015.05.003>

69. Sokolova L.S., Duchkov A.D., Yurchenko N.V., 1986. Thermal conductivity of bituminous argillites from the Bazhenov formation. *Russ Geol. Geophys.* 10, 42-46 (in Russian).
70. Somerton W.H., 1992. Thermal properties and temperature related behavior of rock/fluid systems. *Elsevier, New York*. [https://doi.org/10.1016/S0376-7361\(09\)70024-X](https://doi.org/10.1016/S0376-7361(09)70024-X)
71. Somerton W.H., Boozer G.D., 1960. Thermal characteristics of porous rocks at elevated temperatures. *Annual Fall Meeting of the Los Angeles Basin Section of SPE*, SPE-1372-G, <https://doi.org/10.2118/1372-G>
72. Smith D., 1978. Thermophysical Properties of Conasauga Shale. *Master Thesis. Oak Ridge Y-12 Plant, TN*. <https://www.osti.gov/servlets/purl/6431483>
73. Smith J.W., Johnson D.R. Mechanisms helping to heat oil shale blocks. *Am Chem Soc Prepr, Fuel Chem Div.* 1976;21(6):25-33.
74. Sun Q., Lü C., Cao L., Li W., Geng J., Zhang W., 2016. Thermal properties of sandstone after treatment at high temperature. *Int. J. Rock Mech. Min. Sci.* 85, 60–66. <https://doi.org/10.1016/j.ijrmms.2016.03.006>
75. Vosteen H.-D., Schellschmidt R., 2003. Influence of temperature on thermal conductivity, thermal capacity and thermal diffusivity for different types of rock. *Phys. Chem. Earth.* 28, 499–509. [https://doi.org/10.1016/S1474-7065\(03\)00069-X](https://doi.org/10.1016/S1474-7065(03)00069-X)
76. Wang G., Yang D., Kang Z., Zhao J., 2018. Anisotropy in Thermal Recovery of Oil Shale-Part 1: Thermal Conductivity, Wave Velocity, and Crack Propagation. *Energies.* 11(77). <https://doi.org/10.3390/en11010077>
77. Weaver C.E. Thermal properties of clays and shales. *Technical Report, Oak Ridge, US.*1976.
78. Wong T.F., Brace W.F. Thermal expansion of rocks: some measurements at high pressure. *Tectonophys.* 1979;57:95-117. [https://doi.org/10.1016/0040-1951\(79\)90143-4](https://doi.org/10.1016/0040-1951(79)90143-4)
79. Yanchenko G.A. Information value rising for the rocks expansion temperature coefficients determination experiments. *Min Inf Anal Bull.* 2009;2:110-115. <https://cyberleninka.ru/article/n/o-povyshenii-tochnosti-i-informativnosti-eksperimentov-po-opredeleniyu-temperaturnyh-koeffitsientov-lineynogo-rasshireniya-gornyh>
80. Yarzev V.P., Erofeev A.V. Operating properties and durability of bitumen-polymer composites. *FGBOU VPO, TGTU, Tambov.* 2004. <http://www.tstu.ru/book/elib/pdf/2014/yarcev.pdf>

81. Yu Y. J., Liang W. G., Bi J. L., Geng Y. D., Zhang C. D., Zhao Y. S., 2015. Thermophysical experiment and numerical simulation of thermal cracking and heat transfer for oil shale. *Proceedings of 13th ISRM International Congress of Rock Mechanics, Montreal, Canada*, ISRM-13CONGRESS-2015-178.
82. Yudin V., Korolev A., Afanaskin I., Volpin S., 2015. Heat capacity and thermal conductivity of rocks and fluids of Bazhenov formation rocks – input data for numerical modeling of thermal methods development. *FGU FNC NIISI RAN, Moscow*. ISBN 978-5-93838-059-2 (in Russian). <https://www.niisi.ru/n3.pdf>
83. Zhdanov L.S., Zhdanov G.L. Physics for secondary specialized educational institutions: Textbook. — 4th ed., Revised — M.: Science. Main editorial office of physical and mathematical literature, 1984.
84. Zhou H., Liu H., Hu D., Yang F., Lu J., Zhang F. Anisotropies in Mechanical Behaviour, Thermal Expansion and P-Wave Velocity of Sandstone with Bedding Planes. *Rock Mech Rock Eng.* 2016;49:4497. <https://doi.org/10.1007/s00603-016-1016-y>
85. ASTM C177-13, 2013. Standard Test Method for Steady-State Heat Flux Measurements and Thermal Transmission Properties by Means of the Guarded-Hot-Plate Apparatus. ASTM International, West Conshohocken, PA. <https://www.astm.org/Standards/C177.htm>
86. ASTM E1530-11, 2016. Standard Test Method for Evaluating the Resistance to Thermal Transmission of Materials by the Guarded Heat Flow Meter Technique, ASTM International, West Conshohocken, PA. <https://www.astm.org/Standards/E1530.htm>
87. ASTM D4535-85, 2000. Standard Test Methods for Measurement of Thermal Expansion of Rock Using a Dilatometer. ASTM International, West Conshohocken, PA, 2000, [www.astm.org](http://www.astm.org)
88. ASTM E1269-11. Standard Test Method for Determining Specific Heat Capacity by Differential Scanning Calorimetry. – ASTM International, West Conshohocken, PA. – 2018. – Режим доступа: [www.astm.org](http://www.astm.org). – Загл. с экрана.
89. GOST 25281-82. 1982. Powder metallurgy. Method for determining the density of moldings
90. DTC-300 instrument. <https://www.tainstruments.com/dtc-300/>
91. HAWK Pyrolysis Instrument. <http://www.wildcattechnologies.com>